AFWAL-TR-88-4016

THE BEHAVIOR OF CERAMIC MATRIX, FIBER COMPOSITES UNDER COMBINED IMPACT AND TENSILE STRESSES

D. Clive Phillips, Nicholas Park, Richard J. Lee,
Roy F. Preston and David M. Dawson
Harwell Laboratory
Materials Development Division
Didcot, Oxfordshire, OX11 ORA, UK.

May 1988

Final Report for Period September 1986 - September 1987

Approved for public release; distribution unlimited.

MATERIALS LABORATORY
AIR FORCE WRIGHT AERONAUTICAL LABORATORIES
AIR FORCE SYSTEMS COMMAND
WRIGHT-PATTERSON AIR FORCE BASE, OHIO 45433-6533

UNCLASSIFIED

SECURITY CLASSIFICATION OF THIS PAGE

ADA202518

REPORT DOCUMENTATION PAGE

Form Approved OMB No. 0704-0188

1a. REPORT SECURITY CLASSIFICATION UNCLASSIFIED	1b. RESTRICTIVE MARKINGS
2a. SECURITY CLASSIFICATION AUTHORITY	3. DISTRIBUTION/AVAILABILITY OF REPORT Approved for public Release; Distribution is unlimited.
2b. DECLASSIFICATION/DOWNGRADING SCHEDULE	
4. PERFORMING ORGANIZATION REPORT NUMBER(S) AERE-R12941	5. MONITORING ORGANIZATION REPORT NUMBER(S) AFWAL-TR-88-4016
6a. NAME OF PERFORMING ORGANIZATION Harwell Laboratory (UKAEA) Materials Development Division 6b. OFFICE SYMBOL (If applicable)	7a. NAME OF MONITORING ORGANIZATION Air Force Wright Aeronautical Laboratories Materials Laboratory (AFWAL/MLLN)
6c. ADDRESS (City, State, and ZIP Code) Oxfordshire OX11 ORA, U.K.	7b. ADDRESS (City, State, and ZIP Code) Wright-Patterson AFB OH 45433-6533
8a. NAME OF FUNDING/SPONSORING ORGANIZATION Dept. of the Air Force 8b. OFFICE SYMBOL (If applicable) AFSC	9. PROCUREMENT INSTRUMENT IDENTIFICATION NUMBER F33615-86-C-5144
8c. ADDRESS (City, State, and ZIP Code) Air Force Systems Command Wright-Patterson AFB, OH 45433-6533	10. SOURCE OF FUNDING NUMBERS PROGRAM ELEMENT NO. 62102F; PROJECT NO. 2420; TASK NO 01; WORK UNIT ACCESSION NO. 90
11. TITLE (Include Security Classification) The Behavior of Ceramic Matrix Fiber Reinforced Composites under Combined Impact and Tensile Stresses	
12 PERSONAL AUTHOR(S) D. Clive Phillips, Nicholas Park, Richard J. Lee, Roy F. Preston and David M. Dawson	
13a. TYPE OF REPORT Final 13b. TIME COVERED FROM Sep 86 TO Sep 87	14. DATE OF REPORT (Year, Month, Day) May 88 15. PAGE COUNT 93
16. SUPPLEMENTARY NOTATION	

17. COSATI CODES		
FIELD	GROUP	SUB-GROUP
11	04	
20	11	

18. SUBJECT TERMS (Continue on reverse if necessary and identify by block number)

Impact tests, Fracture, Composite Materials, Ceramic matrix, Damage, Applied stress - tes

19. ABSTRACT (Continue on reverse if necessary and identify by block number)

An investigation has been carried out of the impact behavior of fiber composites with glass and glass-ceramic matrices. The materials, which were selected as model systems for high temperature ceramic composites, consisted of graphite fibers in borosilicate glass and lithium aluminosilicate (LAS) glass-ceramic matrices. Impact testing was carried out on cross-plied material of lay-up $(0^0, 90^0)_{2S}$. Several different types of impact experiments were carried out. In one, specimens were impacted at room temperature by an instrumented falling weight impactor while subjected to a superimposed tensile stress. The amount of damage caused in this test depends on the level of stress and impact energy. The concept of an impact map has been developed: taking total fracture as the failure criterion, an impact map can be constructed in which impact energy is plotted against applied stress. The boundary denoting total failure of a material can be plotted on the impact map and enables a comparison between different test conditions and different materials. Impact maps have been constructed for the two composite systems and it has been shown that at high impact

20. DISTRIBUTION/AVAILABILITY OF ABSTRACT ☐ UNCLASSIFIED/UNLIMITED ☒ SAME AS RPT ☐ DTIC USERS	21. ABSTRACT SECURITY CLASSIFICATION UNCLASSIFIED
22a NAME OF RESPONSIBLE INDIVIDUAL DAVID I.G. JONES	22b TELEPHONE (Include Area Code) 513 255-1355 22c. OFFICE SYMBOL AFWAL/MLLN

DD Form 1473, JUN 86 Previous editions are obsolete. SECURITY CLASSIFICATION OF THIS PAGE

UNCLASSIFIED

19. Abstract (Continued)

energies the borosilicate glass composite is superior to the LAS glass-ceramic composite, while at low energies the opposite is true. This transition in behavior is reflected in differences in morphology of fracture under the different test conditions. Data are provided which enable the glass and glass ceramic composites to be compared with graphite-epoxy composites on the same impact map: the graphite-epoxy is superior to these ceramic composites. Falling weight impact measurements have been carried out on the borosilicate glass composite over the temperature range 400°C to 650°C. This encompasses the temperature at which the matrix becomes ductile at 580°C. The impact damage in the whole of this range is substantially more severe than under the same impact conditions at room temperature, with considerably more delamination being displayed. Ballistic impact tests on both composite systems have been carried out using a gas driven ball gun operating at impact velocities between 70 ms^{-1} and 140 ms^{-1}. These velocities were much higher than those of the falling weight impact test, which were between 1 ms^{-1} and 3.5 ms^{-1}. The damage in the ballistic test is more localized than in the falling weight test and is confined mainly to a hole punched through the specimen, with little significant differences in appearance between the two ceramic composites. This is different than the falling weight test in which damage is considerably more extended and there are more significant differences in appearance between the two composites. Slow, controlled, fracture tests employing the same loading geometry as the falling weight test have enabled some features of the development of damage to be identified. The borosilicate glass and glass-ceramic composites were selected for this program because it was expected, from earlier work, that they would have different fiber-matrix bond strengths and consequently different interlaminar shear strengths, works of fracture, and other toughness-related properties. A modest materials development program was carried out to optimize the materials, and is reported. Measurements of flexural strength, interlaminar shear strength and work of fracture of unidirectional materials are reported. Although the two materials did have different interlaminar shear strengths and works of fracture, the relationship between these properties was not as would be expected from simple theory. Measurements of matrix microcracking have been carried out and fibre-matrix bond strengths calculated from the microcrack spacing as lying in the range 5-25 MPa. These too do not relate well to the interlaminar shear strengths. This may be due, at least partly, to inhomogeneity in fibre-matrix distribution. Some further materials development may be necessary to obtain fully optimized material.

FOREWORD

This report describes work undertaken by personnel of the Materials Development Division, Harwell Laboratory, England, for the Metals Behavior Branch, Metals and Ceramics Division, Materials Laboratory, Air Force Wright Aeronautical Laboratories (AFWAL/MLLN), Wright-Patterson Air Force Base, Ohio. This work was administered under the direction of Dr. D.I.G. Jones (AFWAL/MLLN), under Contract No. F33615-86-C-5144. The program of research was conducted at the Harwell Laboratory under the leadership of Dr. D.C. Phillips, with material optimization and manufacture undertaken by R.F. Preston and D.M. Dawson, and experimental testing undertaken by N. Park and R.L. Lee. This report describes work conducted from September 1986 through September 1987.

We are grateful to Dr. A. Briggs for his assistance in the optimization and manufacture of materials; to Dr. R. Davidson for advice on impact testing and useful discussions; to Dr. R.W. Davidge for his overall encouragement and support; and to Mr. R.F. Mousley and Mr. D. Scott of RAE Farnborough for carrying out the ballistic impact tests.

TABLE OF CONTENTS

LIST OF ILLUSTRATIONS

1. INTRODUCTION

1.1 Scope

The overall objective of the work described here was to determine the effect of impact on ceramic matrix fiber composites.

One of the principal motives for developing fibre reinforced ceramics is the very considerable increase in toughness which can be obtained compared with monolithic ceramics. Increased toughness is clearly an important goal for this class of materials but it is difficult to quantify its usefulness because of the non-applicability of linear elastic fracture mechanics. In practice an important feature of ceramic composites, related to toughness, is their ability to tolerate damage induced by impact while under normal operating stresses as, for example, a turbine blade under centrifugal stress impacted by debris.

Consequently, the programme had several subsidiary objectives. One, was to assess the usefulness of impacting pre-stressed test specimens as a means of evaluating the toughness of ceramic composites. Another was to determine the effect of changes in one of the basic materials properties, the fiber-matrix bond strength, on toughness and resulting impact response. The study was therefore carried out on two different model systems consisting of graphite fibers in glass and glass-ceramic matrices, which were expected from previous work to produce different fiber-matrix bond strengths. Additional objectives were to assess the effect of temperature and impact velocity.

Several different experiments were carried out and are reported here including:

Instrumented drop-weight impact at room temperature.

Drop-weight impact at temperatures at which matrix softening occurred.

Ballistic impact at room temperature.

Subsidiary micromechanics experiments.

1.2 Background

1.2.1 Ceramic Matrix Fiber Composites

The increasing availability, during the last decade, of high strength ceramic fibers and whiskers, with the potential of acceptable costs, has prompted excitement at the prospect of developing high strength ceramic composite systems which could operate for prolonged periods of time at very high temperatures in oxidizing, and other aggressive, atmospheres[1,2]. Particularly important applications for such materials exist in gas turbine engines for aircraft, where the advantages of a higher temperature capability and reduced density compared with nickel based superalloys could result in the development of engines of considerable superiority over existing engines.

The successful development of ceramic composites for such applications depends on two main factors. All the existing fibres have severe disadvantages at present: e.g. graphite because of oxidation above 400°C; Nicalon SiC because of its non-stoichiometry leading to chemical reactions and microstructural re-arrangement at around 1000°C; alumina because of reactions with oxide matrices leading to too strong a bond between fibers and matrix. There is thus a need for the development of fibers with improved high temperature capability and/or the development of fibre surface treatments or coatings which will inhibit internal changes in the fiber, or reactions with the gaseous environment or with the matrix. The existence of different fibers and of different fibre surface modifications will result in composites with a range of fiber-matrix bond strengths and thus a range of mechanical properties.

The other, parallel, need is to understand the significance in engineering terms of the mechanical properties of these composite materials. The anisotropy and local inhomogeneity of composite materials make them behave differently than conventional monolithic materials, and there is a need to interpret carefully their mechanical properties and evolve engineering design techniques based on a fundamental understanding of the properties. Fortunately, there is considerable experience in this from the vast body of work on polymer composites, but there are significant differences between polymer composites and ceramic composites and

therefore the adaptation of polymer composite background to ceramic composites must proceed with caution.

This report describes work on toughness and damage tolerance of graphite fiber reinforced glasses and glass-ceramics. These may be regarded as models for true high temperature systems. Their advantages for this purpose are that: they can be fabricated with a range of fiber- matrix bond strengths[3,4]; they demonstrate many of the features of true high temperature systems, such as matrix microcracking[5]; and because the effects of matrix plasticity can become evident at relatively low temperatures, $\sim$ 500°C, the transition from a brittle matrix to a more ductile matrix can be studied more conveniently than would be possible for a true high temperature system.

Although these composites are treated here as model materials because they cannot operate in air for long periods of time at temperatures greater than 400°C, because of fiber oxidation, in non-oxidising atmospheres the glass-ceramic composite can have excellent properties to temperatures potentially well in excess of 1000°C. Therefore for non- oxidising atmospheres they can be regarded as moderate-to-high temperature systems.

1.2.2 Toughness and Damage Tolerance

Toughness, although sometimes regarded narrowly as the linear elastic fracture mechanics concept of critical stress intensity factor, is more generally a class of properties, rather than a single property. The unifying concept behind the different toughness parameters is that they are all, properly, a measure of the amount of energy absorbed when a material fractures[6,7].

Much research has been carried out into the fracture of fiber composites. The anisotropy and inhomogeneity of unidirectional materials and multi-directional laminates made from unidirectional laminae make their fracture a complex process. For example the fracture of a multi-directional laminate can typically involve a sequence of events such as the development of multiple cracks parallel to fibers, delamination between plies, and a resulting failure which is not localized and not caused by self-similar crack growth[8,9].

Historically, early work concentrated on attempting to understand the factors which control strength and toughness in unidirectional fiber composites. Crack propagation perpendicular to fibers was investigated by artificially constraining the crack to propagate in the required direction. In this way the energy absorption mechanisms in composites, including fiber reinforced glasses and glass-ceramics, were investigated and the important toughening mechanisms such as pull-out, debonding and post-debond friction identified and quantified[4,10,19]. Crack propagation parallel to fibers, in polymer composites, has also been investigated and the development of a process zone, due to fibers tieing the fracture surfaces, and the variation of fracture energy with crack length have been identified and the consequences for crack stability discussed[12,13]. As well as identifying the energy absorption processes, work of this type showed that a fracture mechanics approach could sometimes be employed with unidirectional fiber composites under the artificial conditions where cracks were constrained by experimental techniques to propagate in the required directions[4,11]. For multi-directional materials, the complexity of the fracture processes produced a conceptual problem and research has shown that although a linear elastic fracture mechanics, or related, approach can sometimes be made to work under artificial circumstances of crack constraint, it has very limited general applicability[8,9,11]. As well as linear elastic fracture mechanics, many other related two or three parameter approaches have been used, such as the point stress and average stress criteria, but it is widely recognized that all of these are of very limited value and at present there is no valid, single, toughness parameter which can be used in the selection and design of composite materials. Instead a pragmatic approach is necessary, depending upon the practical application of the material. One approach which is being widely researched for polymer matrix fiber composites is the concept of damage tolerance - the remaining strength of the material after it has been damaged or after a severe stress concentration has been otherwise introduced[14].

Ceramic matrix fiber composites have potential applications where their impact behaviour - including ballistic impact, may be important. It is known from previous work on polymer matrix fiber composites that the loss of strength of a fiber composite under simultaneous impact and tensile stress can be much more severe than under the sequential conditions of impact followed by tensile stress[15-18]. Figure 1 shows this effect for a graphite fiber reinforced epoxide

composite, for which the direction of impact was perpendicular to the direction of the tensile stress, Figure 2. In Figure 1 the data on the upper (broken) line were obtained by impacting the specimens while initially unstressed, and then measuring their residual (remaining) strengths in the tensile test. The data on the lower (solid) line were obtained by impacting the specimens while they were subjected to a superimposed tensile stress. In such an experiment it is necessary to impact several specimens under a range of stress at a given impact energy to determine the boundary between fracture and non-fracture and the solid line of Figure 1 represents that boundary. This effect has been studied in some detail for polymer matrix composites and its severity is known to depend on the strength of the fiber-matrix bond. The combined effects of impact and tension could be important for applications of ceramic composites, for example a turbine blade under high centrifugal stress. An important objective of the programme was to study these aspects of the damage tolerance of ceramic matrix fiber composites.

2. EXPERIMENTAL

2.1 Fabrication

Composites were manufactured by the slurry impregnation route which was first developed at Harwell[1,3]. Figure 3 shows the process for impregnating a continuous tow of carbon fiber with glass or ceramic powder. The tow passes initially up a vertical column and over a pulley, to reduce kinks and twists as the tow is unwound, and then around a series of PTFE rollers where it is subjected to two jets of air, the function of which is to fan the fibers out over the width of the rollers and spread the tow into a tape. The jets are arranged so that there is no net force on the tow in the direction of travel. The tape is then passed through a tank and saturated by total immersion in a slurry of an organic binder, matrix powder and a solvent. The slurry is agitated by air fed through a sintered metal disc which forms the bottom of the tank. The impregnated tape is reduced to a controlled width, typically 1 cm, and wound with a small overlap onto a former while still wet. In this condition each turn bonds with its neighbour. After air drying, the tape can be cut from the drum in the form of a self-supporting sheet, sufficiently strong to enable it to be handled in preparation for subsequent shaping and hot-pressing operations.

Composites were manufactured from Hysol Grafil, high modulus, unsized graphite fiber combined with borosilicate glass and lithium aluminosilicate powders. The borosilicate glass was Corning Pyrex glass, supplied by J. Bibby Science Products Ltd., ball-milled to pass through a mesh < 45 mm. The lithium alumino-silicate glass-ceramic was obtained from Pilkinton, designed Code 693 - mixed ZrO_2/TiO_2 nucleated, also ball-milled to < 45 μm.

The matrix slurry composition was 20.6% of glass or glass-ceramic in a 2.1% polyethylene oxide binder and 77.3% analytical grade water (ph 5.5 to 7.5). The last two constituents were supplied by BDH Ltd. of Poole, England. This slurry composition was optimized to give a consistent pre-preg fiber loading of approximately 40 volume %. After hot pressing the material had a low porosity of <2%.

Optimization of hot-pressing parameters involved an investigation of an time/temperature/pressure matrix of process conditions. Optimization was carried out using a small die assembly to produce specimens 50 mm x 15 mm x 1 mm, from which were machined flexural test specimens 50 mm x 6 mm x 1 mm These were tested in an Instron testing machine at a rate of 0.5 mm min^{-1}.

For the graphite/borosilicate material a matrix of 27 experiments gave the results in Table 1. The optimum hot-pressing conditions involved heating to 850°C; application of a pressure of 12 MPa for 7 minutes; cooling to 400°C under load and then unloading.

An additional requirement for glass-ceramic materials is the ceraming conditions needed to provide good refractory capability. Table 2 presents the results of the optimization studies for the glass-ceramic composites. The optimum hot-pressing and ceraming conditions were: heating to 1275°C at a fast heating rate; application of a pressure of 12 MPa for 7 minutes; cooling to 400°C under load and then unloading. Figure 4 illustrates the effect of ceraming temperature on the crystallinity and crystal form of lithium aluminosilicate.

The optimized fabrication conditions were subsequently used to manufacture larger plates, 100 mm x 100 mm x 2 mm, both cross-plied $(0°,90°)_{2S}$ and unidirectional, from which impact specimens were obtained. Previous work had shown that there are no problems in scaling up from the small die assembly of the optimization studies, to the larger plate die. Each plate consisted of 8 plies.

2.2 Static Mechanical Testing

Static mechanical testing, for the purpose of providing baseline data, was confined to flexural testing. Flexural strengths were measured in 3-point bending on specimens of dimensions 50 x 6 x 1 mm with a span of 40 mm at a crosshead speed of 0.5 mm min^{-1}. Shear strengths were obtained by 3-point bending of short beam specimens of dimensions 20 x 6 x 3 mm with a span to depth ratio of 3.66:1. Works of fracture[10] were obtained by controlled fracture in bending of specimens of dimensions 50 x 6 x 5 mm.

2.3 Instrumented Impact Testing

Instrumented impact testing was carried out at room temperature using a CEAST Modular, Falling Weight, Instrumented Impact Machine. This was interfaced via an AFS/Mk3 advanced fractographic unit to an Apple Microcomputer which uses the potential energy of the impactor and the load-time data to generate load, velocity and absorbed energy as a function of time and displacement. The impact machine was combined with a modified Hounsfield Tensometer to enable the specimens to be stressed in tension.

The equipment is illustrated schematically in Figure 5 and shown in Figure 6. Specimens, typically 100 mm long x 25 mm wide x 2 mm thick, were mounted horizontally in the Hounsfield Tensometer : this is a small, flat-bed, test machine which can apply loads up to 2 tonnes. The specimen was gripped by means of screw action grips with serrated faces. The span between these grips was fixed at 50 mm, see Figure 7. The static tensile load applied to the specimen was measured via a Maywood Instruments U-4000 load cell, which has a 2.5 tonne capacity, connected to a Vishay Ellis-20 digital strain indicator.

Impact was applied by means of a falling weight tup. The tup weight was variable but was normally 1.5 kg in these experiments: the point of impact was a hemisphere either of diameter 20 mm, for extended damage, or 6 mm, for localized damage. In all the work reported here a 6 mm diameter point of impact was used. Althought the point of impact was a hemisphere, it was mounted on a cone. Thus at impact energies at which total penetration occurred, the cross-section of the impactor increased as it drove through the specimen with consequent increase in damage. Drop height was also variable, and in these experiments up to 1 metre. The tup was a proprietary system, supplied by CEAST SpA: it contains a strain gauge system which is interfaced via the CEAST Advanced Fractoscope System Mk.3 to an Apple Microcomputer. The CEAST tup strain gauge has a maximum capacity which allows impact loads of up to 2 tonnes to be measured.

On completion of an impact test the CEAST system can automatically provide a time-sequence print-out of: force on the point of the tup; energy absorbed by the tup during the impact event; velocity of the tup; displacement; and combinations of

these. This analysis is carried out from the input of the force versus time data and the initial potential energy (mass x height, mgh) of the tup: velocity, displacement and energy are inferred from these by simple mechanics.

2.4 Impact Testing at Elevated Temperatures

For impact testing at elevated temperatures a vertical tube furnace was designed and constructed. This is illustrated in Figure 8. Both ends of the furnace were closed to allow a non-oxidising (nitrogen) atmosphere to be maintained around the specimen. The top end contained a centrally positioned ring assembly incorporating a thin membrane of aluminium foil. This was pierced by the impactor prior to its contact with the composite specimen within. The specimen holder reproduced the end conditions of the room-temperature pre-stressed impact tests, and locating pins allowed it to be aligned accurately on the framework within the furnace. For these experiments a non-instrumented tup was used. Specimens were not pre-stressed during these tests.

2.5 Ballistic Impact

Ballistic impact testing was undertaken on equipment at the Royal Aircraft Establishment, Farnborough, UK. Using this equipment, a 6 mm steel ball was fired at impact velocities between 70 ms^{-1} and 140 ms^{-1}. The specimens were mounted in the same jig used for the elevated temperature impact tests (Figure 8), thus giving the same constraining conditions as in the stressed impact tests. Specimens were not pre-stressed during these tests.

3. RESULTS

3.1 Mechanical Properties at Room Temperature

The baseline mechanical properties of the unidirectional carbon fiber reinforced borosilicate glass and LAS glass-ceramic composites are shown in Table 3.

The flexural strength of the unidirectional borosilicate glass composite was 900 MPa while that of laminates made from it were: $(0°/90°)_{2S}$ = 560 MPa; $(90°/0°)_{2S}$ = 300 MPa.

3.2 The Effect of Temperature on the Strength of Borosilicate Glass Composites

The transition from brittle to ductile behaviour at elevated temperatures was determined from the change in interlaminar shear strength (ILSS) with increasing temperature. Values of the ILSS determined for unidirectional material are given in Table 4 and show that a brittle/ductile transition occurred just below 580°C.

3.3 Instrumented Impact Testing

Impact behaviour was studied over a range of energies and applied tensile loads. All impact testing was carried out on cross-plied material of lay-up $(0°,90°)_{2S}$. The test procedure employed was as follows. The specimen was mounted on the Tensometer and a tensile load applied. The impactor was then dropped onto the centre of the specimen from a height which defined the impact energy (E = mgh). The specimen was then removed and examined visually for damage. Each specimen was subjected to only one impact test. For each impact energy a number of specimens were tested over a range of applied tensile loads.

For specimens impacted under zero applied tensile load: at very low values of E no visible damage was observed; at higher values some indentation damage and cracking occurred but some residual tensile strength was retained; as E was further increased damage became progressively more severe and residual tensile strength decreased; finally an energy (E_{max}) was reached at which total fracture of the specimen occurred.

For specimens impacted at a constant impact energy, less than E_{max}: as the applied tensile load was increased from zero for successive specimens, damage increased as the applied tensile load increased, but the specimen retained some residual strength until eventually a load was reached at which total fracture occurred and the specimen had zero residual strength.

A plot of impact energy against applied stress can be regarded as an impact fracture map. For a given impact energy there is a critical applied tensile stress at which total fracture occurs and the residual strength is zero. Plots of this fractured/unfractured boundary over a range of impact energies are shown on the impact fracture maps for the borosilicate glass composite in Figure 9 and LAS glass-ceramic composite in Figure 10.

The data obtained from an instrumented impact event are in the form of a force versus time plot. From this and the initial potential energy of the impactor are derived the absorbed tup energy, velocity and tup displacement. Examples of impact data and their presentation, as well as the corresponding photographs of the post-impact appearance of the specimens are shown in Figures 11 through 22 for the LAS glass-ceramic specimens and Figures 23 through 34 for the borosilicate glass specimens. In these photographs top and bottom faces, and a side view, are shown. Other data about the specimens, applied stresses and information obtained from the impact event graphs are shown in Table 5 for the LAS glass-ceramic specimens and Table 6 for the borosilicate glass specimens. The variation of maximum recorded impact force, which was not always the first recorded peak force, over a range of impact velocities for both non-fractured and fractured material is shown in Figures 35 and 36. Also shown are the peak forces recorded from the slow indentation experiments.

The photographs and corresponding impact data traces illustrate some of the key observations made during these experiments.

For the LAS glass-ceramic system, Figures 13 and 16 are a series of photographs showing the increase in damage of specimens impacted at 2J energy as tensile stress was increased from 20 MPa to 47.5 MPa. At the lower stresses a hemispherical indentation was produced on the front face with splitting and spalling of strips of plies on the rear face. This damage increased until at the

highest stress the specimen broke in two separate pieces. Some of the corresponding force-time and force-displacement curves, such as Figure 11 for specimen LAS1.05, show macroscopic peaks which may be associated with ply failures. The very high frequency peaks are noise associated with resonances and other extraneous features. Figures 19 and 22 are photographs showing the increase in damage of specimens impacted at 4J energy as stress was increased from zero to 10 MPa. At this higher energy, damage at 5 MPa stress was similar to the ballistic damage, to be described later, with complete penetration. At the higher applied stresses at which total fracture occurred, fracture was a more widespread process than at the lower impact energy.

For the borosilicate glass system, Figure 25 is a photograph of damage obtained at 1J impact and applied stresses of 40 MPa and 70 MPa, while Figures 28, 31 and 34 show the effects due to increasing energy with examples at 2J, 6J and 8J. A point to note is the much more extensive damage which occurred as impact energy was increased, the 1J impacted specimen failing with an almost planar fracture while the higher energy specimens showed much more extensive damage.

In general, at the higher impact energies the borosilicate glass composites exhibited much more extensive and fibrous (hairy) damage than the LAS glass-ceramic composites, but this was much reduced as the impact energy was decreased. A further difference between the two composite systems occurred in the force-time and force-displacement curves. The macroscopic peaks which were very apparent in some of the LAS glass-ceramic composite tests, and which may be associated with individual ply failures, were less apparent in the borosilicate glass composite tests.

3.4 Slow Fracture Experiments

In order to clarify the processes occurring in an impact test, slow indentation experiments were carried out. The instrumented tup was mounted on a floor standing Instron, screw driven, testing machine and the Hounsfield Tensometer was located across the bed of the Instron so that the specimen could be pre-stressed by the Tensometer and then slowly 'impacted' by the tup at a rate of 100 mm min^{-1}. All specimens were of cross-plied material of lay-up $(0°,90°)_{2S}$.

The advantage of this test was the controlled nature of the impact/indentation process, which permitted identification of specific damage events at different stages in the fracture process. In an impact test the earlier stages of fracture are usually obscured by later damage. The most noticeable features in the tests were the occurrence of major load peaks and some inflections on the rising and falling parts of the load trace. These peaks and inflections corresponded to microscopic fracture events. Specimens were indented until characteristic load peaks were reached and the damage at those points is described below. It should be noted that it was not possible to relate the peaks to a single event such as 0° ply failure and that further work is necessary to clarify the relationship between the features in the load trace and microstructural fracture events.

3.4.1 LAS Glass-ceramic Composite

Figure 37 shows the load-displacement traces obtained at various stages in the slow fracture of a series of LAS glass-ceramic specimens.

(a) Specimen LAS8-43 shows the trace when the specimen was completely fractured. This force versus displacement plot was characterised by the presence of two distinct peaks.

(b) Specimen LAS8-45 was indented until just after the first peak at a displacement of 0.8 mm. A shallow indent was visible on the top surface. No delamination or ply splitting was visible along the specimen edges. The under surface exhibited a region of localised delamination with some fiber fracture giving the appearance of a small, circular plate being spalled away. A crack ran perpendicularly from this region to one of the edges, through the two bottom plies.

(c) Specimen LAS8-44 was tested to a point just after the second peak. The indent on the top surface was larger and about 2 mm in depth. Some splitting between the fibers in the top 0° ply to one side of the indent mark was visible. The greater tup penetration and associated material push-through had increased the area of delamination on the under surface. Three distinct plate-like regions were present. The perpendicular crack observed with specimen LAS8-45 had progressed a stage further, and had resulted in the specimen fracturing over half of its width. No delamination or ply splitting was visible along the specimen edges.

(a) Returning to (a), this specimen (LAS8-43) was indented until complete fracture. The plate-like regions of delaminated material were visible on the under surface. A very small amount of delamination was present along the specimen edges. Very little fiber pull-out was noticeable on the fracture face.

3.4.2 Borosilicate glass composite

The force vs. displacement plot for this material at total fracture was again characterised by two distinctive peaks, see Figure 38a (specimen BOR7-40). This specimen while not completely fractured, suffered considerable delamination damage similar to that observed in the impact work.

(b) Specimen BOR7-41 was indented until just after the first characteristic peak had been reached at a displacement of 1.4 mm. A small indent was visible, about 2 mm in diameter, with a 5 mm crack each side running parallel to the 0° fibers. The underside exhibited little damage apart from two or three barely visible cracks running parallel to the 0° fibres. The most serious damage was observed along the edges. Considerable ply splitting and delamination was present in the 90° plies over the whole 50 mm specimen span.

(c) Specimen BOR8-43 was indented until just before the second peak. The damage was similar to that observed with BOR7-41, but was more advanced. The indentation on the top surface was larger and both the top and bottom surfaces exhibited a much greater amount of splitting between the 0° fibers. A perpendicular crack meandered its way between the outermost splits in the bottom 0° ply, i.e. across a region about a quarter of the specimen width. Again, substantial splitting/cracking was present in the 90° plies

(d) Specimen BOR7-42 showed the damage state reached just after the second peak. Damage was more extensive than in BOR8-43. Splitting parallel to the fibers was more widespread in the top and bottom 0° plies. Again, considerable delamination/splitting was observed at the specimen edges along the whole length of the test span. The perpendicular meandering crack observed in the undersurface of BOR8-43 had gone a stage further and almost traversed the complete specimen width.

(e) Specimen BOR8-44 was indented beyond the second peak. Far more splitting parallel to the fibers was visible on the top surface, with some of these cracks extending the length of the specimen span. Splitting/cracking visible along the edges was considerable. The perpendicular crack on the under surface eventually traversed the complete specimen width.

(a) Returning to (a), this specimen (BOR7-40) was indented until the tup displacement was 4 mm. The damage observed was considerably worse than with BOR8-44. The greater amount of splitting/cracking in the 90° plies resulted in fiber fracture perpendicular to the 0° fibres in the bottom three 0° plies

3.5 Effect of Temperature on Impact Behavior

Static mechanical testing showed that the brittle/ductile transition temperature for the borosilicate glass composites lay between 570°C and 580°C. Subsequently, impact tests were carried out over the temperature range 400°C to 650°C on cross-plied material of lay-up $(0°,90°)_{2S}$. Photographs of specimens impacted at 0.5J and 1J are shown in Figures 39 and 40 respectively. In these tests the impactor had a mass of 0.85 kg.

The specimens impacted at 0.5J exhibited splitting/cracking in the 90° plies. Tup penetration was limited but the small amount of material "push-through" produced a perpendicular crack which traversed the specimen width for impacts at 600°C and 650°C. The 0.5J impact at 580°C completely fractured the specimen. Some splitting parallel to the 0° fibres was present in the top ply. From its surface appearance, it is possible that this specimen may have suffered some oxidation.

The specimens impacted at 1J exhibited a markedly different damage appearance to those impacted at 0.5J. The specimen impacted at 400°C was expected to suffer damage similar to an impact under equivalent conditions at room temperature because at that temperature the matrix was still brittle. In practice, the damage sustained at 400°C was similar to that obtained with the specimen impacted at 0.5J at 600°C. Again considerable splitting in the 90° plies was visible. A crack perpendicular to the 0° fibres in the bottom ply traversed the complete specimen width and propagated up through three-quarters of the specimen thickness. The top surface impact crater was 4 mm in diameter. The specimen impacted at 580°C

exhibited a brittle fracture breaking at its middle and at the extremities of the span. No delamination or splitting in the 90° plies was visible along the edges. Fiber pull-out was small and the fracture surfaces were relatively flat. Specimens impacted at 600°C and 650°C both fractured at mid-span and both suffered similar damage. In both cases, considerable delamination and splitting/cracking in the 90° plies occurred. Splitting parallel to the 0° fibres was a noticable feature of these specimens giving the final fracture specimen a distinctly fibrous appearance. From its appearance it is possible that some oxidation of the carbon fibers may have occurred to the specimen tested at 600°C.

Specimens impacted at 0.75J exhibited damage features similar to the 1J impacts. The damage sustained at 580°C was similar to that obtained with a 1J impact at 600°C. The specimen had fractured at mid-span and sufferred some fibre and matrix fracture at the span extremities. Considerable delamination and splitting/cracking was present in the 90° plies. Splitting parallel to the 0° fibers was again in evidence giving the specimen a fibrous appearance. Specimens impacted at 600°C and 650°C exhibited similar damage. In both cases, impact caused the bottom six to eight plies to be pushed out while keeping the top ply intact at the specimen edges i.e. the specimen still possessed some residual strength. These delaminated regions completely fractured at the mid-span, but were hinged at the span extremities. The fracture surfaces were again distinctly fibrous or "hairy".

To summarise: the appearance of the fracture morphology of these elevated temperature, low impact energy specimens was quite different than that of the low energy, room temperature impacts, even at a temperature of 400°C at which the matrix was still brittle. Damage tended to be more extensive and more akin to the high impact energy, room temperature, specimens. In most cases considerable delamination occurred in a far more pronounced way than at room temperature, perhaps suggesting that interply thermal mismatch stresses were of increasing importance. As temperature and energy were varied, similar damage was observed at 0.5J at 600°C, 0.75J at 580°C, and 1.0J at 400°C, i.e. as energy increased the temperature at which similar damage occurred decreased.

3.6 Ballistic Impacts

LAS glass-ceramic specimens impacted under ballistic conditions are shown in Figure 41, and the borosilicate glass specimens are shown in Figure 42. All specimens were of cross-plied material of lay-up $(0°,90°)_{2S}$. The rear surfaces of the specimens are shown in these figures. Damage to the front surface was confined to a round hole caused by the projectile. No delamination or ply splitting/cracking was visible along the specimen edges. As can be seen in the figures, impact damage becames more localised as the velocity increased. This is shown for the borosilicate glass specimens, Figure 42. An impact at 70 ms^{-1} has resulted in a greater amount of damage in the bottom ply than that observed at 140 ms^{-1}. A similar trend is visible with the LAS glass-ceramic composite material, Figure 41, although the damaged carbon fibers obscure the penetration hole. Equivalent impact energies are also noted in these two figures to enable a comparison between high velocity low mass impacts (ballistic) and low velocity high mass impacts (the instrumented drop weight impact tests) shown in previous photographs.

At the high velocities of these ballistic tests differences in fracture morphology between the two composite systems were much less obvious than in the lower velocity experiments.

3.7 Matrix Microcracking

Microcracking was observed in both the LAS and borosilicate unidirectional composites tested in 3-point flexure. This cracking was more easily observed in the LAS glass-ceramic composite than in the borosilicate glass composite, Figure 43. The separation between matrix microcracks can be used to estimate the fibre-matrix bond strength by a procedure described more fully in Reference 1 and 5. The non-uniform spacing between cracks made the measurement of a meaningful, average crack spacing difficult, but some regions of uniform cracking could be isolated and measurements were carried out on these.

The fiber/matrix bond strength can be determined from the equation[5]:

$$\tau = \frac{(\sigma_m)_u \, V_m \, r}{k \, V_f \, 2 \, t} \qquad (3.1)$$

where τ is the fiber matrix bond strength, $(\sigma_m)_u$ is the strength of the matrix, V_m is the matrix volume fraction (0.6), r is the fiber radius (4×10^{-6} m), k is a constant which is usually less than 1 (taken as 0.5), V_f is the fibre volume fraction (0.4) and t is the crack spacing. Average crack spacings measured from fractured borosilicate glass and LAS glass-ceramic composite specimens were 0.24 mm and 0.14 mm respectively.

Ideally, $(\sigma_m)_u$, the stress in the matrix at which microcracking commences, should be derived from the stress in the composite at which cracking is observed to begin, or at which the stress-strain curve becomes non-linear, through the equation:

$$(\sigma_m)_u = \frac{\sigma_c}{[1 + V_f \, (\frac{E_f}{E_m} - 1)]} \qquad (3.2)$$

where σ_c is the stress in the composite at which matrix microcracking occurs, E_f and E_m are the moduli of the fiber and matrix respectively. In practice, because of experimental difficulties, it was not possible to measure $(\sigma_m)_u$ accurately for both the composite systems in the time available. A value was estimated for the LAS composite from the stress at which the stress-strain curve became non-linear: this gave a value of $(\sigma_m)_u$ of approximately 590 MPa. Earlier work[5] on graphite-borosilicate composites showed that $(\sigma_m)_u$ for a 40 volume % composite was typically 200 MPa. When these values are employed in Equation (3.1) with the measured microcrack spacings they yield values of the fibre-matrix bond strength of 5 MPa for the borosilicate glass composite and 25 MPa for the LAS composite. The values of $(\sigma_m)_u$ used in these calculations are very uncertain and an alternative is to make an estimate based on a similar, typical, guessed value of matrix strength for each material. Assuming values of $(\sigma_m)_u$ for both of 200 MPa yields values of τ of 5 MPa for the borosilicate composite and 9 MPa for the LAS.

In each case, although there is uncertainty in the absolute values, the relative order of the values is unchanged with the borosilicate glass composite having a substantially lower fiber-matrix bond strength than the LAS composite. In contrast the interlaminar shear stresses for these materials were 30 MPa for the borosilicate and 7 MPa for the LAS composites respectively.

4. DISCUSSION

This programme of work set out to address several main questions:

(i) Under combined conditions of impact and superimposed tensile stress, how well do ceramic matrix composites perform?

(ii) What is the effect on impact behaviour of varying the properties of a ceramic matrix composite, in particular: toughness as controlled by the fiber-matrix bond; and matrix ductility as controlled by temperature?

(iii) What is the effect of impactor velocity?

(iv) Do the techniques described here provide a useful approach to comparing and qualifying materials for service applications?

The complete programme described here lasted one year with most of the data, necessarily, being generated towards the end of the programme. A considerable amount of information has been generated in a relatively short time and the full implications of all the data, particularly with respect to question (iv), are still uncertain. In parallel with the programme described here, a separate in-house programme of research on polymer composites and other materials has been undertaken. The results of that are described elsewhere[20] and reference to those results are made in this discussion where they help clarify some of the issues: that programme is still continuing and some of the conclusions given here should be regarded as tentative.

Figure 44 shows the room temperature, energy vs. applied stress, impact fracture map for the glass and glass-ceramic composite systems. At high impact energies the borosilicate glass system is superior to the LAS glass-ceramic system, being able to sustain higher impact energy and/or applied stress before total fracture. At low impact energies, approximately 2.5J in the experiments reported here, the LAS glass- ceramic system was superior. The reasons for this transition in behaviour are not understood at present but there are strong indications that the transition occurs also in the morphology of fracture of the two systems. Figures 23 through 34 showed that at low impact energy the borosilicate glass

system exhibited an almost planar fracture. As impact energy was increased the fracture became more delocalized with much splitting and splintering and the development of fibrous features, to produce a final appearance which intuitively seemed tougher than the more brittle planar fracture.

Further research is needed to determine the reasons for this change in behaviour. A possible hypothesis is that the two different systems possessed different strain-rate sensitivities. It is, perhaps, not intuitively obvious that brittle matrix systems could possess a strain-rate sensitivity, but early work on carbon fiber reinforced glass systems demonstrated that this could occur[4]. In the present experiments the velocity of the impactor, and thus strain-rate, increased as impact energy increased. Figures 35 and 36 compare maximum recorded force as a function of impact velocity. For the borosilicate glass system, Figure 36, the variation of the recorded force over the impact/indentation strain-rate range is of the same order as the experimental scatter, and is almost a constant value. However, with the LAS glass-ceramic system, the force is constant up to an impact of 1.96 ms^{-1} (3J), but apparently increases in value after this point, Figure 35. Again, the large variation in the experimental results may be misleading, considering the damage induced into the materials appears consistent over the test range. Thus the small change in recorded maximum force over the range of impact velocities suggests that strain-rate behavior is not a major problem.

If the effect shown here is reproducible and applies to other ceramic composite systems, it shows that care must be taken in selecting a material on the basis of a simple, unstressed, impact test. The borosilicate glass system would appear superior in such a test but in a practical, operational situation, where the component is under stress at impact the glass-ceramic system would be superior.

Figure 45 shows an impact fracture map for the glass and glass- ceramic matrix composite systems, together with boundaries obtained for graphite fiber epoxy and polymethylmethacrylate ("Perspex/Plexiglas") from Reference 20. The data should be compared with caution because of the different thicknesses and other geometrical differences of the different specimens; however, it is clear that the glass and glass-ceramic composites are considerably inferior to the high performance epoxy composites. This could be a reflection of their poorer static mechanical

properties. The flexural and interlaminar shear strengths of the unidirectional T300/914C graphite-epoxy system are respectively 1520 MPa and 100 MPa, which are much higher than those of the glass/glass-ceramic systems given in Table 3. It would be interesting to compare glass/glass-ceramic composite systems with epoxy composite systems of similar static strengths to determine whether the toughness of the matrix is an important factor - the toughness of epoxy resins is between factors of ten and a hundred greater than inorganic glasses.

The variation of maximum recorded force with applied stress for a range of impact energies is shown in Figures 46 and 47. In the case of th LAS glass-ceramic material, Figure 46, it can be seen that two distinct clusters are formed, i.e. the impacts at 2 and 3J and at 4 and 5J. An important thing to note is the almost constant maximum force recorded for impacts of 2J over a large span of applied stresses. This suggests similar behavior is exhibited by the specimens at the various applied stresses. As mentioned previously (and see Figure 35) the apparent increase in recorded force above 1.961 ms^{-1} (3J), i.e. for specimens subjected to the least applied stresses, may be misleading due to experimental scatter. In general, the maximum recorded force obtained from a specimen that has completely fractured is less than that obtained from a non-fractured specimen. This may be due to the reduced affect of the bending stress component, and hence a reduction in the force required to produce it, with the increased applied static tensile stress necessary to result in material fracture during an impact event.

For the borosilicate glass system, the maximum recorded force shows a wide variation, but is almost constant over the range of applied stresses, especially for the non-fractured specimens. This is also shown in Figure 36. As with the LAS glass-ceramic, the maximum recorded force obtained from a fractured specimen is less than for a non-fractured specimen.

It should be noted that the glass and glass-ceramic composite systems manufactured in this programme did not have the properties, relative to one another, anticipated from earlier work. Table 7 shows the properties of 0° borosilicate glass and LAS glass-ceramic composites published some years ago[4]. The glass-ceramic was a different system than that used in the present programme. It was shown in the earlier work that the different coefficients of thermal expansion and softening temperatures of the matrix materials resulted in

differences in the relative radial shrinkage of fiber and matrix. This produced a different fiber-matrix bond strength reflected in differences in inter- laminar shear strength and toughness, as measured by a work of fracture test.

Table 8 compares works of fracture, interlaminar shear strengths and fiber-matrix bond strengths of the borosilicate glass and glass- ceramic systems manufactured for this programme. On the basis of simple theory, for two composites with different fiber-matrix bond strengths it would be expected that the composite with the higher bond strength would have the higher interlaminar shear strength and the lower work of fracture[4]. Table 8 shows that this simple relationship does not hold for these materials.

In Table 8 the fiber-matrix bond strength is the most basic property. However, the estimates given in the table have a great deal of uncertainty for the reasons described in Section 3.7 and because of the inhomogeneity of the material. The values were estimated from the microcrack spacing[5] and in practice the microcrack spacing was measured in matrix-rich regions. Consequently the absolute values may be in error. However, the relative values will be less in error because similar matrix-rich regions with similar, effective, fiber volume fractions were used. The relative values of work of fracture of the two systems thus agree with the relative values of fiber-matrix bond strengths. There is, however, complete disagreement between the relative values of interlaminar shear strength and those of work of fracture and fiber-matrix bond strength. It is unclear why this is so and further research is required. It may be that the explanation lies in a lack of optimisation of the materials and certainly further optimization is required to improve the homogeneity of the distribution of fibers in the matrix.

The increase in damage at equivalent impact energies on increasing temperature, and the increasing amount of delamination which occurs, is disconcerting. It is unclear why this occurs, especially as it begins at temperatures sufficiently low for matrix ductility not to be important. The delamination suggests that interply thermal mismatch strains become more important as temperature increases, but this is unlikely to be a correct interpretation as the mismatch strains produced during fabrication should decrease as temperature rises. Whatever the reason this is clearly a very important practical effect and needs further research to clarify the issues.

The slow fracture test is useful in providing an insight into the way damage develops during an impact test: a comparison of the slow fracture test, falling weight impact and ballistic impact provides a clear picture of the way the morphology of fracture changes as velocity of impact increases. The qualitative, visual observations reported here provide a starting point for beginning to understand in more quantitative detail the important stages in fracture of ceramic composites. Further observations of this type could provide helpful guidance in the development of materials with improved damage tolerance, as has been the case for polymer composites where it has been shown that ply stacking sequence has a prominent role in controlling toughness and damage tolerance[8,9].

With regard to the ballistic testing, it should be noted that graphite-epoxy composites impacted under similar conditions did not exhibit the complete projectile penetration of the glass and glass-ceramic composites but exhibited instead considerable amounts of delamination within the specimen and cracking in the 90° plies[20]. This may be due to the superior strength of the graphite-epoxy.

In the ballistic impact tests, specimens were impacted at velocities of 70 to 140 ms^{-1}, i.e. two orders of magnitude greater than in the instrumented impact tests. At these high velocities, total projectile penetration occurred. No delamination or cracking in the 90° plies was visible along the specimen edges, as apparent in the photographs of ballistically impacted specimens, Figures 41 and 42. It is noticeable that at the lower velocities, a greater area of damage is created in the bottom two or three plies around the underside of the penetration hole. The high velocity of the projectile in the ballistic impact work inhibits energy absorption mechanisms such as delamination and fiber pull-out. Decreasing the impact velocity causes the impact energy to be dissipated increasingly further outwards from the point of impact, with more widespread damage.

This phenomenon has been observed with ballistically impacted boron/aluminium composites[21,22]. Both these papers show that for unstressed material, increasing the impact velocity decreases the post impact residual strength of the composite. In this case, to 50% of the original strength. This is also accompanied by a transition in the damage morphology, changing from material cracking and delamination to complete projectile perforation. Carlisle et al[21]

showed that there were three distinctive types of damage induced into stressed boron/alunimium material under ballistic impact conditions. Up to a certain impact velocity, specimen damage occurred, gradually decreasing the material's residual strength with increasing velocity, see Figure 48. Beyond this first critical velocity, a region is entered where the impact alone is sufficient to result in complete material fracture. In both these regions, the initiation and propagation of a widespread macroscopic cracking is probable. At the second critical transition velocity, complete projectile penetration is encountered. As the velocity increases still further, the damage due to the impact becomes less widespread. A theoretical limit is reached where the end result is a round hole. The energy to produce this ideal through thickness hole is

$$\pi \gamma t d$$

where γ is the through thickness fracture energy, d the diameter of the projectile, and t is the specimen thickness[23]. The type of damage sustained by the ceramic matrix composites tested in this programme suggests an impact velocity on the extreme right of the non-stressed material curve.

It is interesting to compare the same material impacted with similar impact energies but large differences in impact velocities. An example is LAS3-16 (Figure 19) and LAS2-08 (Figure 41), both impacted with roughly 4J but at velocities of 2.26 ms^{-1} and 100 ms^{-1} respectively. Specimen LAS2-08 has suffered a projectile penetration while LAS3-16 shows signs of a large delamination region on the undersurface, from which the development and propagation of a transverse crack is the likely next step. These two distinctly different damage morphologies make direct comparisons of similar impact energies but highly differing impact velocities suspect. This suggests that the material behaves differently when impacted below approximately 5 ms^{-1} and above 50 ms^{-1}. Below the former limit, the material can be envisaged as behaving in quasi-static equilibrium, i.e. tup penetration is limited and simple elastic beam theory can be applied. The transition to complete projectile penetration as the main material damage suggests a difference in material response to the impact event. The increased momentum of the ballistic impact probably reduces the elastic response of the whole specimen (essential a beam built-in at both ends), with the majority of the impact energy being absorbed in a highly localised region. This leads to highly localised

deformation and damage, finally permitting total projectile penetration given that the impact is sufficient to do so.

Thus, impact velocity does play a significant role in impact induced damage, especially if compared over a very wide range.

Comparisons of the two ceramic matrix composites with graphite-epoxy impacted under similar conditions shows that with the graphite-epoxy, complete projectile penetration was not achieved even at 140 ms^{-1}[20]. Considerable amounts of delamination within these materials and cracking parallel to the fibres in both the 0° and 90° plies was observed. The damage sustained would probably place a graphite-epoxy $(0°,90°)_{2S}$ composite impacted at 140 ms^{-1} in the middle portion of the curve for unstressed material shown in Figure 46. Many papers[23,24,25,26] have studied the impact of CFRP from 10 ms^{-1} upwards. Widespread delamination within these materials has been shown to be a major energy absorbing mechanism. The greater the number of interfaces between plies, i.e. increasing the number of sites for the energy absorbing delaminations, inhibits the spread of damage within the composite[20].

Many features of the combined stress/impact test technique have not been considered here. In particular the report has not addressed in any detail: geometrical problems; the influence of the applied tensile load on the peak force recorded by the impactor; nor the variations of energy absorbed by the impactor under conditions of impact energy and applied stress beyond the critical conditions required for fracture, i.e. away from the fracture boundary of the impact fracture map. Further, in the impact maps presented here, the boundaries represent the transition between the condition of some residual strength and zero residual strength. In practice this may be too severe a criterion and a more conservative criterion may be more realistic: for example, a boundary denoting some design-acceptable value of residual strength such as 50% of the undamaged strength. These aspects will be considered in more detail in the report on in-house work on graphite-epoxy composites and other materials[20].

5. CONCLUSIONS

(1) Impact tests carried out on materials under superimposed tensile stresses enable impact maps to be constructed. Boundaries on these maps enable comparisons of the behaviour of a material under different operating conditions, and of the behaviour of different materials. Impact maps are therefore a useful way of comparing the toughness of composites and other materials.

(2) Cross-plied laminates, $(0°,90°)_{2S}$, of graphite fiber-borosilicate glass were superior to those of graphite fibre-LAS glass-ceramic at impact energies greater than approximately 2.5J but inferior below 2.5J, under total failure conditions. On an impact map this is shown by the fractured/unfractured boundaries of the two materials intersecting.

(3) These differences in behavior were reflected in differences in fracture morphology.

(4) At elevated temperatures, in the range 400°C to 650°C, the impact behavior of the borosilicate glass composite was considerably inferior to the room temperature behavior. This cannot be attributed entirely to softening of the matrix as the borosilicate glass does not soften until 580°C. Specimens impacted at elevated temperatures displayed much more delamination than after room temperature impacts.

(5) Under ballistic impact conditions the two ceramic composites exhibited rather similar fracture morphologies, while under the slower velocity conditions of a falling weight impact test more significant differences between the two materials were apparent.

(6) The impact behavior of the ceramic composites was inferior to that of graphite-epoxy composites.

(7) An estimate of the fiber-matrix bond strength of these materials is possible from measurements of matrix microcracking. Estimates of the fiber-matrix bond strength, measured values of work of fracture, and measured values of interlaminar shear strength, do not relate to each other in the way expected from simple theory.

This may imply that some further materials development is necessary to optimize these materials.

6. RECOMMENDATIONS

This work has demonstrated a useful practical approach to characterizing the toughness of composite materials. In a relatively short time a considerable amount of data and some new concepts have been generated. The techniques described here are sufficiently promising to require further work. In particular:

(1) Impact maps derived from impact tests carried out under superimposed tensile stress are a useful way of comparing the behaviour of different materials. The zero residual strength criterion employed in the current work may be too severe for many practical applications. An investigation of a less severe criterion should be carried out, for example, a residual strength of 50% of the undamaged strength.

(2) Further work is necessary to understand the effects of specimen geometry and end constraints in order to be able to extrapolate to practical situations, so that the technique can become more than a materials-comparison test.

(3) Graphite fiber reinforced glass and glass-ceramic systems are useful for modelling the behavior of higher temperature systems because they can be produced with different fiber-matrix bond strengths (τ_i). Further work is necessary to understand the relationship between τ_i, interlaminar shear strength and toughness-related properties.

(4) Impact maps should be derived for other, more practical, ceramic matrix composites such as SiC/LAS and compared with those of more conventional materials.

(5) Impact maps are useful too for polymer composites such as graphite-epoxy and should be derived for these systems.

(6) Further work is necessary to understand the micromechanics of damage development in ceramic matrix composites under impact. The slow fracture technique described in this report is a useful method of studying damage development.

(7) Further investigations of the effect of temperature on toughness-related properties are important for ceramic matrix composites.

REFERENCES

1. D.C. Phillips, 'Fibre reinforced ceramics,' Chapter 10 (pp. 373 to 428) of Handbook of Composite Materials, Vol. 4, Fabrication of Composites, Ed. A. Kelly and S.T. Mileiko, North Holland Publishing Co., (1983), and as AERE-R10056.

2. D.C. Phillips, 'Fibre reinforced ceramics (for high temperature technologies),' in Ceramic Composites for High Temperature Engineering Applications, Ed. R.W. Davidge, Published by the Commission of the European Communities, EUR 9565 EN, 1985.

3. R.A.J. Sambell, D.C. Phillips and D.H. Bowen, 'The technology of carbon fibre reinforced glasses and ceramics,' in Carbon Fibres, Their Place in Modern Technology, Proc. Int. Conf. 1974, (Plastics Institute, London), AERE-R7612, (1974).

4. D.C. Phillips, 'Interfacial bonding and the toughness of carbon fibre reinforced glasses and glass-ceramics,' J. Materials Science, 9, 1847-1854, (1974), and as AERE-R7594.

5. D.C. Phillips, R.A.J. Sambell and D.H. Bowen, 'The mechanical properties of carbon reinforced pyrex glass,' J. of Materials Science, 7, (1972), pp. 1454-1464.

6. D.C. Phillips and B. Harris, 'The strength, toughness and fatigue properties of polymeric composites,' Chapter 2, (pp. 47-156), of "Polymer Engineering Composites", Ed. by M.O.W. Richardson, Published by Applied Science Publishers Ltd., 1977.

7. R.W. Davidge and D.C. Phillips, 'The significance of impact data for brittle non-metallic materials,' J. of Materials Science, 7, (1972), pp. 1308-1314.

8. R.J. Lee and D.C. Phillips, 'The damage tolerance of high performance composites,' Pub. in "Composite Structures", Ed. I.H. Marshall, Applied Science Publishers, London, 1981, (Proceedings of the 1st International Conference on Composite Structures, Paisley, 1981), pp. 536-554.

9. R.J. Lee and D.C. Phillips, 'Fracture toughness testing of high performance laminates,' Presented at "Testing, Evaluation and Quality Control of Composites," Sept. 1983, Guildford, Surrey. (Organised Butterworth Scientific Ltd.). Published in Conference Proceedings.

10. D.C. Phillips, 'The fracture energy of carbon fibre reinforced glass,' J. of Materials Science, 7, (1972), 1175-1191; and as AERE-R6916.

11. D.C. Phillips, 'The fracture mechanics of carbon fibre laminates,' J. of Composite Materials, 8, (1974), pp. 130-141; and as AERE-R7443.

12. J.M. Scott and D.C. Phillips, 'Carbon fibre composites with rubber toughened matrices,' J. of Materials Science, 10, (1975), pp. 551-562, and as AERE-R7793.

13. D.C. Phillips and G.M. Wells, 'The stability of transverse cracks in fibre composites,' J. Materials Science Letters, 1, No. 8, Aug. 1982, and as AERE-R10482, March 1982.

14. See for example AGARD Conference Proceedings No. 355, Characterisation, analysis and significance of defects in composite materials, AGARD-CP-355, 1983.

15. B.R. Butcher, 'The dynamic notch toughness of fibre composites - Part 1,' Composites, January 1976, p. 12, AERE-R7801.

16. B.R. Butcher, 'The dynamic notch toughness of fibre composites - Part 2,' Composites, April 1976, p. 81, AERE-R7802.

17. B.R. Butcher, 'Impact resistance of unidirectional CFRP under tensile stress,' Fibre Sci. and Tech., (1979), p. 295, AERE-R8843.

18. B.R. Butcher and P.J. Fernback, 'Impact resistance of unidirectional CFRP under tensile stress: Further experimental variables,' Fibre Sci. and Tech., (1981), p. 41, AERE-R9576.

19. B. Harris, J. Morley and D.C. Phillips, 'Fracture mechanisms in glass reinforced plastics,' J. of Materials Science, 10, (1975), 2050-2061.

20. D.C. Phillips, N. Park, R.J. Lee and R. Davidson, 'The impact behaviour of composites under applied stress - The development of impact maps,' AERE-R12942, in preparation.

21. J.C. Carlisle, R.L. Crane, W.J. Jaques and L.T. Montulli, 'Impact damage effects on boron-aluminium composites,' Composite Reliability, ASTM STP 580, 1975, pp. 458-470.

22. J. Awerbuch and H.T. Hahn, 'Hard object impact damage of metal matrix composite,' Journal of Composite Materials, Vol. 10, July 1976, p 231-257.

23. S.M. Bishop and G. Dorey, 'The effect of damage on the tensile and compressive performance of carbon fibre laminates', AGARD-CP-355.

24. B.V. Sankar and C.T. Sun, 'Low velocity impact damage in graphite-epoxy laminates subjected to tensile initial stresses', AIAA Journal, Vol. 24, No. 3, 1986, p. 470-471.

25. S.P. Joshi and C.T. Sun, 'Impact induced fracture in a laminated composite', Journal of Composite Materials, Vol. 19, Jan. 1985, p. 51-66.

26. S.P. Joshi and C.T. Sun, 'Impact-induced fracture in a quasi-isotropic laminate,' Journal of Composite Technology and Research, Vol. 9, No. 2 1987, p. 40-46.

Table 1

Hot pressing optimization matrix for aligned graphite fiber/ borosilicate glass composite

Loading Temp. (°C)	Consolidation			Unloading Temp. (°C)	Density (g cm^{-3})	Mean Strength (MPa)	WoF* (kJm^{-2})
	Temp. °C	Pressure (MPa)	Time (min.)				
500	930	10	5	930		184	
930	930	10	5	930	1.90	213	1.2
500	1030	10	5	400	2.02	165	1.2
1030	1030	10	5	1030	1.95	186	1.4
930	930	10	5	930	1.96	410	10.1
935	935	10	7	935	1.75	234	
930	930	10	7	930			
1025	1025	10	7	1025	1.80	396	
930	930	10	7	930	1.90	540	
930	930	10	7	930		540	
1025	1025	10	7	1025	2.00	380	
850	850	10	7	850	2.05	752	
825	825	10	7	825	1.97	736	15
800	800	10	7	800	1.97	760	
775	775	10	7	775	1.86	650	
850	850	10	7	850	1.91	840	17
850	850	15	7	850	1.85	864	
850	850	5	7	850	1.86	813	
850	850	12	7	850	1.87	840	20
850	850	12	7	400	1.91	922	23
850	850	12	2	400	1.90	840	20
850	850	12	60	400	1.97	775	
850	850	12	15	400		786	
850	850	12	15	400	2.00	820	
850	850	12	7	400	2.01	894	22
850	850	12	7	400	2.00	902	24
850	850	12	7	400	1.99	889	23

* Work of fracture.

Table 2

Hot-pressing and ceraming optimization matrix for aligned graphite/lithium aluminosilicate composite

Consolidation			Ceraming			Unloading Temp. °C	Density g cm^{-3}	Mean Flexural Strength MPa	WoF* kJ m^{-2}
Temp. °C	Pressure MPa	Time Min.	Temp. °C	Pressure MPa	Time Min.				
800	12	1	-	-	-	400	2.0	340	4
900	12	1	Some ceraming			400	1.9	94	Delaminated
1000	12	7	-	-	-	Ceramed prior to consolidation - did not consolidate.			
1200	12	7	-	-	-	500	1.8	125	Delaminated
1250	12	7	-	-	-	500	2.1	685	~6
1275	12	7	-	-	-	500	2.0	770	8
1300	12	7	-	-	-	500	2.2	830	2.5
800	12	1	1200	12	10	400	2.0	404	6
850	12	1	1200	0	10	850	1.7	220	4
1275	12	7	-	-	-	500	2.1± 0.1	600± 100	8±2

* Work of fracture.

Table 3

Baseline properties for borosilicate glass and LAS glass-ceramic composites containing 40 volume % of unidirectional graphite fibers

Property	Borosilicate Glass	LAS Glass-Ceramic Matrix
Flexural Strength (MPa)	900	600
Shear Strength (MPa)	30	7
Work of Fracture ($kJ\ m^{-2}$)	20	8

Table 4

Variation of ILSS with temperature

Temp °C	b mm	d mm	P kg	τ MPa	Comments
530	4.75	3.61	53	22.7	
550	4.70	3.56	39	17.2	
560	4.75	3.54	37	16.0	
560	3.41	3.41	50	21.6	
570	4.95	3.43	48	20.8	
580	4.74	3.53	35	15.4	
580	4.92	3.51	-	-	Plastic (viscous) flow
590	4.83	3.63	-	-	Plastic (viscous) flow

Table 5

Data from instrumented impact tests on the LAS glass-ceramic composite

Specimen Number	Width (mm)	Thickness (mm)	C.S.A.[1] (mm^2)	Applied Load (kN)	Applied Stress (MPa)	Impact Energy[2] (J)	Impact Velocity (ms^{-1})	Maximum Force[3] (N)	Total Energy[4] (J)	Comments
LAS1-04	24.73	1.72	42.54	0.43	10.0	2	1.601	345	2.00	
LAS1-05	24.69	1.68	41.48	0.83	20.0	2	1.601	355	2.00	
LAS5-28	24.51	1.70	41.67	0.83	20.0	2	1.601	365	2.00	
LAS6-31	24.78	1.62	40.14	1.00	25.0	2	1.601	435	2.00	
LAS6-32	24.42	1.72	42.00	1.16	27.5	2	1.601	400	2.00	
LAS1-06	24.76	1.71	42.34	1.27	30.0	2	1.601	370	2.00	
LAS6-33	24.77	1.70	42.11	1.26	30.0	2	1.601	405	2.00	
LAS7-34	24.84	1.64	40.74	1.43	35.0	2	1.601	400	2.00	
LAS7-35	24.74	1.49	36.86	1.47	40.0	2	1.601	390	2.00	
LAS7-36	24.79	1.68	41.65	1.87	45.0	2	1.601	395	2.00	
LAS7-37	24.84	1.60	39.74	1.89	47.5	2	1.601	230	-	Fractured
LAS7-39	24.78	1.63	40.39	0.61	15.0	3	1.961	330	3.00	
LAS7-38	24.65	1.54	37.96	0.66	17.5	3	1.961	295	-	Fractured
LAS3-13	24.62	1.87	46.04	0.00	0.0	4	2.265	620	4.00	
LAS3-16	24.61	2.23	54.88	0.00	0.0	4	2.265	715	4.00	
LAS3-18	24.85	2.30	57.16	0.29	5.0	4	2.265	690	4.00	
LAS4-20	24.72	2.34	57.84	0.43	7.5	4	2.265	905	-	Fractured
LAS1-02	24.71	1.38	34.10	0.34	10.0	4	2.265	250	1.33	Fractured
LAS3-14	24.82	1.91	47.41	0.47	10.0	4	2.265	475	1.63	Fractured
LAS1-01	24.38	1.46	35.59	0.71	20.0	4	2.265	400	-	Fractured
LAS4-21	24.75	2.18	53.96	0.00	0.0	5	2.532	650	5.00	
LAS5-29	24.78	2.00	49.56	0.12	2.5	5	2.532	620	5.00	

(1) C.S.A. = Cross-sectional area.
(2) Initial potential energy of impactor.
(3) Maximum force recorded by the instrumented tup.
(4) Total energy recorded during the impact by the instrumented tup.

Table 6

Data from instrumented impact tests on the borosilicate glass composite

Specimen Number	Width (mm)	Thickness (mm)	C.S.A.[1] (mm^2)	Applied Load (kN)	Applied Stress (MPa)	Impact Energy[2] (J)	Impact Velocity (ms^{-1})	Maximum Force[3] (N)	Total Energy[4] (J)	Comments
BOR5-25	24.80	2.40	59.52	2.38	40.0	1	1.132	505	1.00	
BOR5-27	24.65	2.43	59.90	3.59	60.0	1	1.132	630	1.00	
BOR5-30	24.82	2.40	59.57	3.87	65.0	1	1.132	470	-	Fractured (Just!)
BOR5-29	24.85	2.43	60.39	4.23	70.0	1	1.132	695	0.79	Fractured
BOR5-28	24.87	2.36	58.69	4.70	80.0	1	1.132	480	0.36	Fractured
BOR4-19	24.80	2.60	64.48	1.61	25.0	2	1.601	325	2.00	
BOR4-21	24.70	2.72	67.18	1.85	27.5	2	1.601	425	2.00	
BOR4-20	24.79	2.64	65.45	1.96	30.0	2	1.601	350	-	Fractured
BOR4-22	24.87	2.53	62.92	2.20	35.0	2	1.601	300	0.53	Fractured
BOR3-17	24.51	2.50	61.62	1.23	20.0	4	2.265	540	4.00	
BOR3-18	24.78	2.46	60.96	1.37	22.5	4	2.265	360	-	Fractured
BOR2-12	24.82	2.31	57.33	0.86	15.0	6	2.774	575	6.00	
BOR3-15	24.50	2.48	60.76	1.06	17.5	6	2.774	380	3.48	Fractured
BOR3-16	24.73	2.50	61.83	1.08	17.5	6	2.774	255	1.63	Fractured
BOR3-14	24.72	2.35	58.09	1.16	20.0	6	2.774	400	1.40	Fractured
BOR2-07	24.87	2.18	54.22	0.00	0.0	8	3.203	560	8.00	
BOR2-09	24.86	2.13	52.95	0.53	10.0	8	3.203	600	8.00	
BOR2-11	24.82	2.33	57.83	0.72	12.5	8	3.203	480	-	Fractured
BOR8-46	24.80	2.07	51.34	0.64	12.5	8	3.203	600	-	Fractured
BOR2-10	24.86	2.38	59.17	0.89	15.0	8	3.203	615	-	Fractured
BOR4-23	24.63	2.70	66.50	0.00	0.0	9	3.397	400	-	Fractured
BOR12-65	24.67	2.48	61.18	1.53	25.0	2	1.601	925	2.00	
BOR12-64	24.52	2.45	60.07	1.80	30.0	2	1.601	450	2.00	
BOR11-61	24.63	2.22	54.68	0.82	15.0	6	2.774	465	6.00	
BOR11-62	24.64	2.24	55.19	1.10	20.0	6	2.774	620	6.00	
BOR11-63	24.45	2.21	54.03	1.35	25.0	6	2.774	360	-	Fractured
BOR12-66	24.64	2.47	60.86	0.76	12.5	8	3.203	650	8.00	

(1) C.S.A. = Cross-sectional area.
(2) Initial potential energy of impactor.
(3) Maximum force recorded by the instrumented tup.
(4) Total energy recorded during the impact by the instrumented tup.

Table 7

Mechanical properties and microstructural details of unidirectional composites made from two different types of carbon fiber in borosilicate glass[a] and lithium aluminosilicate glass-ceramic[b] taken from References 1 and 4

Material	Microstructural details (V_o)				Mean Strength (MPa)		Mean Work of Fracture (kJ/m^2)
	Volume of Fiber V_f	Volume of Matrix V_m	Volume of Open Porosity V_{op}	Volume of Closed Porosity V_{cp}	Bend Strength	Interlaminar Shear Strength	
Borosilicate glass and high modulus fiber	45.9	52.4	0.6	1.1	459	59	3.1
Borosilicate glass and high strength fiber	48.9	46.0	0.3	4.9	575	71	3.6
Glass-ceramic and high modulus fiber	49.5	41.6	7.3	1.6	588	32	4.5
Glass-ceramic and high strength fiber	45.7	40.7	4.7	9.0	574	26	10.3

(a) Borosilicate glass: $\Delta T = 500°C$, $\alpha = 3.5 \times 10^{-6} °C^{-1}$.

(b) Glass-ceramic: $\Delta T = 1000°C$, $\alpha = 2.0 \times 10^{-6} °C^{-1}$.

Table 8

Estimated fiber-matrix bond strengths and related properties of the borosilicate glass and LAS glass-ceramic systems. The values were obtained from measurements at room temperature on composites containing 40 volume % of unidirectional fibers

	Work of Fracture ($kJ\ m^{-2}$)	Interlaminar Shear Strength (MPa)	Fibre-matrix Bond Strength (MPa)
Borosilicate glass composite	20	30	5
LAS glass-ceramic composite	8	7	25

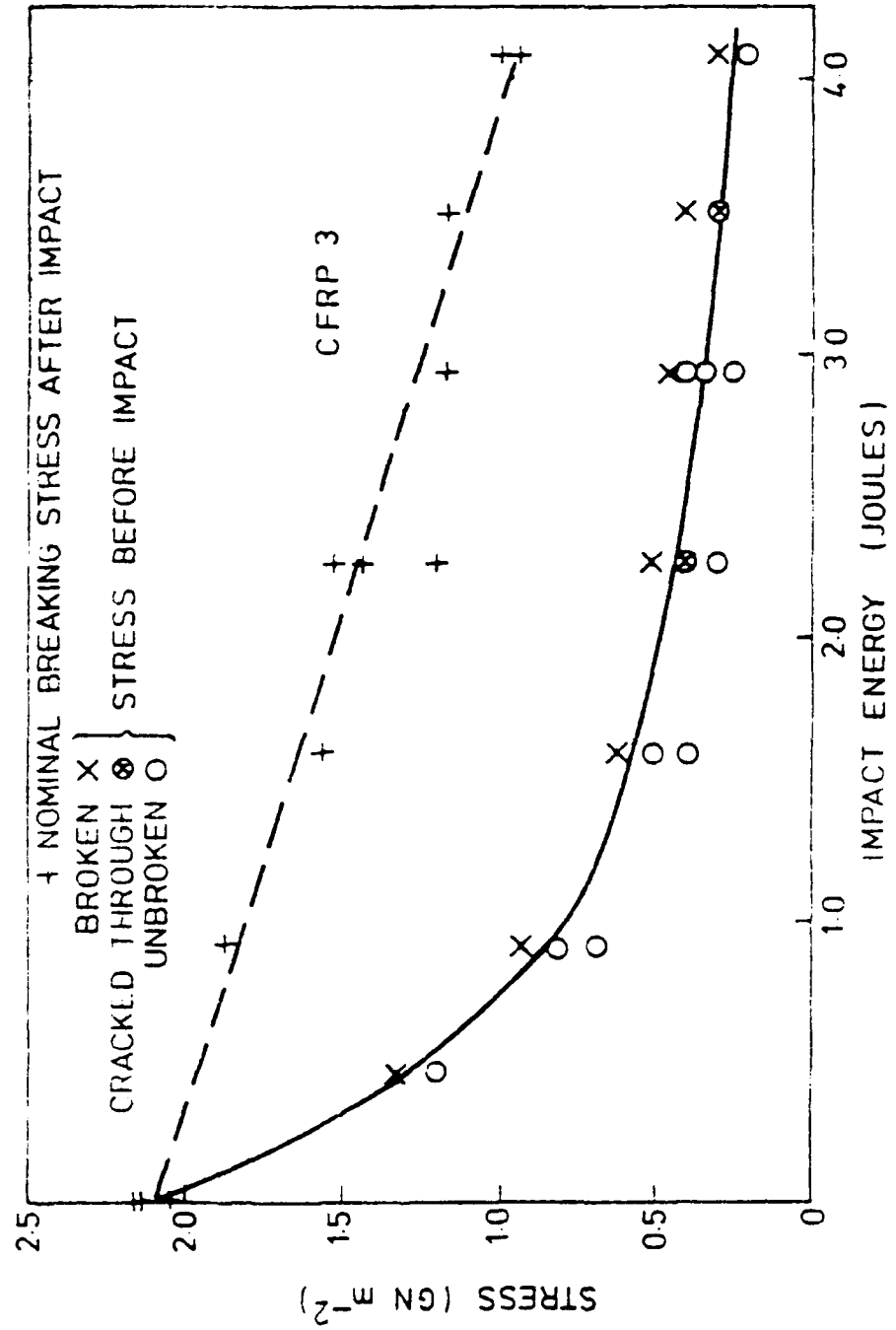

FIGURE 1. Results of static and dynamic tests on a CFRP.

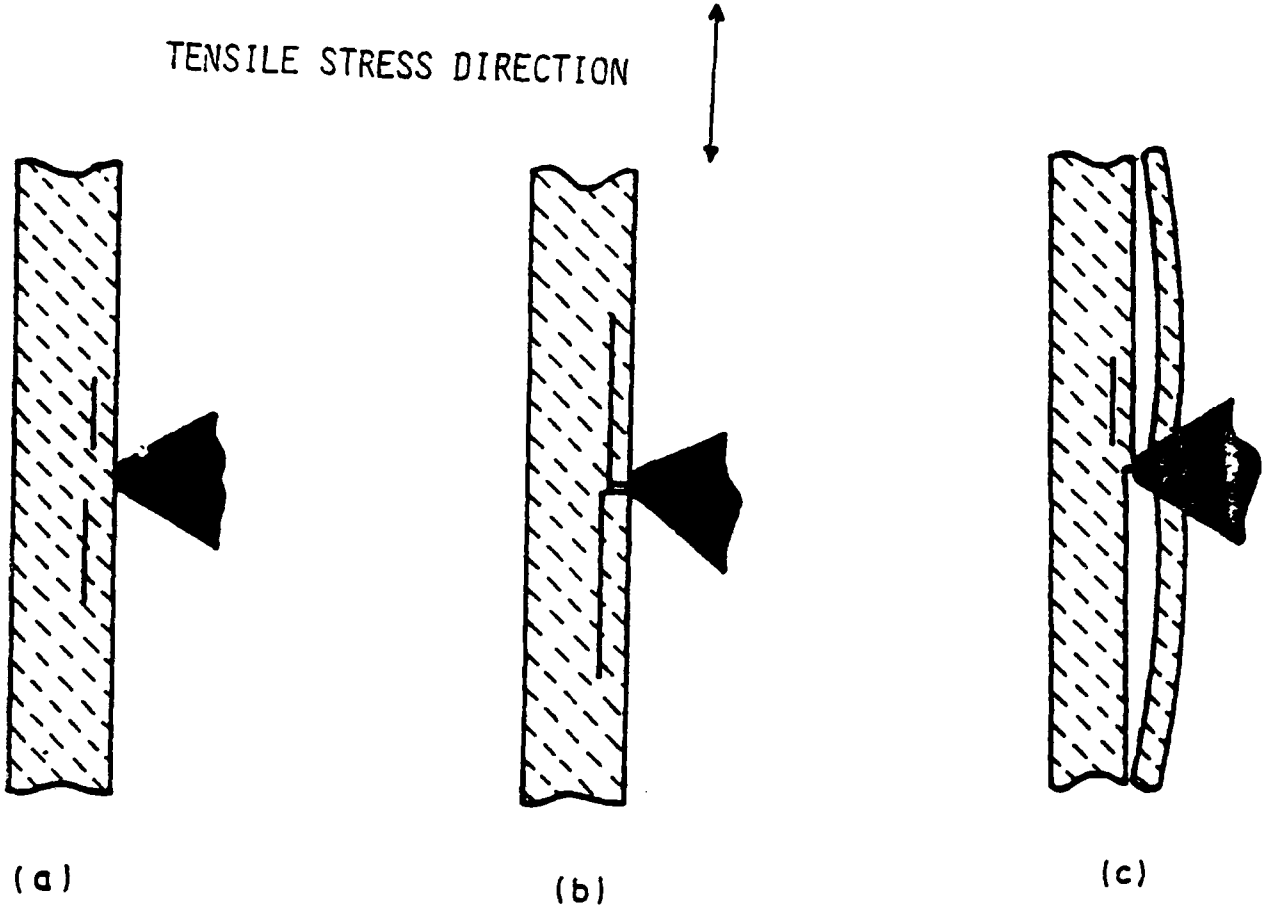

FIGURE 2. Sequence of cracking in a CFRP under combined axial tensile loading and transverse impact loading.

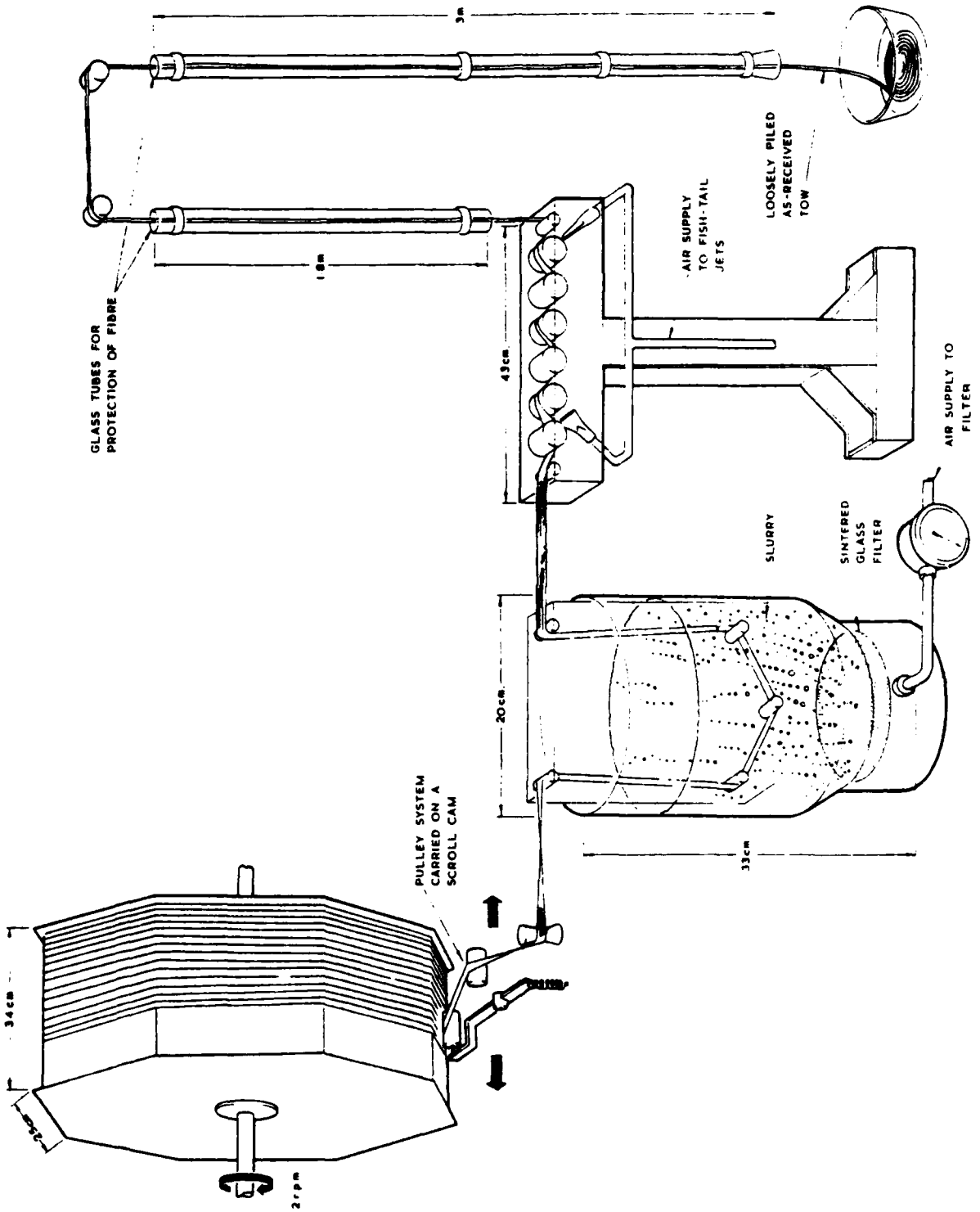

FIGURE 3. Fibre impregnation and tape winding equipment.

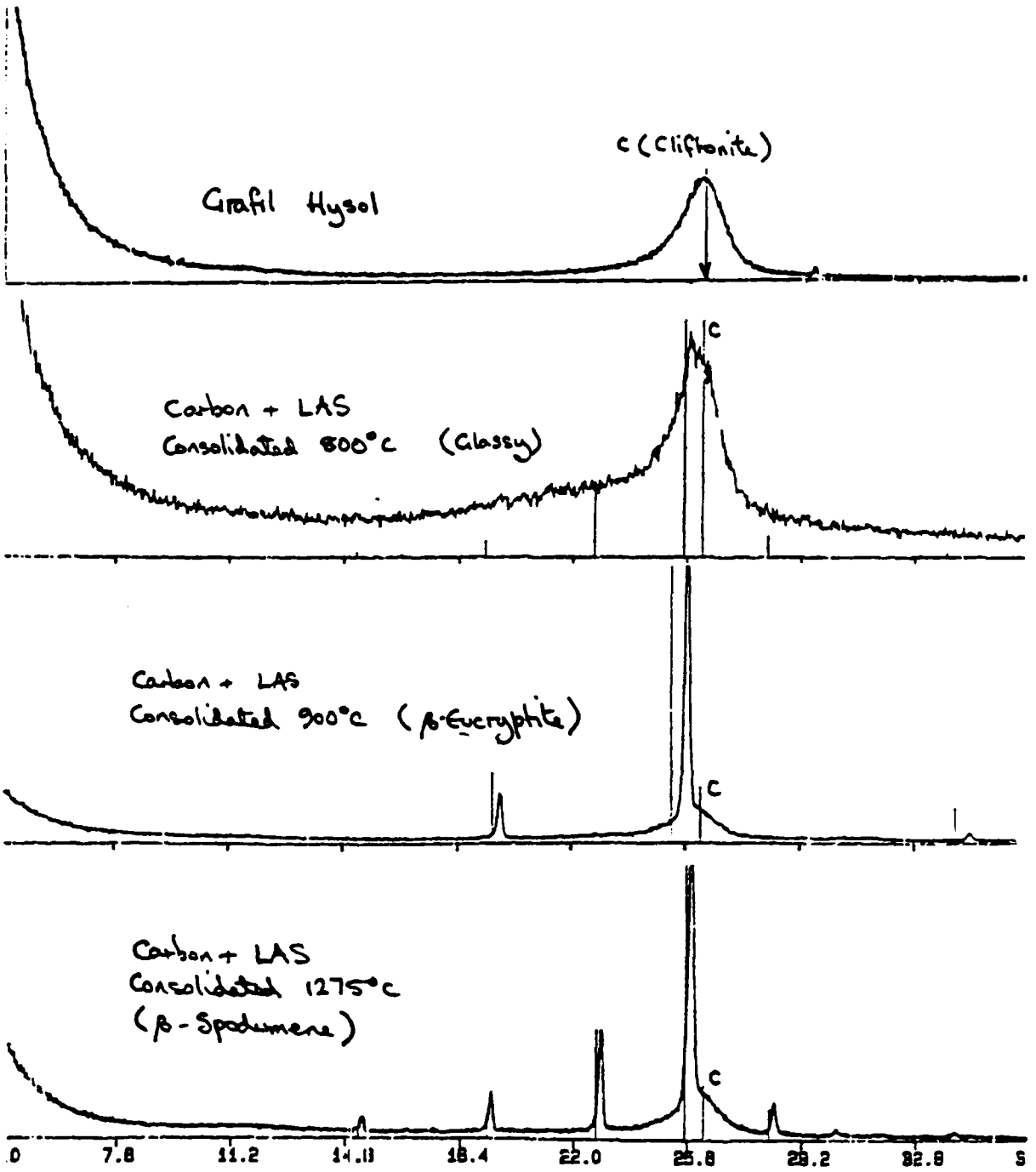

FIGURE 4. X-ray diffraction spectra of graphite/LAS composites as a function of consolidation/ceraming temperature.

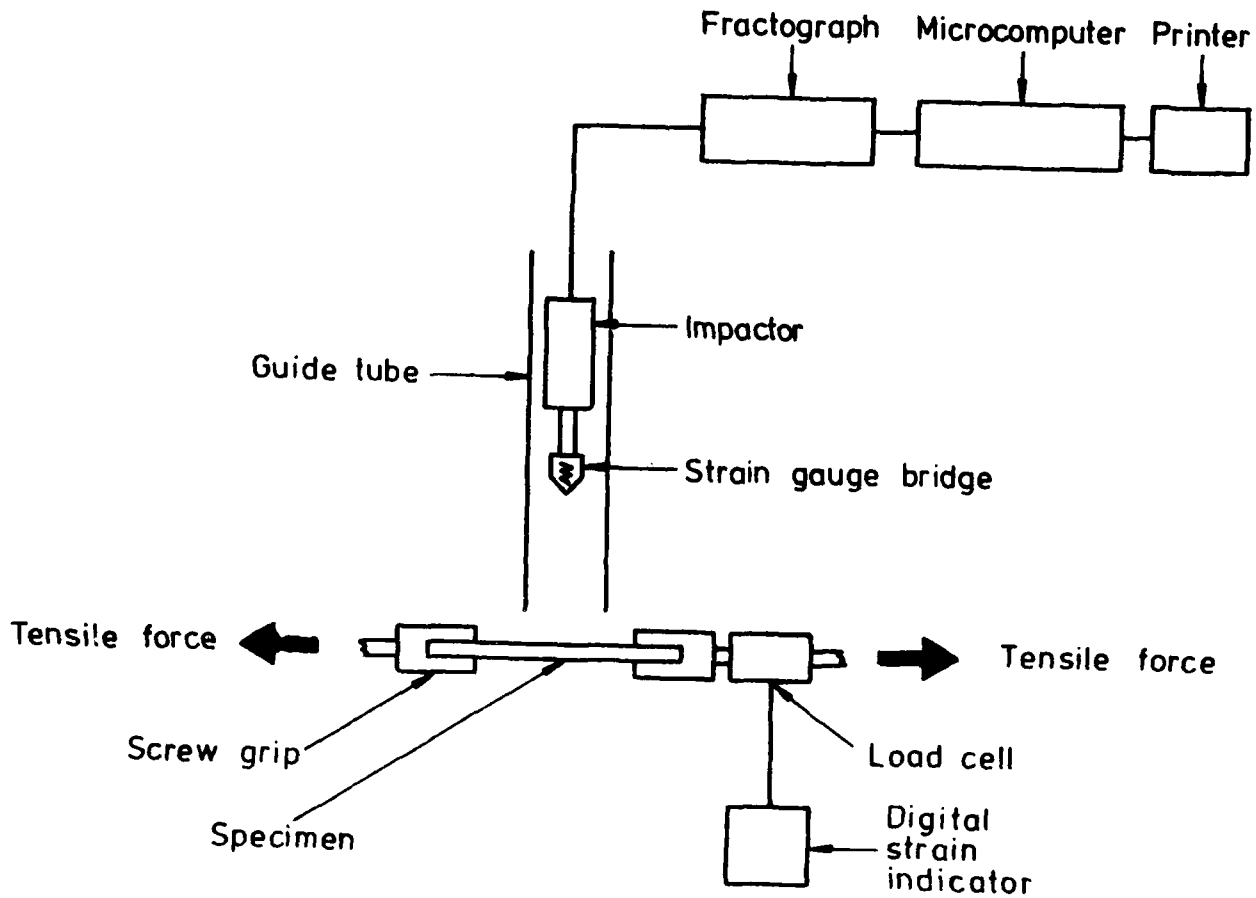

FIGURE 5. Schematic diagram of the impact equipment.

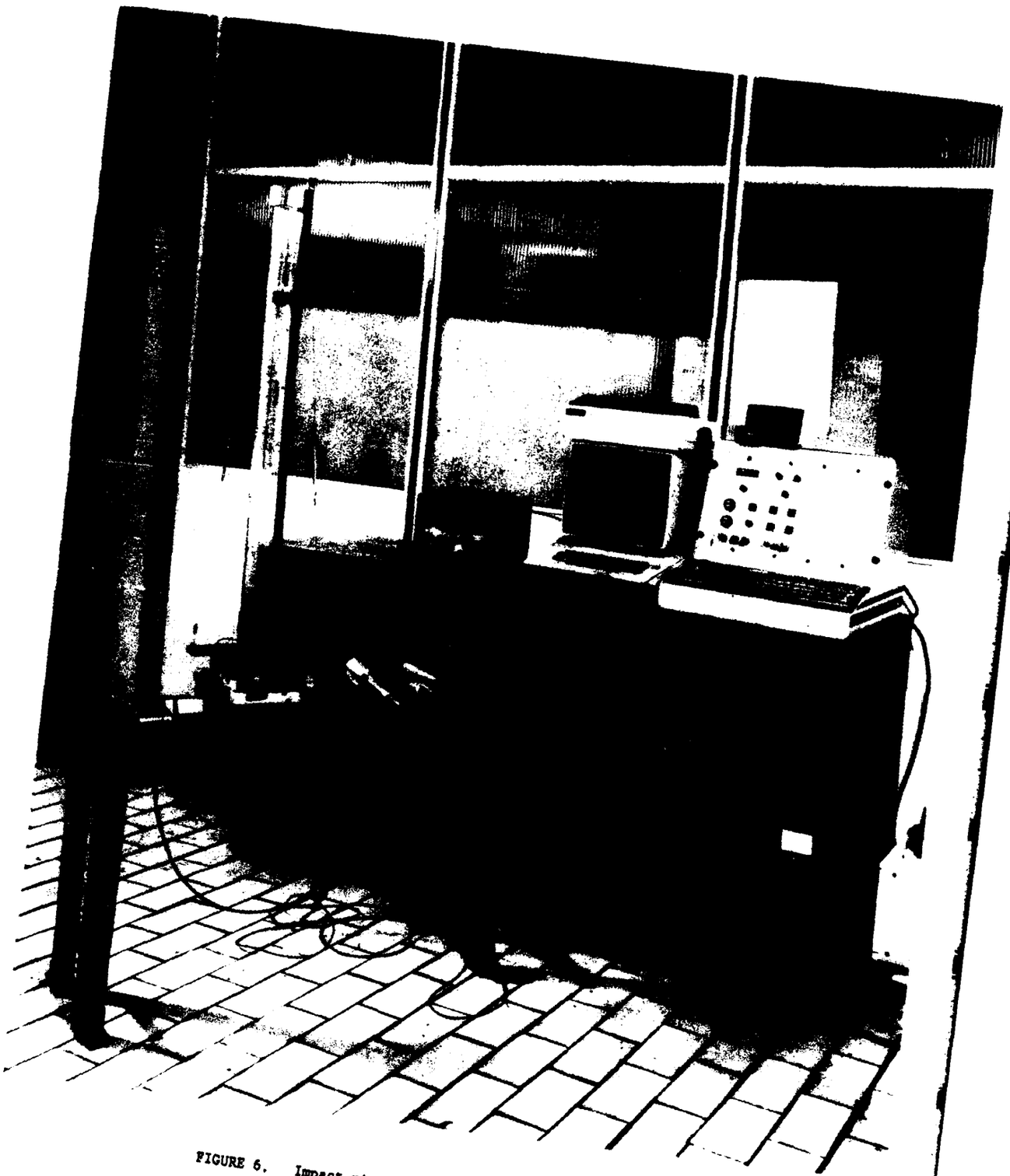

FIGURE 6. Impact rig and associated electronic hardware.

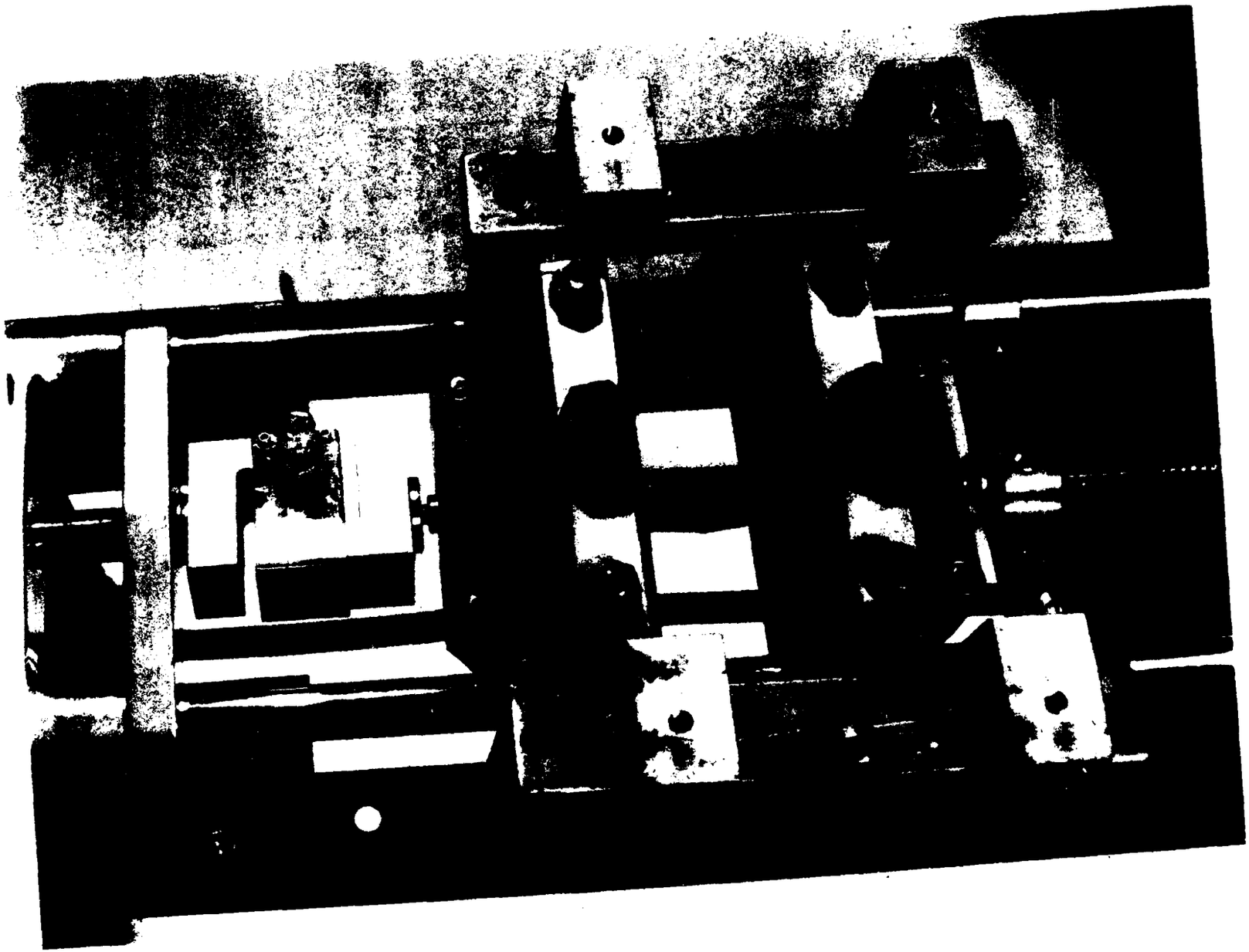

FIGURE 7. Specimen configuration in the tensometer grips.

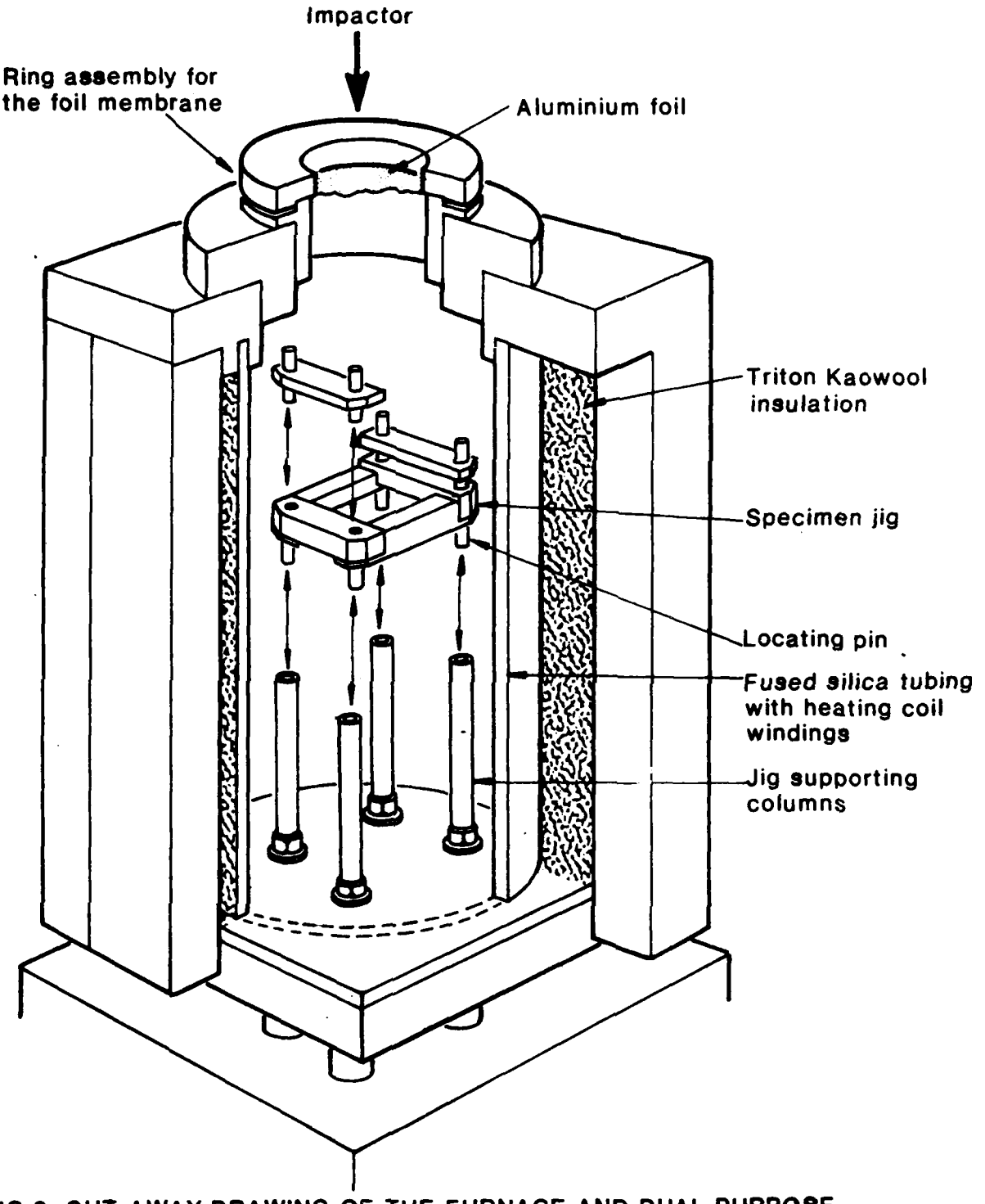

FIG.8. CUT-AWAY DRAWING OF THE FURNACE AND DUAL PURPOSE SPECIMEN JIG USED IN THE VARIOUS IMPACT EXPERIMENTS

FIBER MATERIAL	GRAFIL H. M. CARBON
MATRIX MATERIAL	BOROSILICATE GLASS
MATERIAL LAY-UP	(0,90,0,90)s
IMPACTOR TYPE	6 mm CONICAL IMPACTING TUP
IMPACTOR MASS	1.56 kg
SPECIMEN SPAN	50 mm

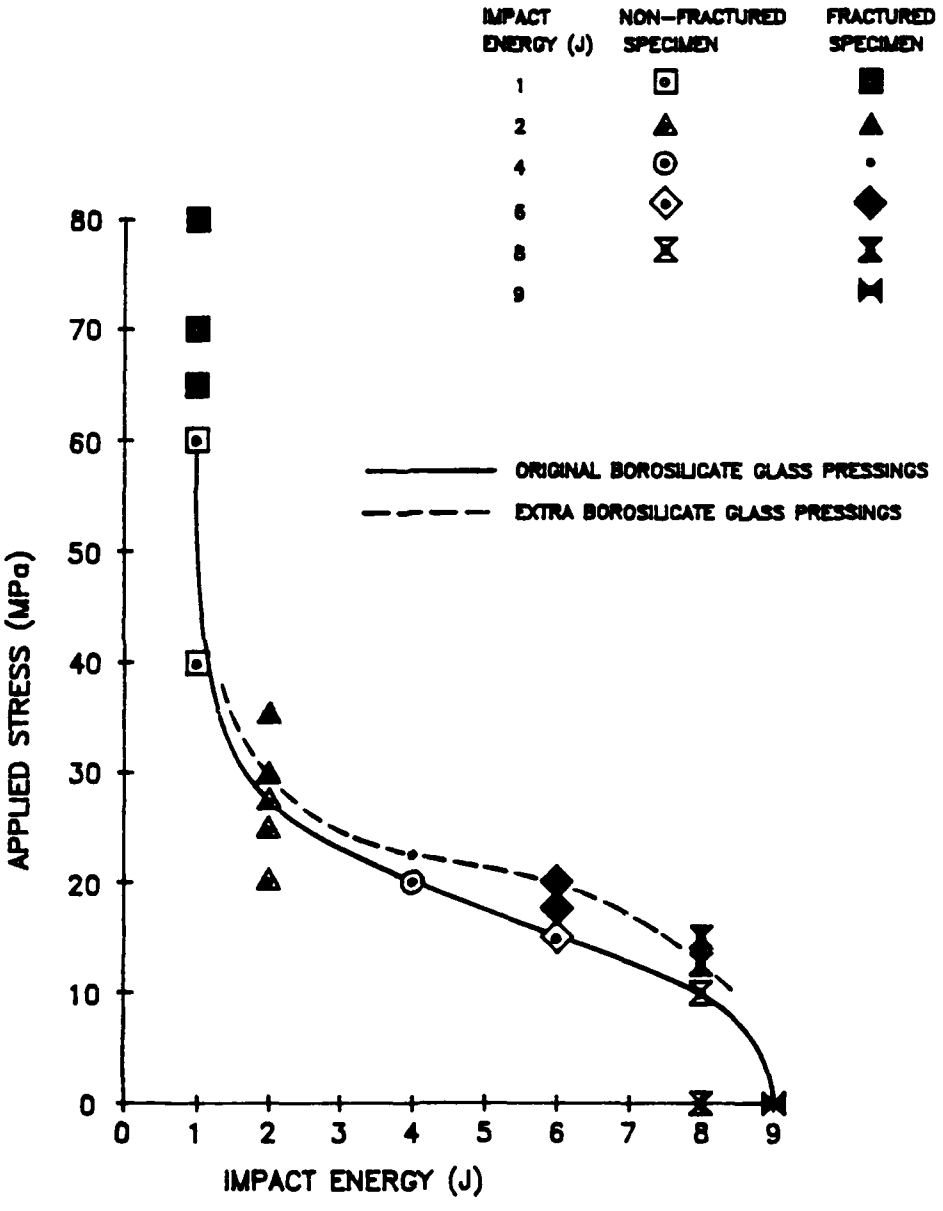

FIGURE 9. Variation of the FRACTURE/NO FRACTURE boundary over a range of impact energies and applied stresses for the borosilicate glass composite.

FIBER MATERIAL	GRAFIL H. M. CARBON
MATRIX MATERIAL	LAS GLASS–CERAMIC
MATERIAL LAY–UP	$(0,90,0,90)_S$
IMPACTOR TYPE	6 mm CONICAL IMPACTING TUP
IMPACTOR MASS	1.56 kg
SPECIMEN SPAN	50 mm

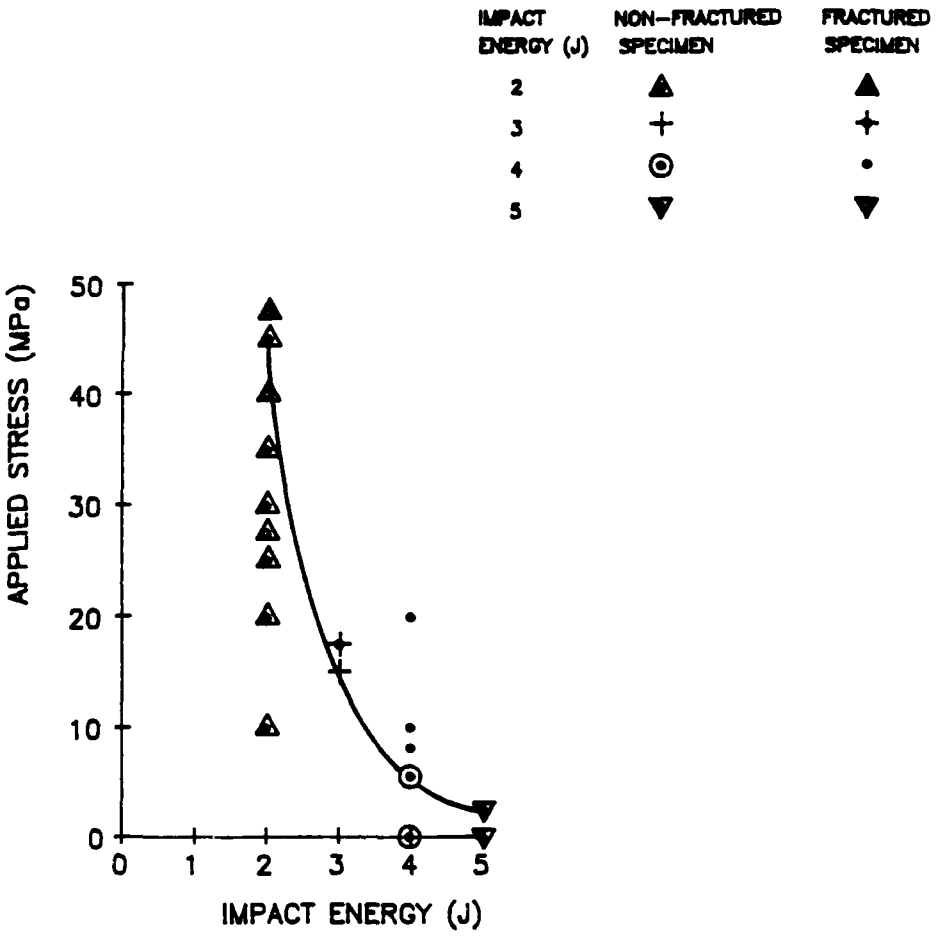

FIGURE 10. Variation of the FRACTURE/NO FRACTURE boundary over a range of impact energies and applied stresses for the LAS glass–ceramic matrix composite.

SPECIMEN NUMBER LAS1-05

MATERIAL : FIBER Grafil Carbon Fiber
MATRIX Lithium Alumina Silicate Glass-ceramic
LAY-UP (0,90,0,90)s

IMPACTOR TYPE :- 6 mm Conical Tup		Impact Energy	= 2.00 J
Mass of Impactor	= 1.56 kg	Drop Height	= 0.13 m
		Impact Velocity	= 1.60 m/s
Specimen Span	= 50.00 mm	Applied Stress	= 20.00 MPa
Specimen Width	= 24.69 mm	Max. Recorded Force	= 355.00 N
Specimen Thickness	= 1.68 mm	Max. Recorded Energy	= 2.00 J

POST IMPACT CONDITION :-

1. Specimen has not fractured.
2. An impact crater is present on the top surface. No other visible damage on the top surface, ie there is no visible cracking parallel to fiber direction in top 0' ply. Some delamination is visible along one edge.
3. Material push-through beneath the point of impact has resulted in the spallation of a localized region of delaminated material on the bottom 0' ply. This is roughly square in shape, with cracking parallel and perpendicular to the fibers traversing and surrounding this delaminated region.

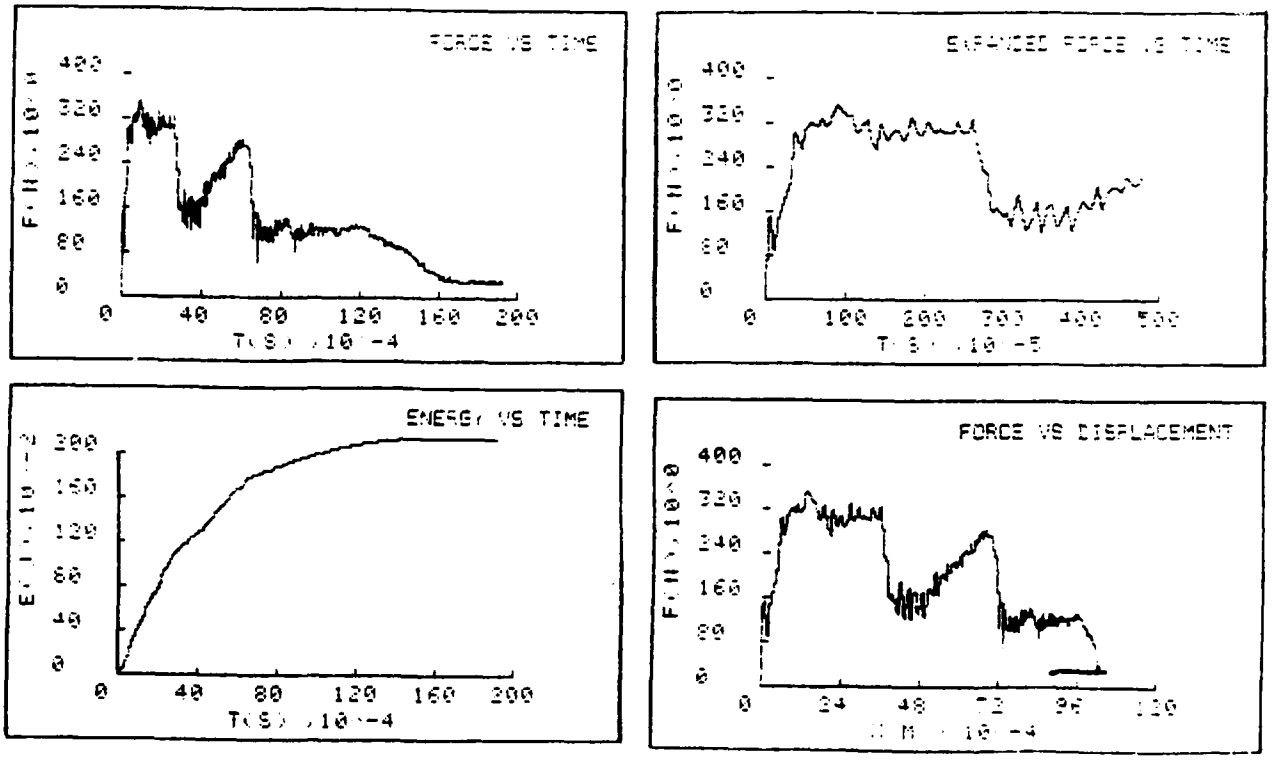

FIGURE 11. Impact data obtained for the LAS glass-ceramic specimen LAS1-05.

SPECIMEN NUMBER LAS7-34

MATERIAL : FIBER Grafil Carbon Fiber
MATRIX Lithium Alumina Silicate Glass-ceramic
LAY-UP (0,90,0,90)s

IMPACTOR TYPE :- 6 mm Conical Tup		Impact Energy	= 2.00 J
Mass of Impactor	= 1.56 kg	Drop Height	= 0.13 m
		Impact Velocity	= 1.60 m/s
Specimen Span	= 50.00 mm	Applied Stress	= 35.00 MPa
Specimen Width	= 24.84 mm	Max. Recorded Force	= 400.00 N
Specimen Thickness	= 1.64 mm	Max. Recorded Energy	= 2.00 J

POST IMPACT CONDITION :-
1. Specimen has not fractured.
2. A smaller impact crater than in LAS1-05 is present. There is limited splitting parallel to fibers in the top 0' ply on one side of the impact mark.
3. No delamination visible at edges.
4. Material push-through beneath the point of impact has resulted in the spallation of a localized region of delaminated material on the bottom 0' ply. This is roughly square in shape.

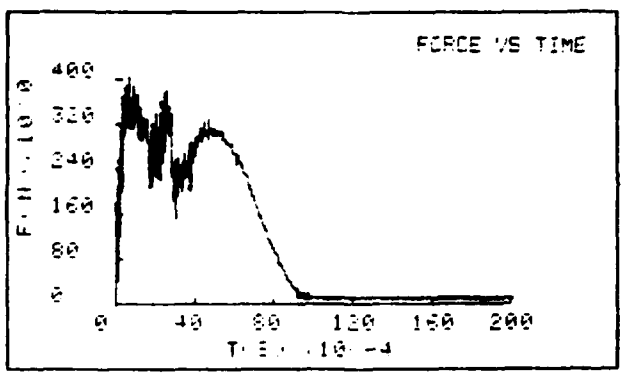

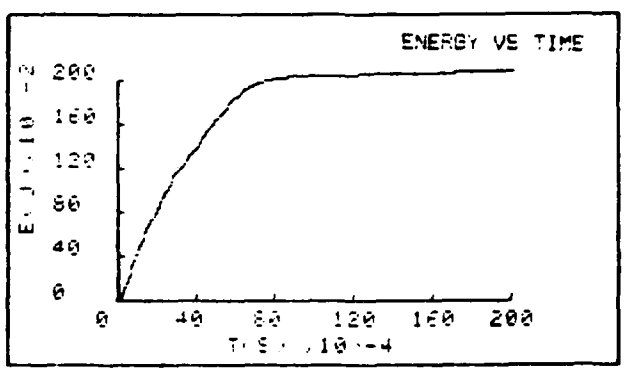

FIGURE 12. Impact data obtained for the LAS glass-ceramic specimen LAS7-34.

INSTRUMENTED IMPACT TESTING OF STRESSED COMPOSITES

MATERIALS : FIBRE — GRAFIL HIGH MODULUS CARBON
MATRIX — LAS GLASS–CERAMIC
LAY–UP — (0,90,0,90)s

TESTING CONDITIONS : BUILT–IN ENDS
6mm CONICAL IMPACTING TUP
WEIGHT OF IMPACTOR = 1.56kg
SPECIMEN SPAN = 50mm
IMPACT ENERGY = 2J
IMPACT VELOCITY = 1.601m/s

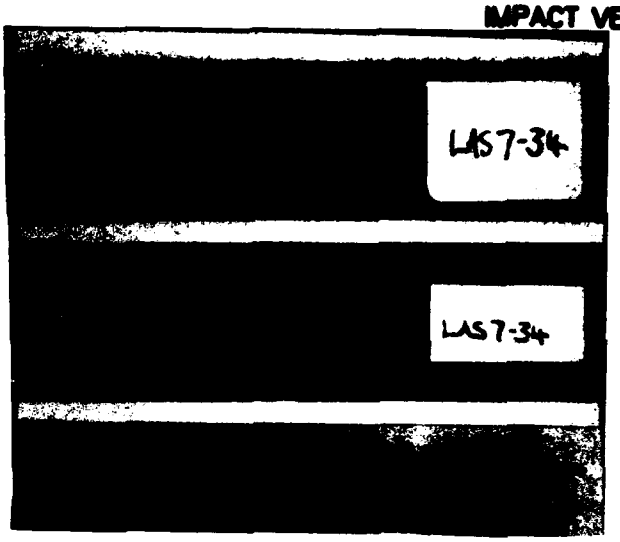

APPLIED STRESS = 35.0MPa
SPECIMEN NUMBER : LAS7–34

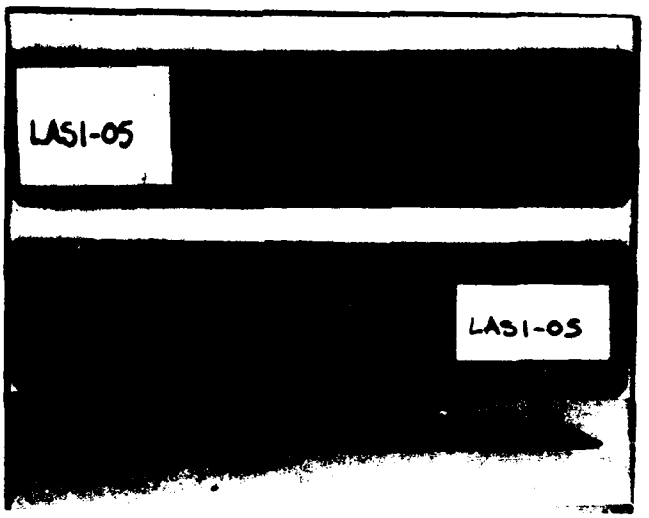

APPLIED STRESS = 20.0MPa
SPECIMEN NUMBER : LAS1–05

0mm 50mm

FIGURE 13. Damage sustained by the LAS glass-ceramic composite specimens LAS7-34 and LAS1-05 during an impact.

SPECIMEN NUMBER LAS7-36

MATERIAL : FIBER Grafil Carbon Fiber
MATRIX Lithium Alumina Silicate Glass-ceramic
LAY-UP (0,90,0,90)s

IMPACTOR TYPE :- 6 mm Conical Tup		Impact Energy	= 2.00 J
Mass of Impactor	= 1.56 kg	Drop Height	= 0.13 m
		Impact Velocity	= 1.60 m/s
Specimen Span	= 50.00 mm	Applied Stress	= 45.00 MPa
Specimen Width	= 24.79 mm	Max. Recorded Force	= 395.00 N
Specimen Thickness	= 1.68 mm	Max. Recorded Energy	= 2.00 J

POST IMPACT CONDITION :-

1. Specimen has not fractured.
2. Impact mark is very shallow. Splitting parallel to 0' fibers in the top ply is present. A perpendicular crack meandering from the impact point has reached one of the edges and almost to the other.
3. There is no visible delamination along the edges. A through thickness crack is present at the edge at which the meandering perpendicular cracks on the top and bottom 0' plies meet.
4. There is less material push-through than is typical encountered with the lower stressed material. This has resulted in a localized delaminated region. The meandering perpendicular crack on the bottom 0' ply crosses about 7/8ths the specimen width.

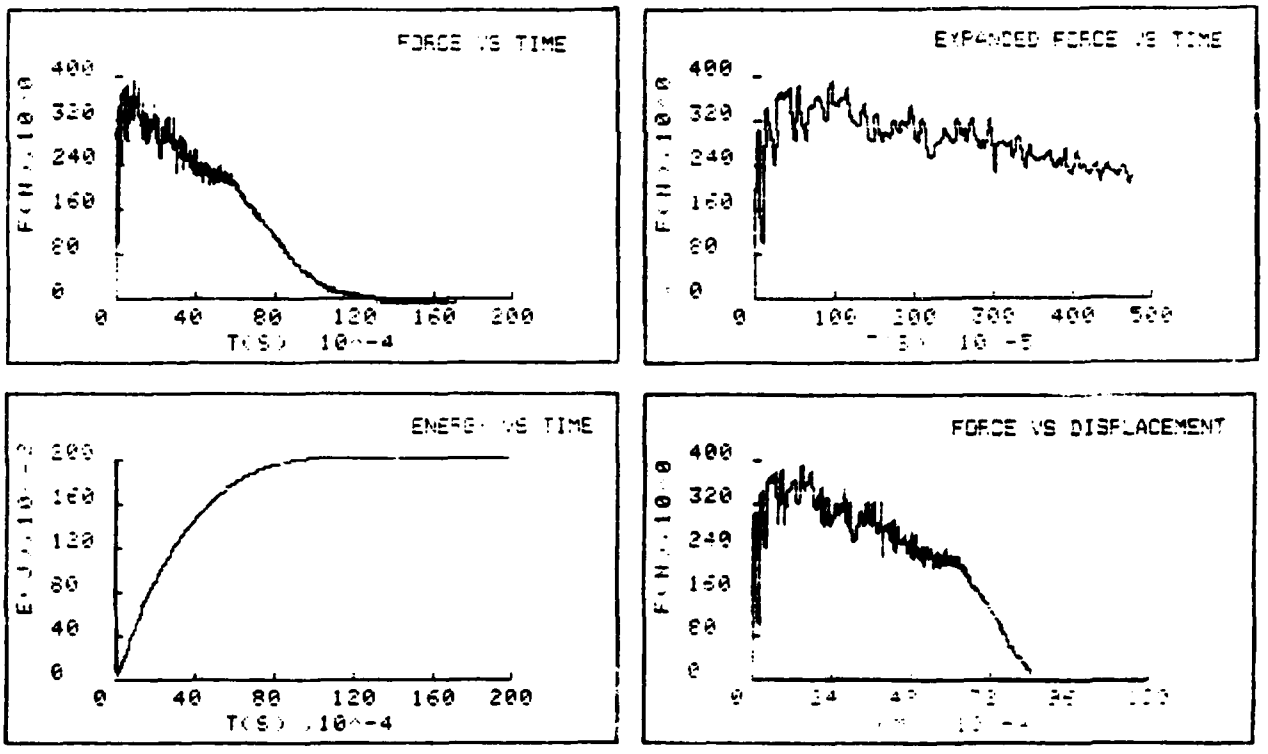

FIGURE 14. Impact data obtained for the LAS glass-ceramic specimen LAS7-36.

SPECIMEN NUMBER LAS7-37

MATERIAL : FIBER Grafil Carbon Fiber
MATRIX Lithium Alumina Silicate Glass-ceramic
LAY-UP (0,90,0,90)s

IMPACTOR TYPE :- 6 mm Conical Tup			Impact Energy	=	2.00 J
Mass of Impactor	=	1.56 kg	Drop Height	=	0.13 m
			Impact Velocity	=	1.60 m/s
Specimen Span	=	50.00 mm	Applied Stress	=	47.50 MPa
Specimen Width	=	24.84 mm	Max. Recorded Force	=	230.00 N
Specimen Thickness	=	1.60 mm	Max. Recorded Energy	=	-- J

POST IMPACT CONDITION :-

1. Specimen has fractured.
2. The impact mark is small. Little or no splitting parallel to the fibers is visible the top and bottom 0° plies.
3. Very little fiber pull-out can be seen along the fracture face. Little delamination is present in this specimen.
4. No obvious impactor penetration and as a consequence there is very little material push-through.
5. Material fracture has occurred at the mid-span of the specimen and near to one of the span ends.

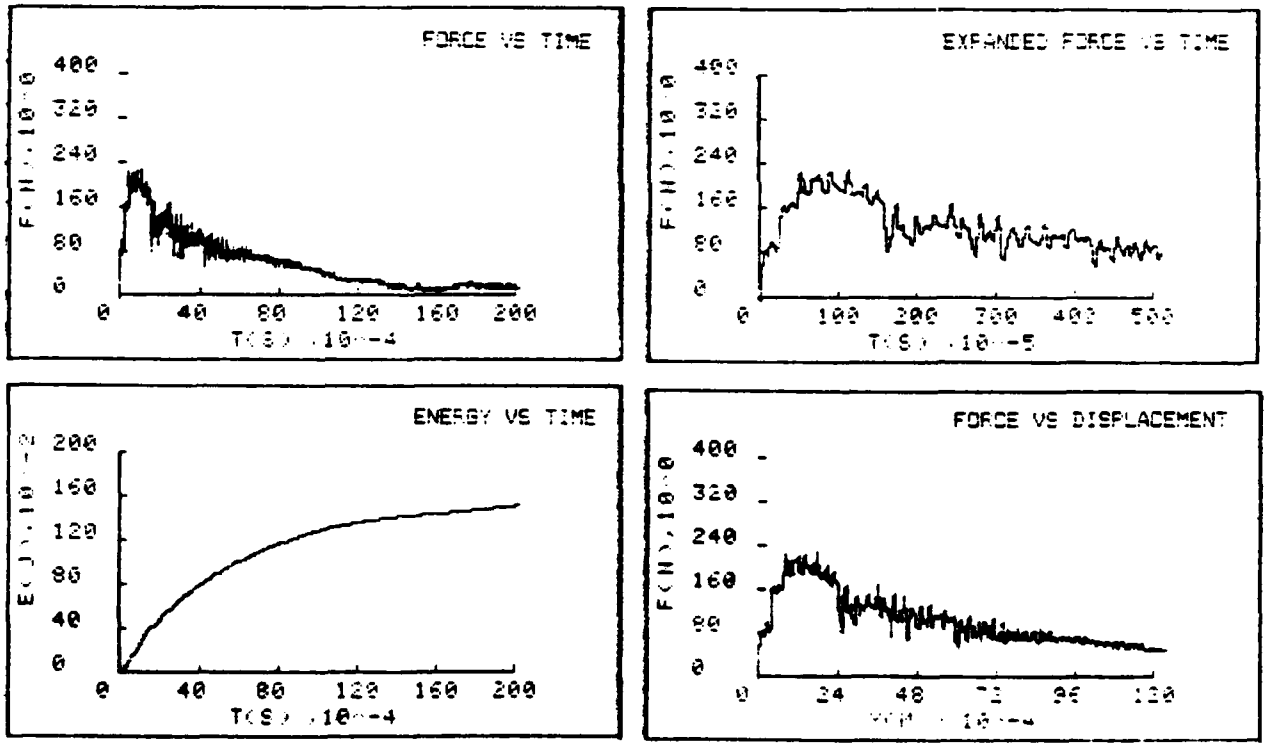

FIGURE 15. Impact data obtained for the LAS glass-ceramic specimen LAS7-37.

INSTRUMENTED IMPACT TESTING OF STRESSED COMPOSITES

MATERIALS : FIBRE — GRAFIL HIGH MODULUS CARBON
MATRIX — LAS GLASS–CERAMIC
LAY–UP — (0,90,0,90)s

TESTING CONDITIONS : BUILT–IN ENDS
6mm CONICAL IMPACTING TUP
WEIGHT OF IMPACTOR = 1.56kg
SPECIMEN SPAN = 50mm
IMPACT ENERGY = 2J
IMPACT VELOCITY = 1.601m/s

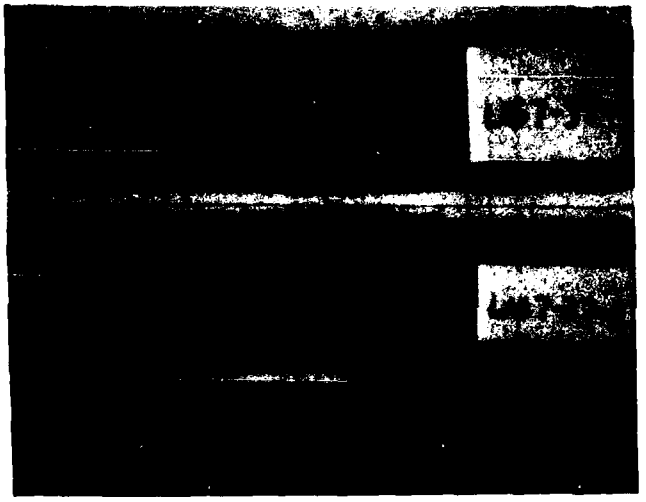

APPLIED STRESS = 47.5MPa
SPECIMEN NUMBER : LAS7–37

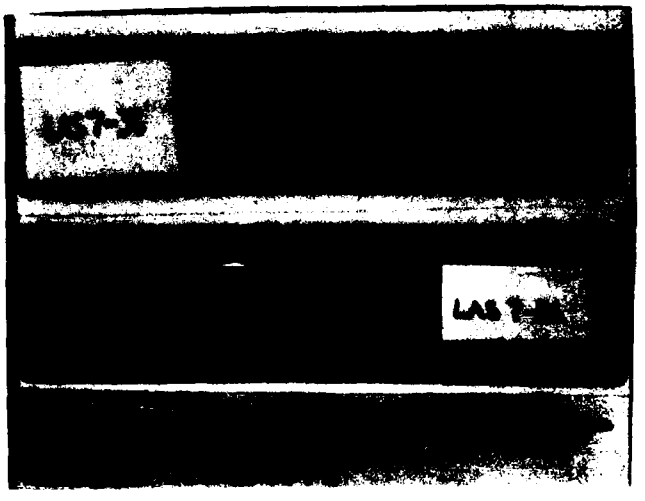

APPLIED STRESS = 45.0MPa
SPECIMEN NUMBER : LAS7–36

0mm 50mm

FIGURE 16. Damage sustained by the LAS glass-ceramic composite specimens LAS7-37 and LAS7-36 during an impact.

SPECIMEN NUMBER LAS3-16

MATERIAL : FIBER Grafil Carbon Fiber
MATRIX Lithium Alumina Silicate Glass-ceramic
LAY-UP (0,90,0,90)s

IMPACTOR TYPE :- 6 mm Conical Tup		Impact Energy	= 4.00 J
Mass of Impactor	= 1.56 kg	Drop Height	= 0.26 m
		Impact Velocity	= 2.26 m/s
Specimen Span	= 50.00 mm	Applied Stress	= 0.00 MPa
Specimen Width	= 24.61 mm	Max. Recorded Force	= 715.00 N
Specimen Thickness	= 2.23 mm	Max. Recorded Energy	= 3.00 J

POST IMPACT CONDITION :-
1. Specimen has not fractured.
2. An impact crater is present on the top surface. There is little other visible damage on the top surface.
3. Material push-through beneath the point of impact has resulted in the spallation of a localized region of delaminated material on the bottom 0° ply. This is area is roughly square in shape.

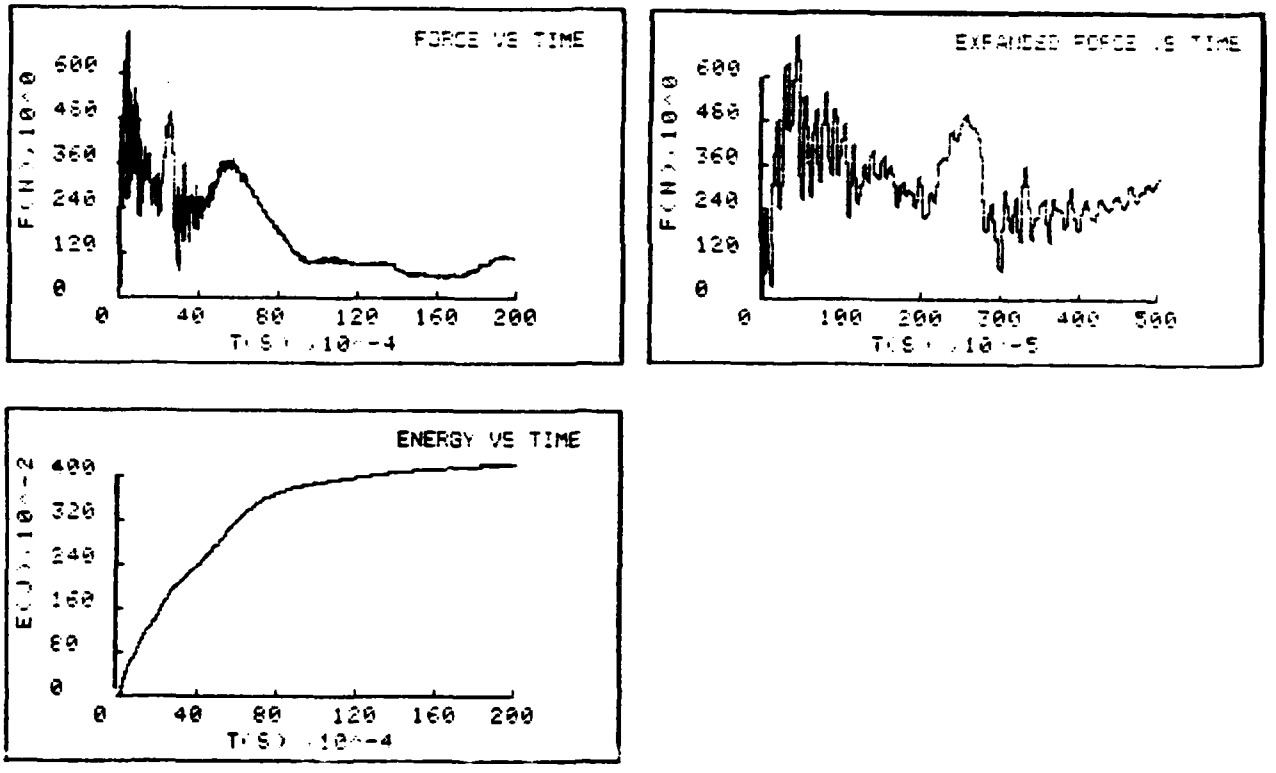

FIGURE 17. Impact data obtained for the LAS glass-ceramic specimen LAS3-16.

SPECIMEN NUMBER LAS3-18

MATERIAL : FIBER Grafil Carbon Fiber
MATRIX Lithium Alumina Silicate Glass-ceramic
LAY-UP (0,90,0,90)s

IMPACTOR TYPE :- 6 mm Conical Tup		Impact Energy	= 4.00 J
Mass of Impactor	= 1.56 kg	Drop Height	= 0.26 m
		Impact Velocity	= 2.26 m/s
Specimen Span	= 50.00 mm	Applied Stress	= 5.00 MPa
Specimen Width	= 24.85 mm	Max. Recorded Force	= 690.00 N
Specimen Thickness	= 2.30 mm	Max. Recorded Energy	= 4.00J

POST IMPACT CONDITION :-

1. Specimen has not fractured.
2. Even though there is relatively little tup penetration (similar to that in LAS3-16), the impact has resulted in the spallation of a plate-like region from the under surface (again similar in size to that formed in specimen LAS3-16).
3. There is no visible cracking on the top surface or delamination along the specimen edges.

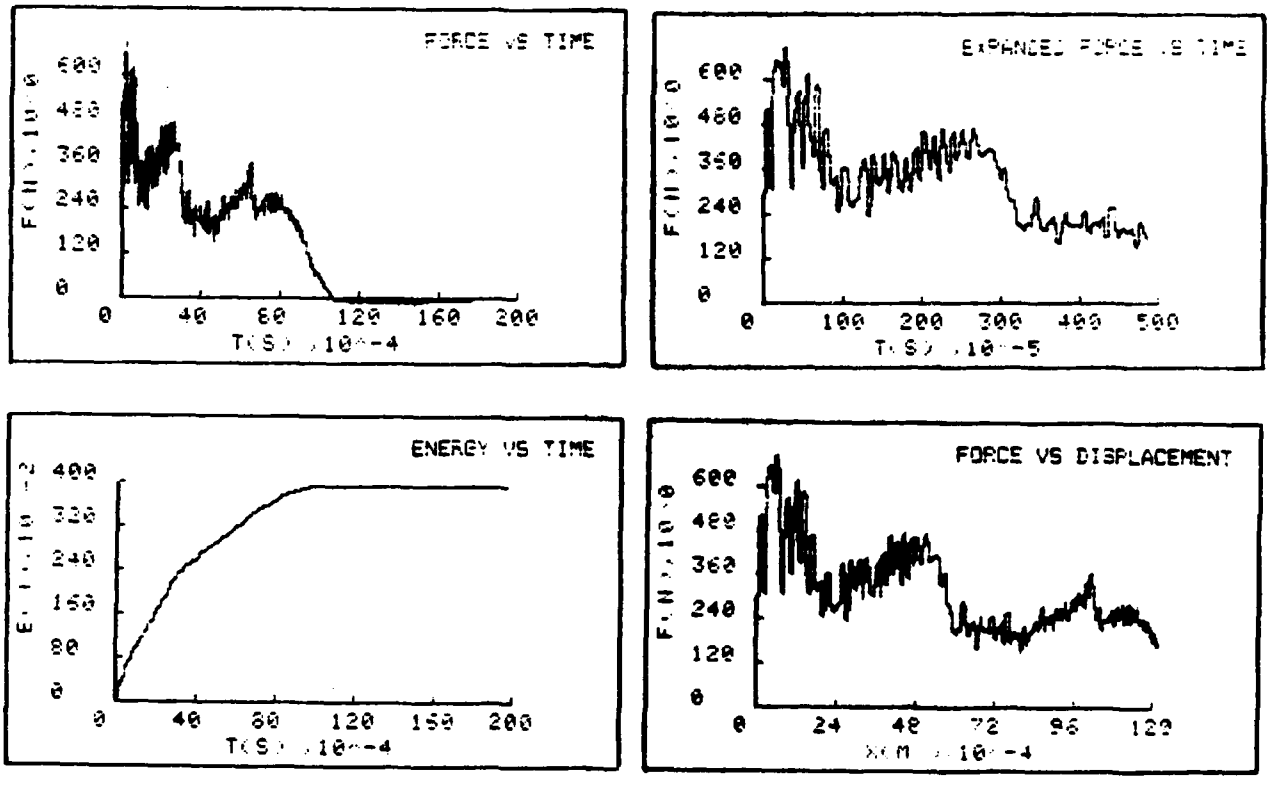

FIGURE 18. Impact data obtained for the LAS glass-ceramic specimen LAS3-18.

INSTRUMENTED IMPACT TESTING OF STRESSED COMPOSITES

MATERIALS : FIBRE — GRAFIL HIGH MODULUS CARBON
MATRIX — LAS GLASS–CERAMIC
LAY–UP — (0,90,0,90)s

TESTING CONDITIONS : BUILT–IN ENDS
6mm CONICAL IMPACTING TUP
WEIGHT OF IMPACTOR = 1.56kg
SPECIMEN SPAN = 50mm
IMPACT ENERGY = 4J
IMPACT VELOCITY = 2.265m/s

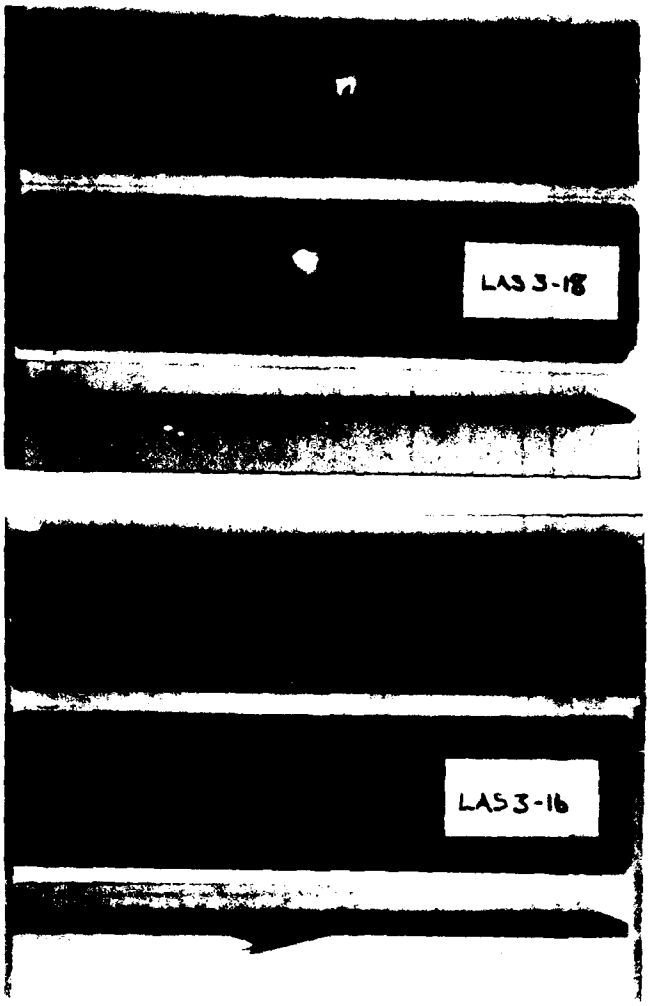

FIGURE 19. Damage sustained by the LAS glass-ceramic composite specimens LAS3-18 and LAS3-16 during an impact.

SPECIMEN NUMBER LAS4-20

MATERIAL : FIBER Grafil Carbon Fiber
MATRIX Lithium Alumina Silicate Glass-Ceramic
LAY-UP (0,90,0,90)s

IMPACTOR TYPE :- 6 mm Conical Tup			Impact Energy	=	4.00 J
Mass of Impactor	=	1.56 kg	Drop Height	=	0.26 m
			Impact Velocity	=	2.26 m/s
Specimen Span	=	50.00 mm	Applied Stress	=	7.50 MPa
Specimen Width	=	24.72 mm	Max. Recorded Force	=	905.00 N
Specimen Thickness	=	2.34 mm	Max. Recorded Energy	=	4.00 J

POST IMPACT CONDITION :-

1. Specimen has fractured.
2. More delamination is to be seen in this specimen than in LAS1-02.
3. Fiber pull-out is limited, although long "fingers" of fibers are present due to cracking parallel to the fibers on the top and bottom surfaces and local delamination at the adjacent interfaces.
4. No obvious impactor penetration, and as a consequence there is very little material push-through.
5. Material fracture has occurred at the mid-span of the specimen and near to one of the span ends.

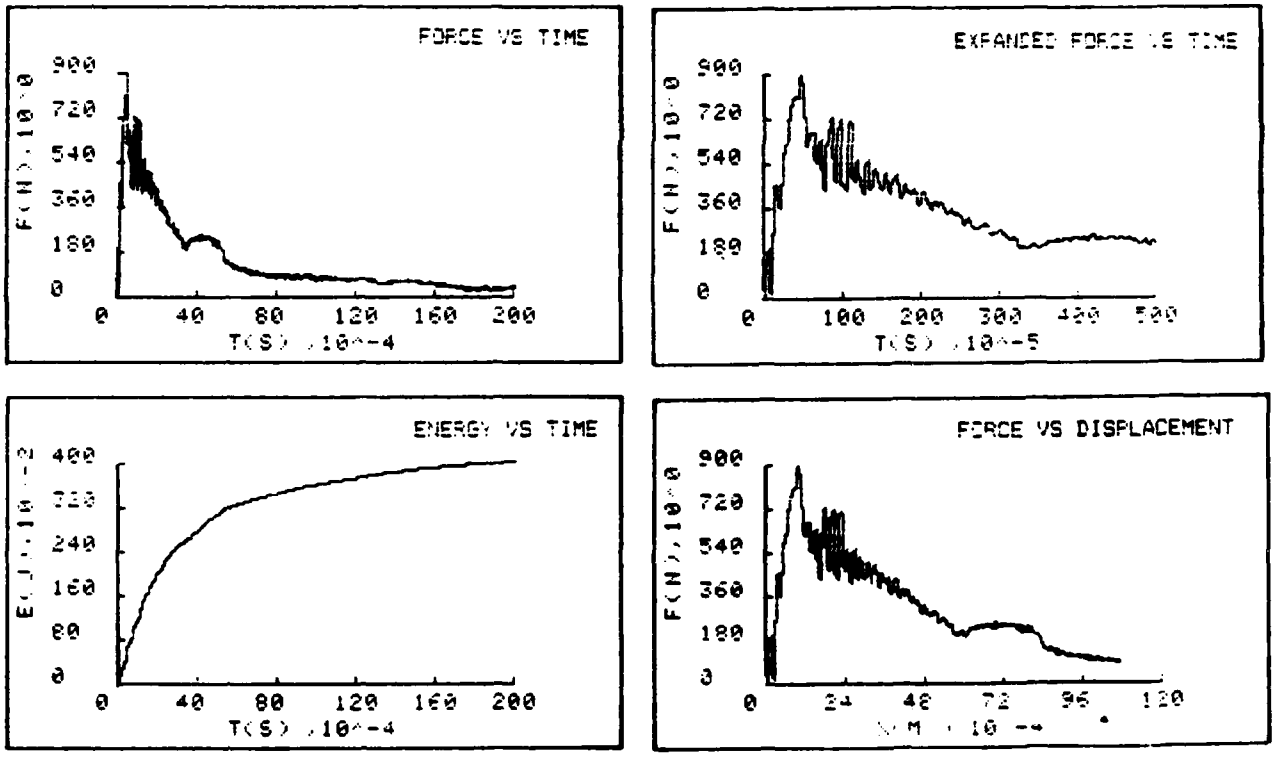

FIGURE 20. Impact data obtained for the LAS glass-ceramic specimen LAS4-20.

SPECIMEN NUMBER LAS1-02

MATERIAL : FIBER Grafil Carbon Fiber
MATRIX Lithium Alumina Silicate Glass-Ceramic
LAY-UP (0,90,0,90)s

IMPACTOR TYPE :- 6 mm Conical Tup		Impact Energy	= 4.00 J
Mass of Impactor	= 1.56 kg	Drop Height	= 0.26 m
		Impact Velocity	= 2.26 m/s
Specimen Span	= 50.00 mm	Applied Stress	= 10.00 MPa
Specimen Width	= 24.71 mm	Max. Recorded Force	= 250.00 N
Specimen Thickness	= 1.38 mm	Max. Recorded Energy	= 1.33 J

POST IMPACT CONDITION :-

1. Specimen has fractured.
2. Very little delamination is to be seen in this specimen.
3. Some cracking/splitting parallel to the 0' fibers on the top and bottom layers.
4. No obvious impactor penetration and as a consequence there is very little material push-through.
5. Material fracture has occurred at the mid-span of the specimen and near to one of the span ends.

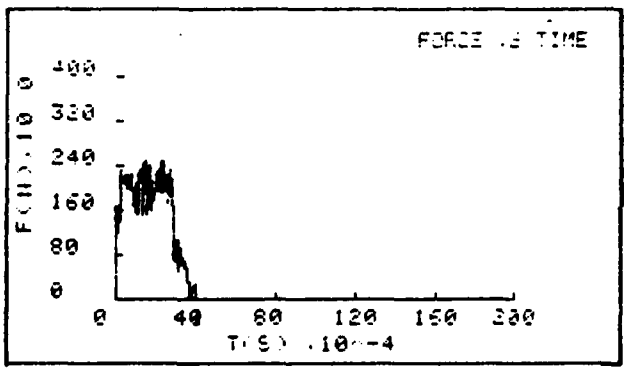

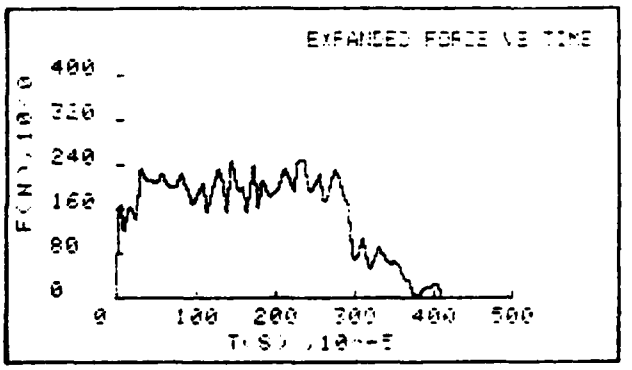

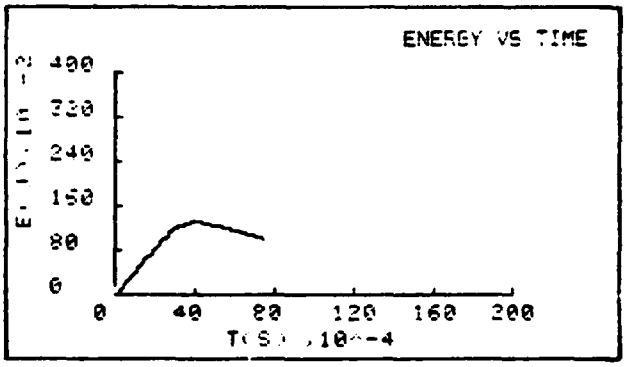

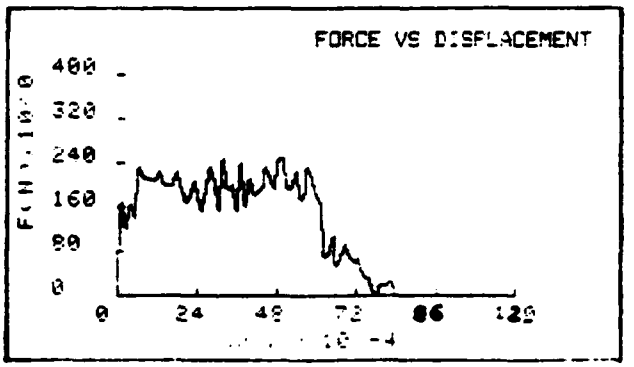

FIGURE 21. Impact data obtained for the LAS glass-ceramic speicmen LAS1-02.

INSTRUMENTED IMPACT TESTING OF STRESSED COMPOSITES

MATERIALS :	FIBRE	GRAFIL HIGH MODULUS CARBON
	MATRIX	LAS GLASS–CERAMIC
	LAY–UP	(0,90,0,90)s
TESTING CONDITIONS :		BUILT–IN ENDS
		6mm CONICAL IMPACTING TUP
		WEIGHT OF IMPACTOR = 1.56kg
		SPECIMEN SPAN = 50mm
		IMPACT ENERGY = 4J
		IMPACT VELOCITY = 2.265m/s

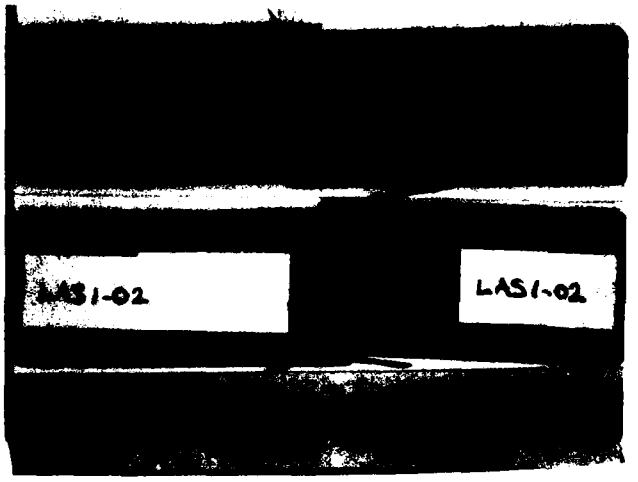

APPLIED STRESS = 10.0MPa
SPECIMEN NUMBER : LAS1–02

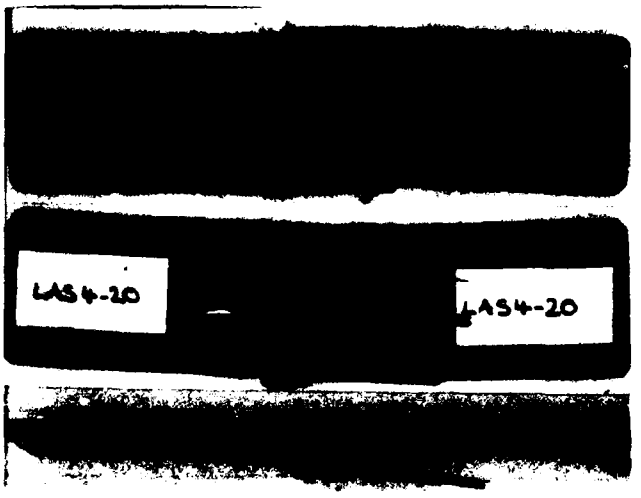

APPLIED STRESS = 7.5MPa
SPECIMEN NUMBER : LAS4–20

0mm 50mm

FIGURE 22. Damage sustained by the LAS glass-ceramic composite specimens LAS1-02 and LAS4-20 during an impact.

SPECIMEN NUMBER BOR5-25
==========

MATERIAL : FIBER Grafil Carbon Fiber
MATRIX Borosilicate Glass
LAY-UP (0,90,0,90)s

IMPACTOR TYPE :- 6 mm Conical Tup			Impact Energy	=	1.00 J
Mass of Impactor	=	1.56 kg	Drop Height	=	0.07 m
			Impact Velocity	=	1.13 m/s
Specimen Span	=	50.00 mm	Applied Stress	=	40.00 MPa
Specimen Width	=	24.80 mm	Max. Recorded Force	=	505.00 N
Specimen Thickness	=	2.40 mm	Max. Recorded Energy	=	1.00 J

POST IMPACT CONDITION :-
1. Specimen has not fractured.
2. Small indentation mark on top surface with some splitting between the fibers either side of the impact point.
3. No delamination is visible along the edges.
4. Slight bulge on the under face indicating internal delamination, and again some splitting between the 0° plies.

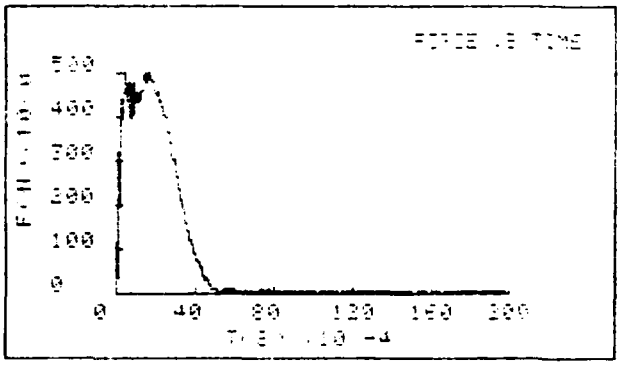

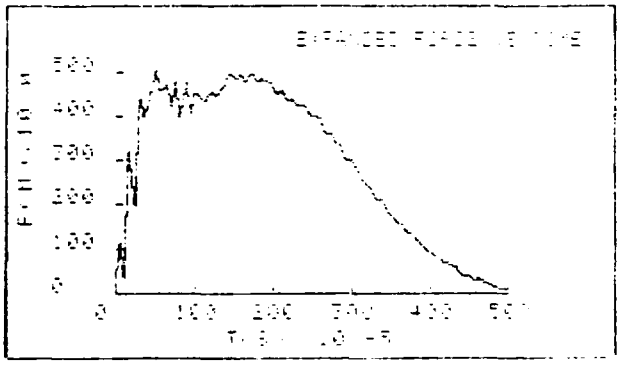

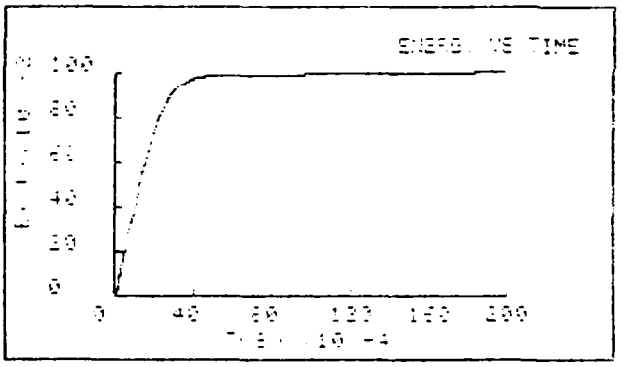

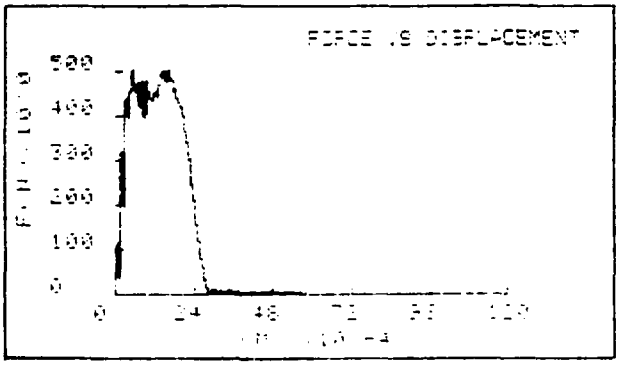

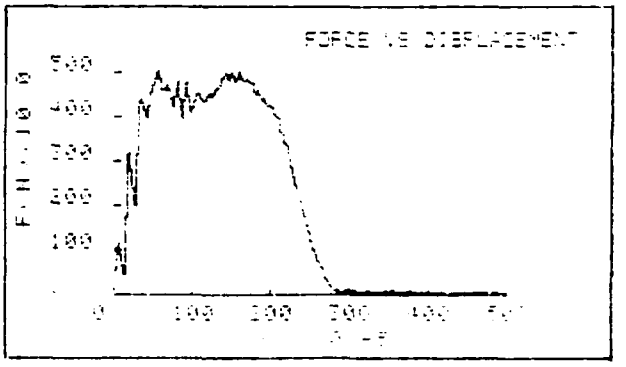

FIGURE 23. Impact data obtained for the borosilicate glass specimen BOR5-25.

SPECIMEN NUMBER BOR5-29

MATERIAL : FIBER Grafil Carbon Fiber
MATRIX Borosilicate Glass
LAY-UP (0,90,0,90)s

IMPACTOR TYPE :- 6 mm Conical Tup		Impact Energy	= 1.00 J
Mass of Impactor	= 1.56 kg	Drop Height	= 0.07 m
		Impact Velocity	= 1.13 m/s
Specimen Span	= 50.00 mm	Applied Stress	= 70.00 MPa
Specimen Width	= 24.85 mm	Max. Recorded Force	= 695.00 N
Specimen Thickness	= 2.43 mm	Max. Recorded Energy	= 0.79 J

POST IMPACT CONDITION :-

1. Specimen has fractured.
2. A small impact mark is visible on the top surface. The fracture crack is perpendicular to the applied stress axis when viewed from the top.
3. Considerable cracking is present in all 90° plies along one edge.
4. Fracture surface has a step-like appearance. Some fiber pull-out is visible. Delamination at the bottom 0°/90° interface has resulted in the deviation of the fracture crack across the bottom 0° ply.

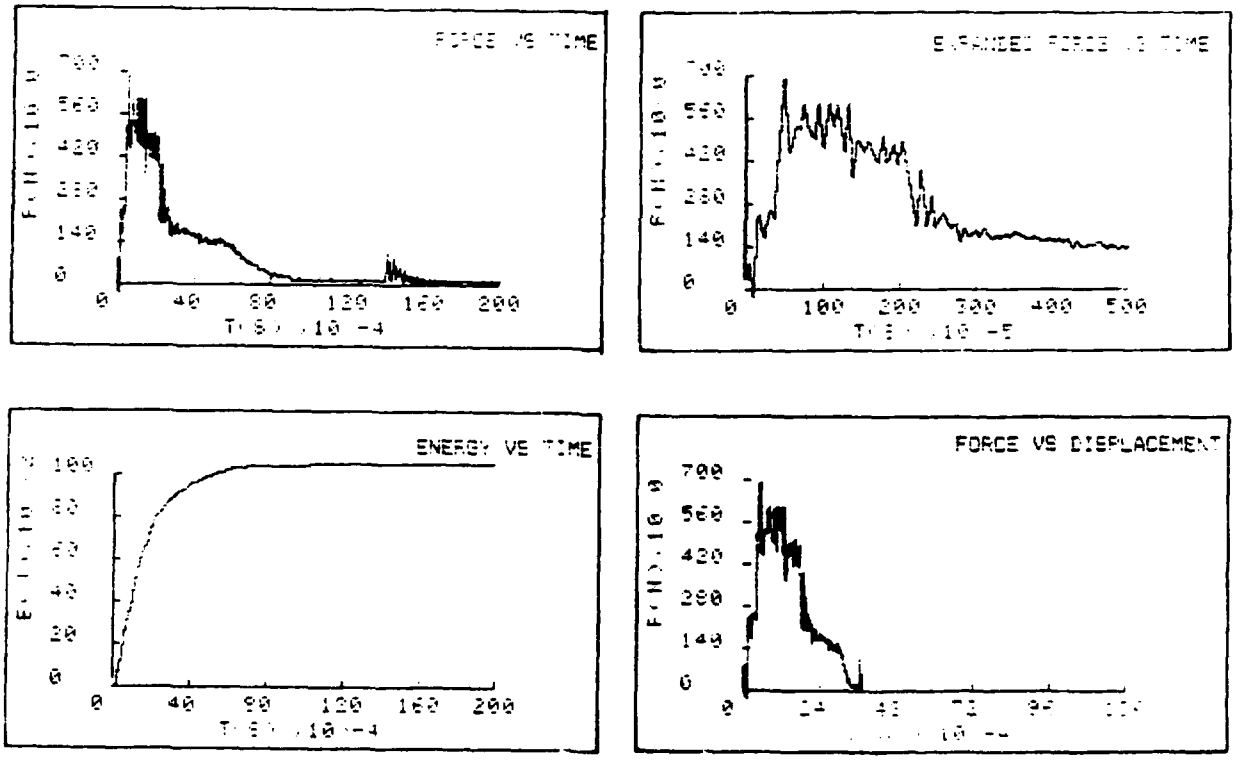

FIGURE 24. Impact data obtained for the borosilicate glass specimen BOR5-29.

INSTRUMENTED IMPACT TESTING OF STRESSED COMPOSITES

MATERIALS : FIBRE — CRAFIL HIGH MODULUS CARBON
MATRIX — BOROSILICATE GLASS
LAY-UP — (0,90,0,90)s

TESTING CONDITIONS : BUILT-IN ENDS
6mm CONICAL IMPACTING TUP
WEIGHT OF IMPACTOR = 1.56kg
SPECIMEN SPAN = 50mm
IMPACT ENERGY = 1J
IMPACT VELOCITY = 1.132m/s

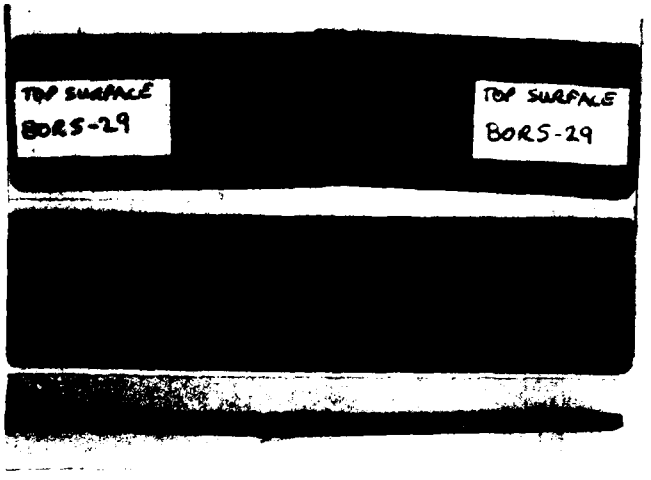

APPLIED STRESS = 70.0MPa
SPECIMEN NUMBER : BOR5-29

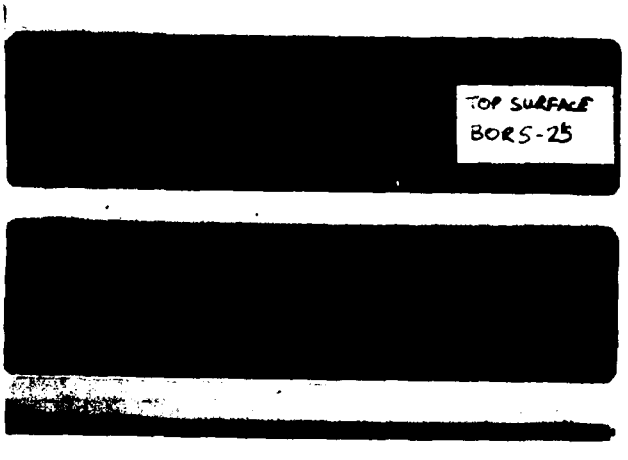

APPLIED STRESS = 40.0MPa
SPECIMEN NUMBER : BOR5-25

0mm 50mm

FIGURE 25. Damage sustained by the borosilicate glass composite specimens BOR5-29 and BOR5-25 during an impact.

SPECIMEN NUMBER BOR4-21

MATERIAL : FIBER Grafil Carbon Fiber
MATRIX Borosilicate Glass
LAY-UP (0,90,0,90)s

IMPACTOR TYPE :- 6 mm Conical Tup			Impact Energy	=	2.00 J
Mass of Impactor	=	1.56 kg	Drop Height	=	0.13 m
			Impact Velocity	=	1.60 m/s
Specimen Span	=	50.00 mm	Applied Stress	=	27.50 MPa
Specimen Width	=	24.70 mm	Max. Recorded Force	=	425.00 N
Specimen Thickness	=	2.72 mm	Max. Recorded Energy	=	2.00 J

POST IMPACT CONDITION :-
1. Specimen has not fractured.
2. Initial surface quality is looks poor! A small impact mark is present on the top surface although some cracking parallel to the 0' fibers is evidence.
3. Considerable cracking/splitting is present in the 90' plies.
4. Bottom surface has a perpendicular crack across the specimen width. This crack has only propagated up through half the specimen thickness. Some splitting parallel to the 0' fibers is present on the under surface.

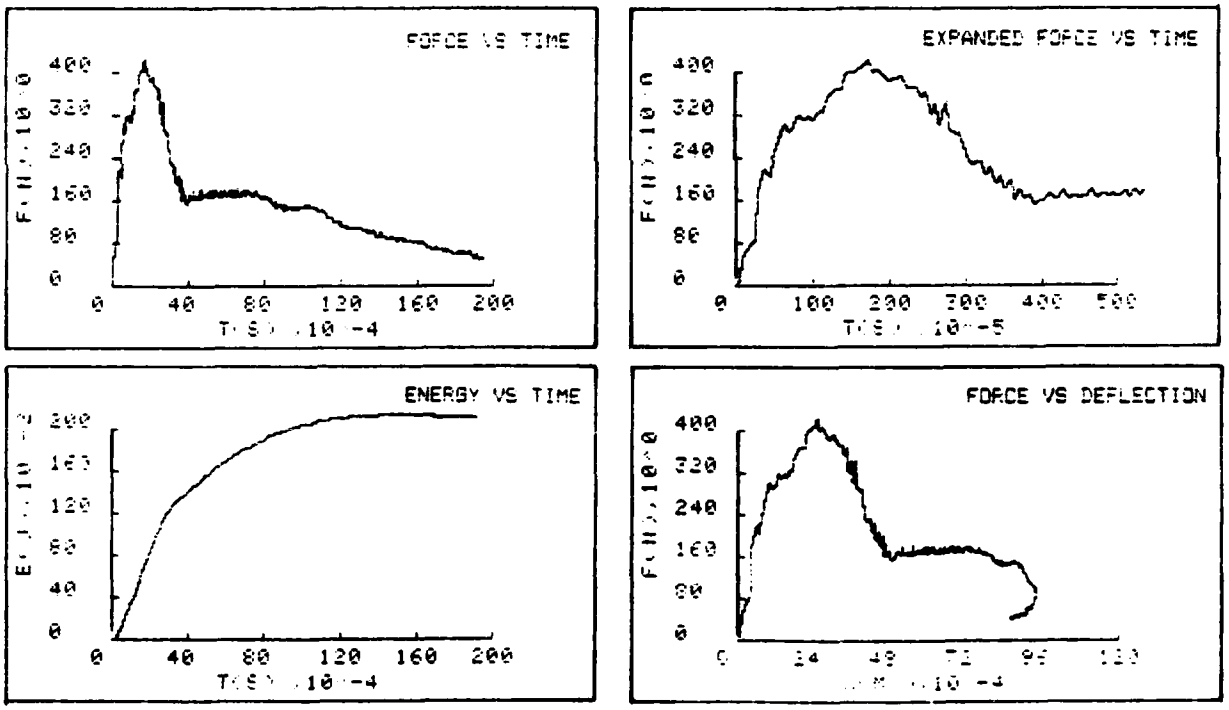

FIGURE 26. Impact data obtained for the borosilicate glass specimen BOR4-21.

SPECIMEN NUMBER BOR4-20

MATERIAL : FIBER Grafil Carbon Fiber
MATRIX Borosilicate Glass
LAY-UP (0,90,0,90)s

IMPACTOR TYPE :- 6 mm Conical Tup			Impact Energy	=	2.00 J
Mass of Impactor	=	1.56 kg	Drop Height	=	0.13 m
			Impact Velocity	=	1.60 m/s
Specimen Span	=	50.00 mm	Applied Stress	=	30.00 MPa
Specimen Width	=	24.79 mm	Max. Recorded Force	=	350.00 N
Specimen Thickness	=	2.64 mm	Max. Recorded Energy	=	-- J

POST IMPACT CONDITION :-

1. Specimen has fractured.
2. Initial surface quality is looks poor! A small impact mark is present on the top surface with extensive splitting parallel to the 0' fibers.
3. Considerable cracking present in the 90' plies. Worse than that observed with both BOR4-19 and BOR4-21.
4. Bottom surface has some splitting parallel to the 0' fibers. The fracture surface is very uneven but is generally perpendicular to the axis of applied stress, with considerable fiber pull-out, giving it a fibrous appearance.
5. Impactor penetration is limited suggesting failure is probably due to specimen flexure.

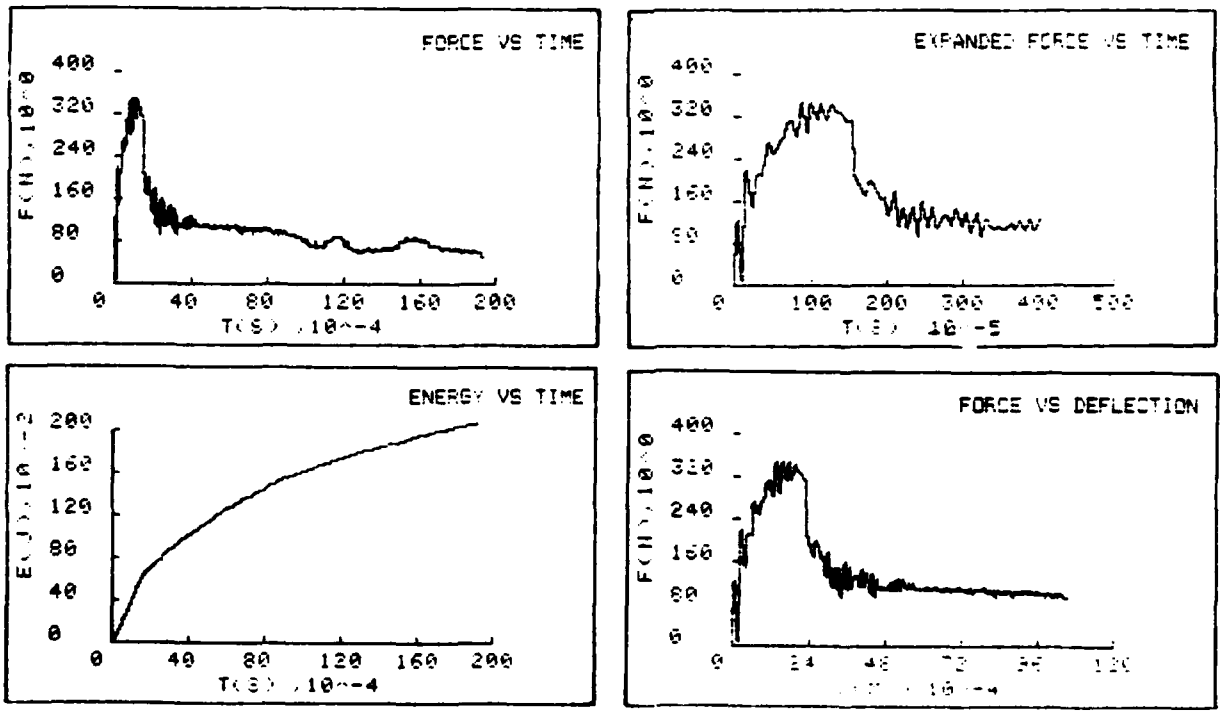

FIGURE 27. Impact data obtained for the borosilicate glass specimen BOR4-20.

INSTRUMENTED IMPACT TESTING OF STRESSED COMPOSITES

MATERIALS : FIBRE — GRAFIL HIGH MODULUS CARBON
MATRIX — BOROSILICATE GLASS
LAY-UP — (0,90,0,90)s

TESTING CONDITIONS : BUILT-IN ENDS
6mm CONICAL IMPACTING TUP
WEIGHT OF IMPACTOR = 1.56kg
SPECIMEN SPAN = 50mm
IMPACT ENERGY = 2J
IMPACT VELOCITY = 1.601m/s

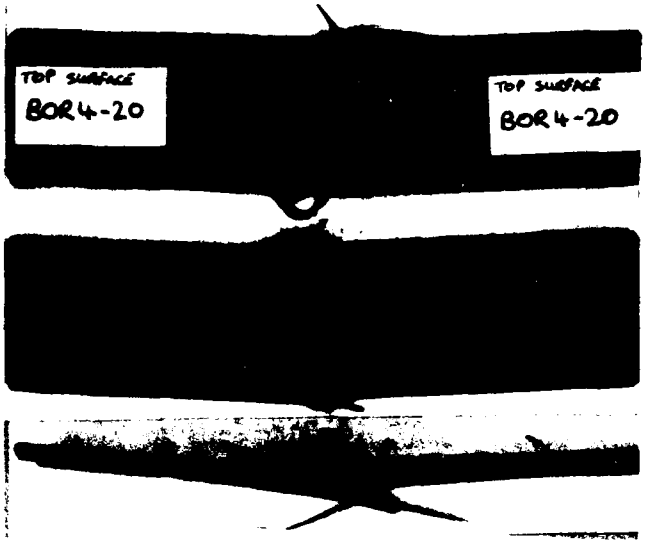

APPLIED STRESS = 30.0MPa
SPECIMEN NUMBER : BOR4-20

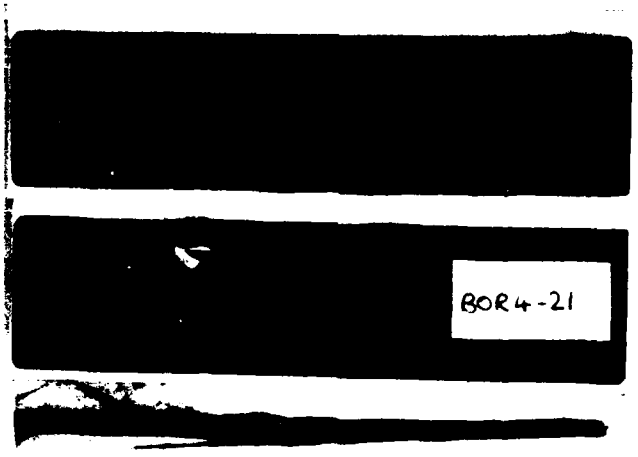

APPLIED STRESS = 27.5MPa
SPECIMEN NUMBER : BOR4-21

0mm 50mm

FIGURE 28. Damage sustained by the borosilicate glass composite specimens BOR4-20 and BOR4-21 during an impact.

SPECIMEN NUMBER BOR2-12

MATERIAL : FIBER Grafil Carbon Fiber
MATRIX Borosilicate Glass
LAY-UP (0,90,0,90)s

IMPACTOR TYPE : 6 mm Conical Tup		Impact Energy	= 6.00 J
Mass of Impactor	= 1.56 kg	Drop Height	= 0.39 m
		Impact Velocity	= 2.77 m/s
Specimen Span	= 50.00 mm	Applied Stress	= 15.00 MPa
Specimen Width	= 24.82 mm	Max. Recorded Force	= 575.00 N
Specimen Thickness	= 2.31 mm	Max. Recorded Energy	= 6.00 J

POST IMPACT CONDITION :-

1. Specimen not fractured.
2. Large impact crater surrounded with short lengths of fractured fibers. Some splitting parallel to the fibers either side of the point of impact.
3. Extensive cracking present in the 90' plies, with considerable delaminatic especially between plies in the bottom half of the specimen.
4. A crack perpendicular to the stress axis has been formed on the under surface, across the specimen width, which has propagated up through more than half the specimen thickness on both sides.
5. Fracture of the lower 0' plies in the composite, combined with the large tup displacement, has resulted in the formation of a ridge (maximum displacement of bottom 0' ply is 10 mm) across the under surface.

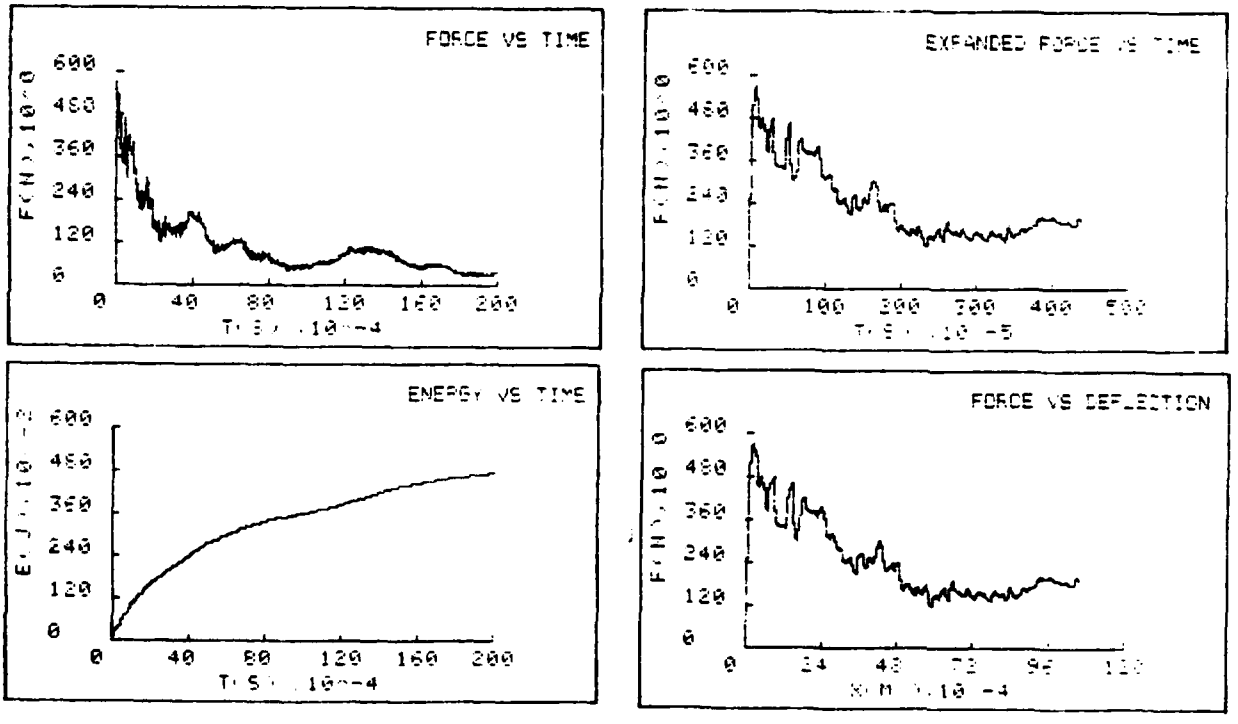

FIGURE 29. Impact data obtained for the borosilicate glass specimen BOR2-12.

SPECIMEN NUMBER BOR3-15

MATERIAL : FIBER Grafil Carbon Fiber
MATRIX Borosilicate Glass
LAY-UP (0,90,0,90)s

IMPACTOR TYPE :- 6 mm Conical Tup		Impact Energy	= 6.00 J
Mass of Impactor	= 1.56 kg	Drop Height	= 0.39 m
		Impact Velocity	= 2.77 m/s
Specimen Span	= 50.00 mm	Applied Stress	= 17.50 MPa
Specimen Width	= 24.50 mm	Max. Recorded Force	= 380.00 N
Specimen Thickness	= 2.48 mm	Max. Recorded Energy	= 3.48 J

POST IMPACT CONDITION :-

1. Specimen has fractured.
2. The top two 0' plies exhibit fiber fracture across the specimen width at four or five places along the specimen span. The other 0' plies have fractured at the extremities of the specimen span and beneath the point of impact.
3. Extensive cracking in the 90' plies and considerable delamination between all the plies is present.
4. Fracture surface exhibits a considerable amount of fiber pull-out giving a fibrous appearance to the post fractured specimen.
5. The large tup displacement coupled with the severe damage mentioned above together with the major perpendicular to the stress axis crack has given the impacted specimen an ad hoc hinge at the original specimen span extremities.

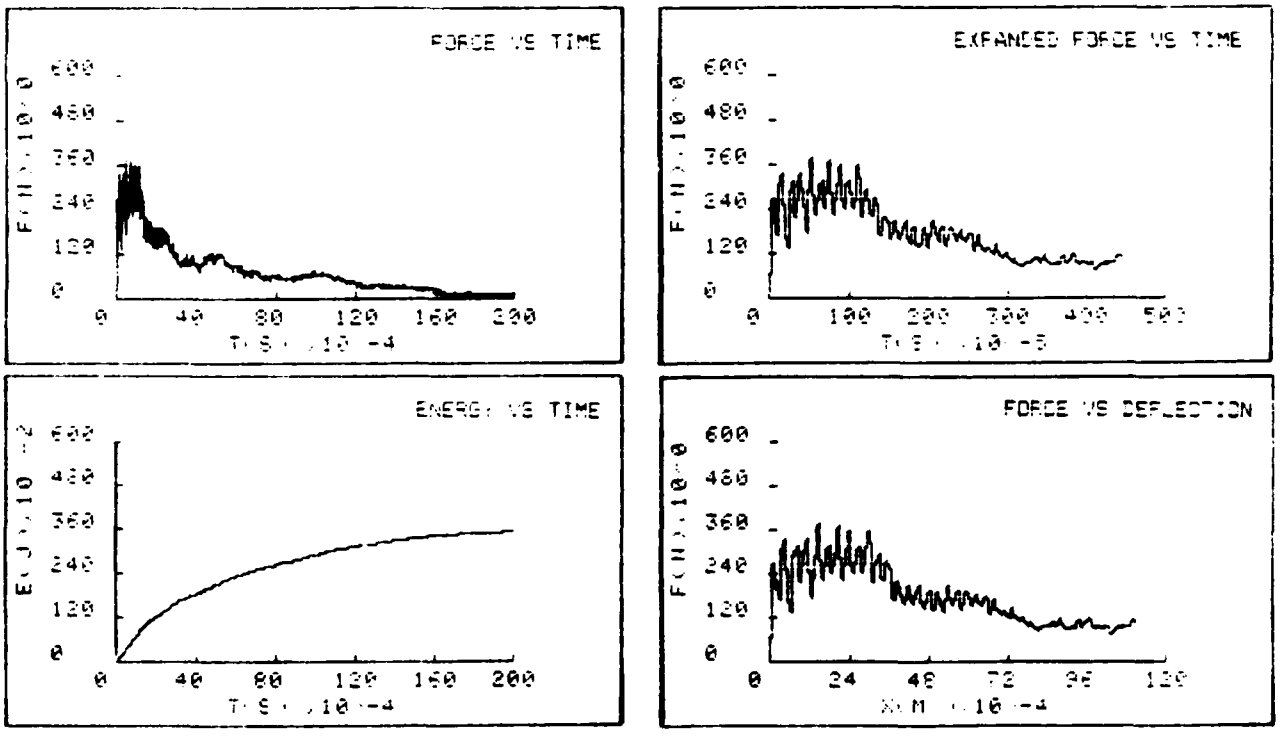

FIGURE 30. Impact data obtained for the borosilicate glass specimen BOR3-15.

INSTRUMENTED IMPACT TESTING OF STRESSED COMPOSITES

MATERIALS : FIBRE — GRAFIL HIGH MODULUS CARBON
MATRIX — BOROSILICATE GLASS
LAY–UP — (0,90,0,90)s

TESTING CONDITIONS : BUILT–IN ENDS
6mm CONICAL IMPACTING TUP
WEIGHT OF IMPACTOR = 1.56kg
SPECIMEN SPAN = 50mm
IMPACT ENERGY = 6J
IMPACT VELOCITY = 2.774m/s

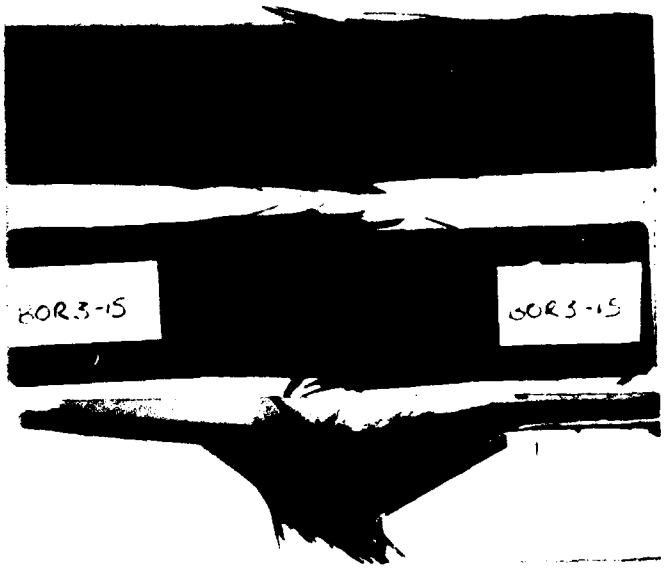

APPLIED STRESS = 17.5MPa
SPECIMEN NUMBER : BOR3–15

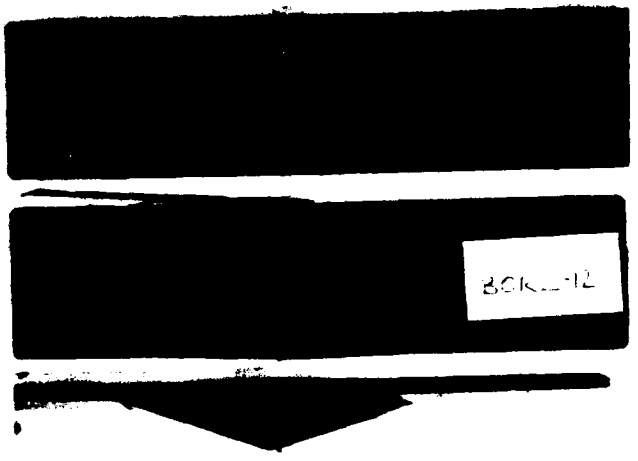

APPLIED STRESS = 15.0MPa
SPECIMEN NUMBER : BOR2–12

0mm 50mm

FIGURE 31. Damage sustained by the borosilicate glass composite specimens BOR3-15 and BOR2-12 during an impact.

SPECIMEN NUMBER BOR11-62 (Extra Pressing)

MATERIAL : FIBER Grafil Carbon Fiber
MATRIX Borosilicate Glass
LAY-UP [0,90,0,90]s

IMPACTOR TYPE :- 6 mm Conical Tup		Impact Energy	= 6.00 J
Mass of Impactor	= 1.56 kg	Drop Height	= 0.39 m
		Impact Velocity	= 2.77 m/s
Specimen Span	= 50.00 mm	Applied Stress	= 20.00 MPa
Specimen Width	= 24.64 mm	Max. Recorded Force	= 620.00 N
Specimen Thickness	= 2.24 mm	Max. Recorded Energy	= 6.00 J

POST IMPACT CONDITION :-
1. Specimen not fractured (impact is slightly off-centre).
2. Deep tup penetration, leaving a hole about 10 mm in diameter. This has resulted in the punching out of an area about half the specimen width, about 20 mm long and about half the specimen thickness (ie delamination has occurred half way through the composite thickness).
3. No widespread delamination is visible.
4. Damaged region is distinctly fibrous.
5. Some longitudinal cracking is present on the under surface.

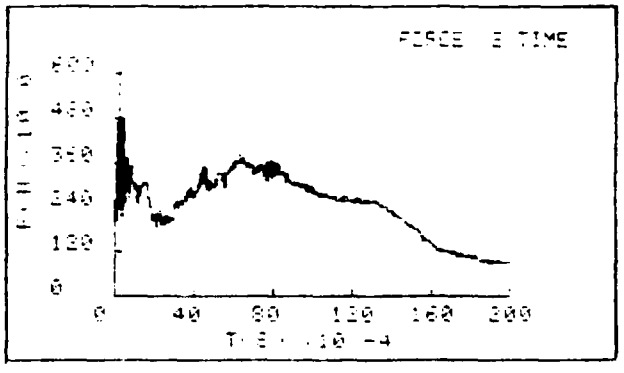

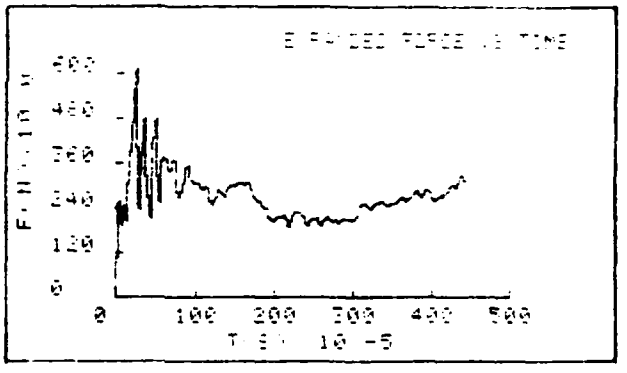

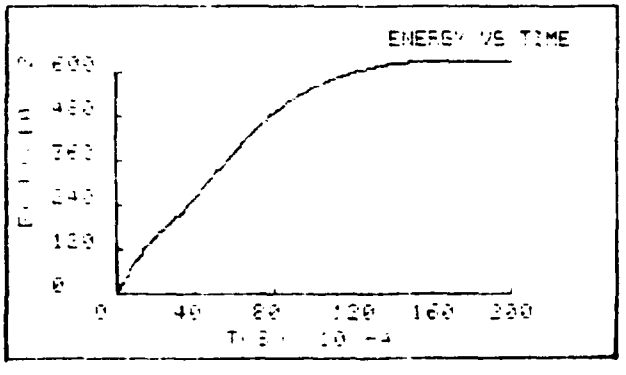

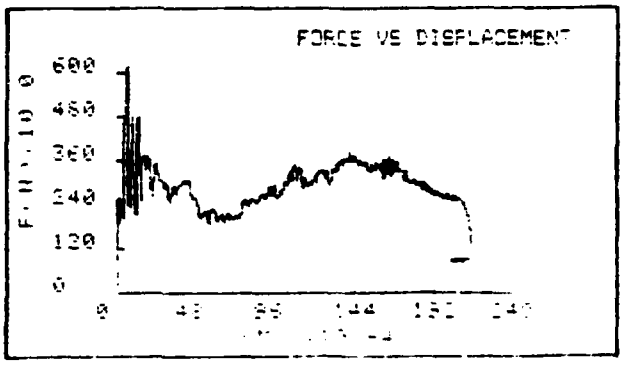

FIGURE 32. Impact data obtained for the borosilicate glass specimen BOR11-62.

SPECIMEN NUMBER BOR12-66 (Extra Pressing)

MATERIAL : FIBER Grafil Carbon Fiber
MATRIX Borosilicate Glass
LAY-UP (0,90,0,90)s

IMPACTOR TYPE :- 6 mm Conical Tup			Impact Energy	=	8.00 J
Mass of Impactor	=	1.56 kg	Drop Height	=	0.52 m
			Impact Velocity	=	3.20 m/s
Specimen Span	=	50.00 mm	Applied Stress	=	12.50 MPa
Specimen Width	=	24.64 mm	Max. Recorded Force	=	650.00 N
Specimen Thickness	=	2.47 mm	Max. Recorded Energy	=	8.00 J

POST IMPACT CONDITION :-

1. Specimen has not fractured.
2. Deep tup penetration has occurred leaving a hole about 14 mm in diameter. This has resulted in the punching out of a region across the specimen width, although varying in length along the axis of applied stress. This has been helped by some initial delamination at the 5th 0'/90' interface
3. Considerable delamination is also visible on one side. This half of the specimen also contains a transverse which has propagated up through the specimen thickness, ie the specimen has fractured over half its width.
4. Damaged area is distinctly fibrous in appearance.

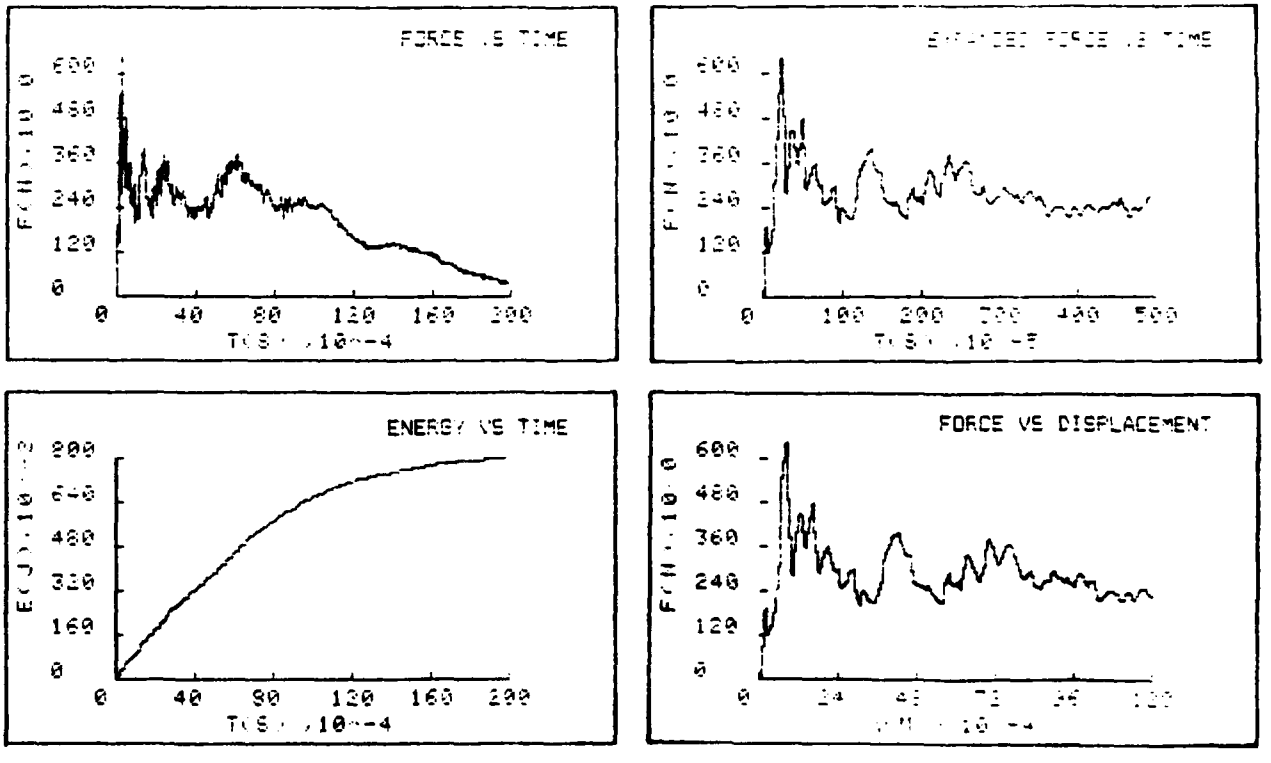

FIGURE 33. Impact data obtained for the borosilicate glass specimen BOR12-66.

INSTRUMENTED IMPACT TESTING OF STRESSED COMPOSITES

MATERIALS : FIBRE — GRAFIL HIGH MODULUS CARBON
MATRIX — BOROSILICATE GLASS (EXTRA PRESSINGS)
LAY-UP — (0,90,0,90)s

TESTING CONDITIONS : BUILT-IN ENDS
6mm CONICAL IMPACTING TUP
WEIGHT OF IMPACTOR = 1.56kg
SPECIMEN SPAN = 50mm

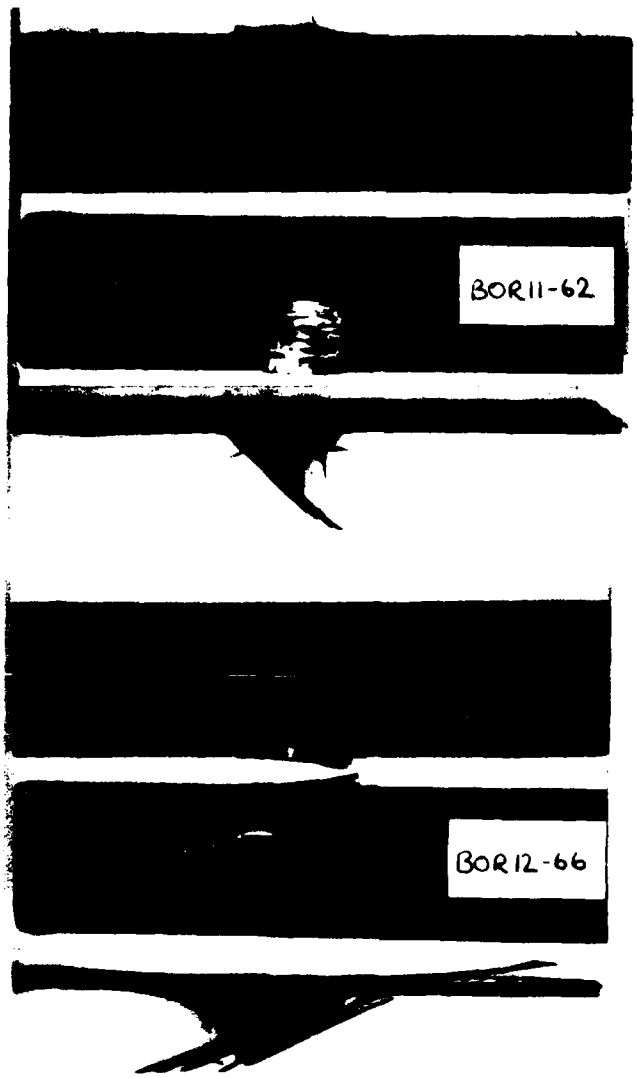

APPLIED STRESS = 20.0MPa
SPECIMEN NUMBER : BOR11-62
IMPACT ENERGY = 6J
IMPACT VELOCITY = 2.774m/s

APPLIED STRESS = 12.5MPa
SPECIMEN NUMBER : BOR12-66
IMPACT ENERGY = 8J
IMPACT VELOCITY = 3.203m/s

0mm 50mm

FIGURE 34. Damage sustained by the borosilicate glass composite specimens BOR11-62 and BOR12-66 during an impact.

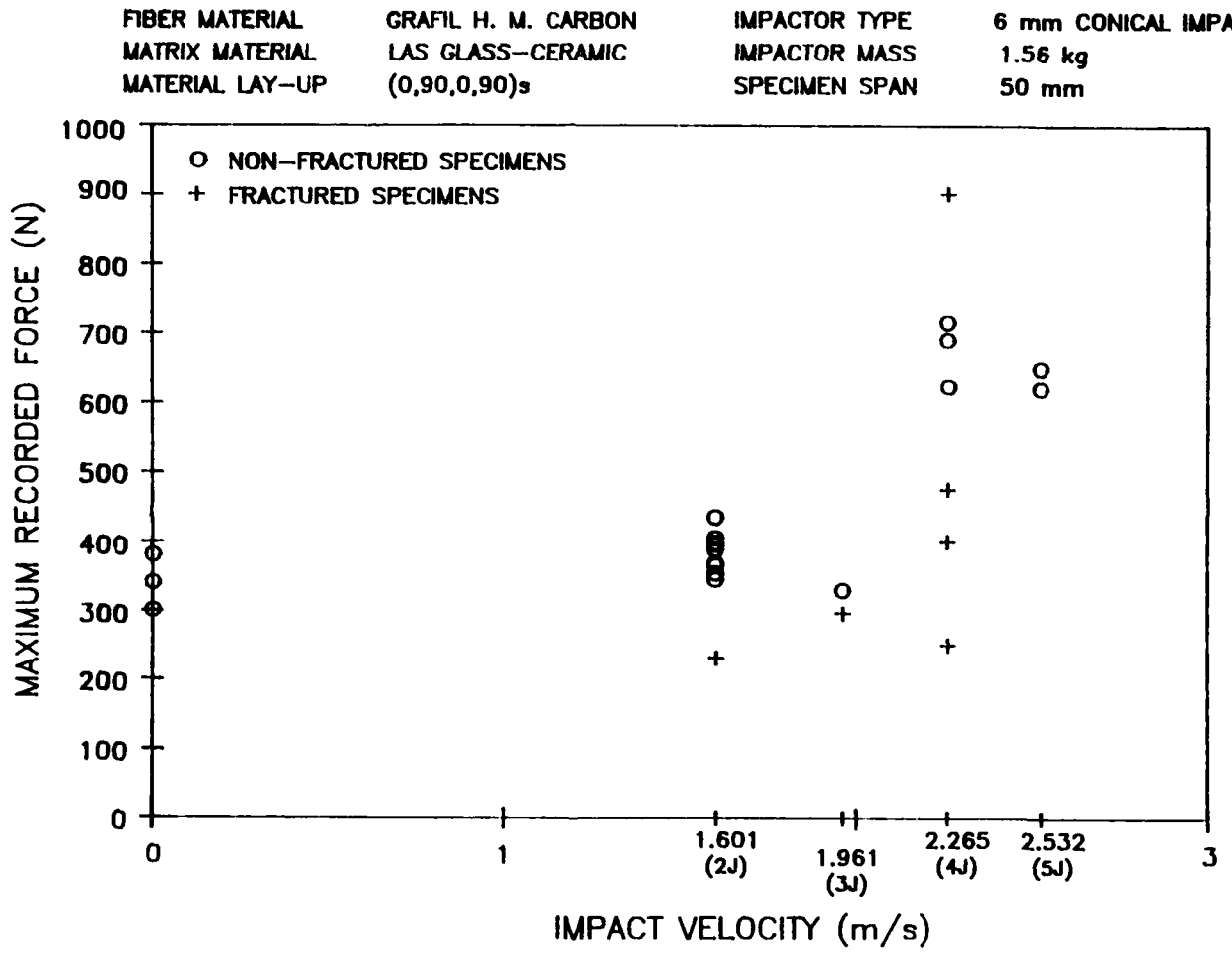

FIGURE 35. Variation of maximum recorded force with impact velocity for the Carbon / LAS glass–ceramic composite material.

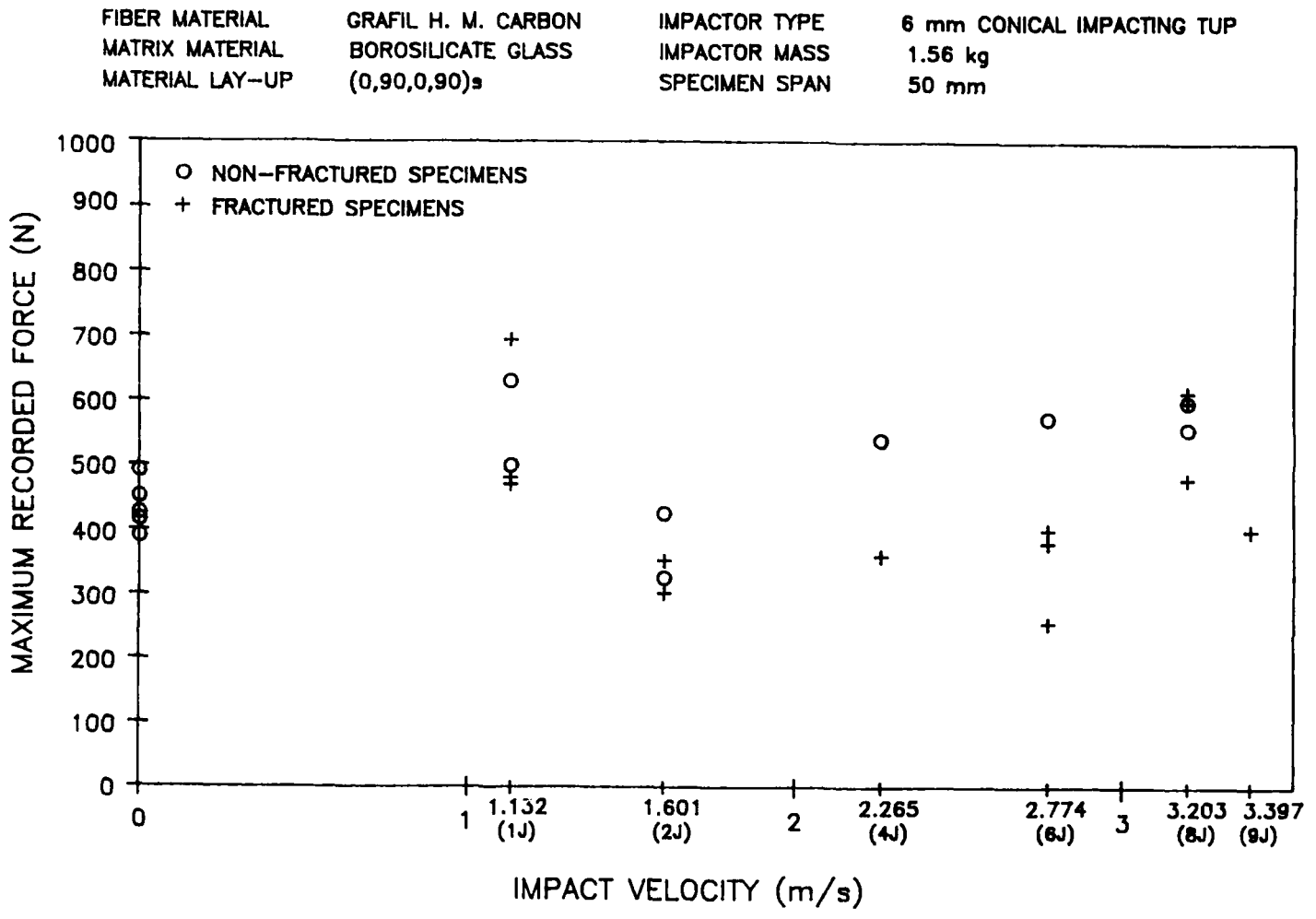

FIGURE 36. *Variation of maximum recorded force with impact velocity for the Carbon / borosilicate glass composite material.*

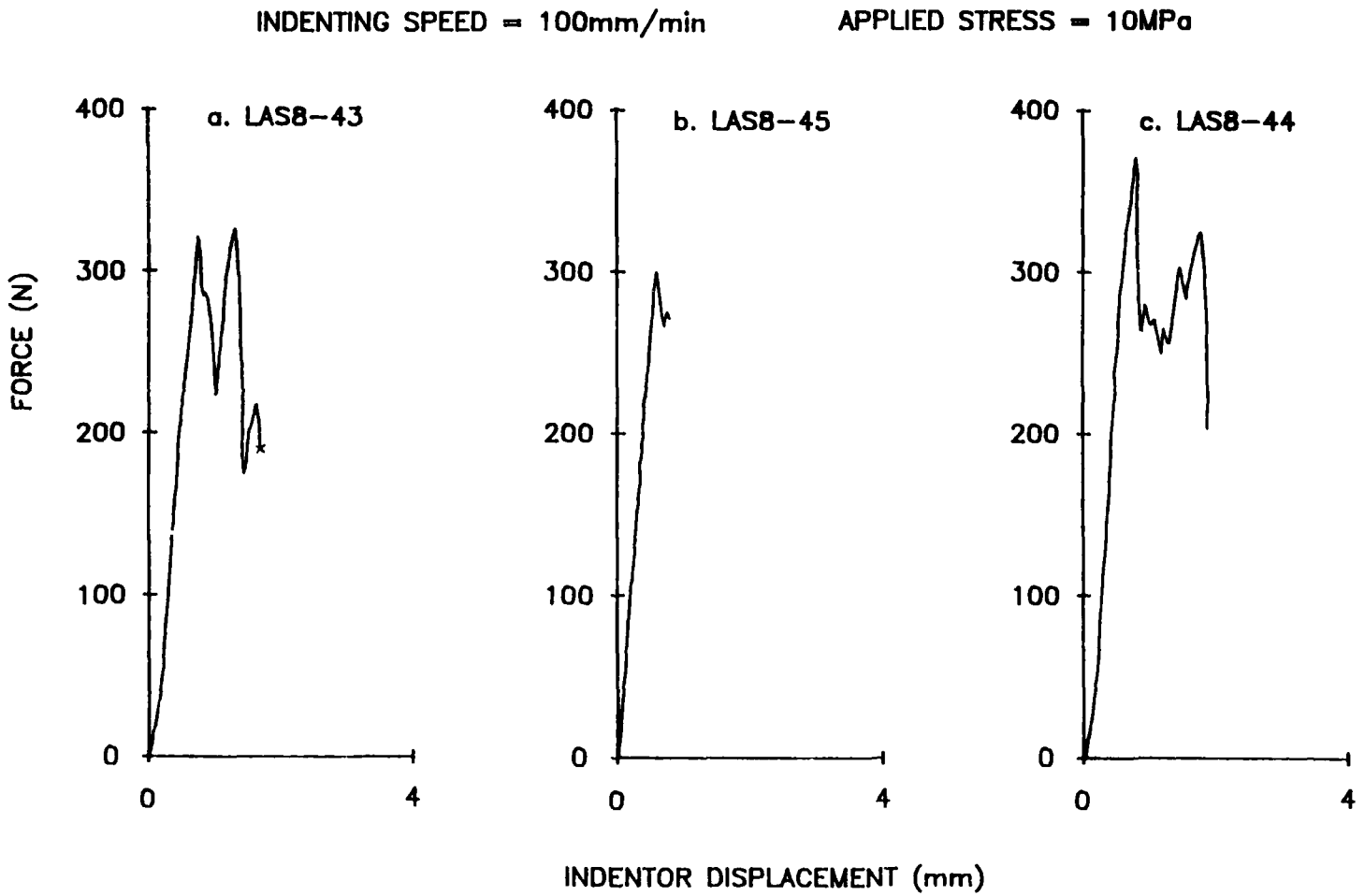

FIGURE 37. Plots of force vs indentor displacement obtained from the slow indentation experiments on the LAS glass-ceramic composite

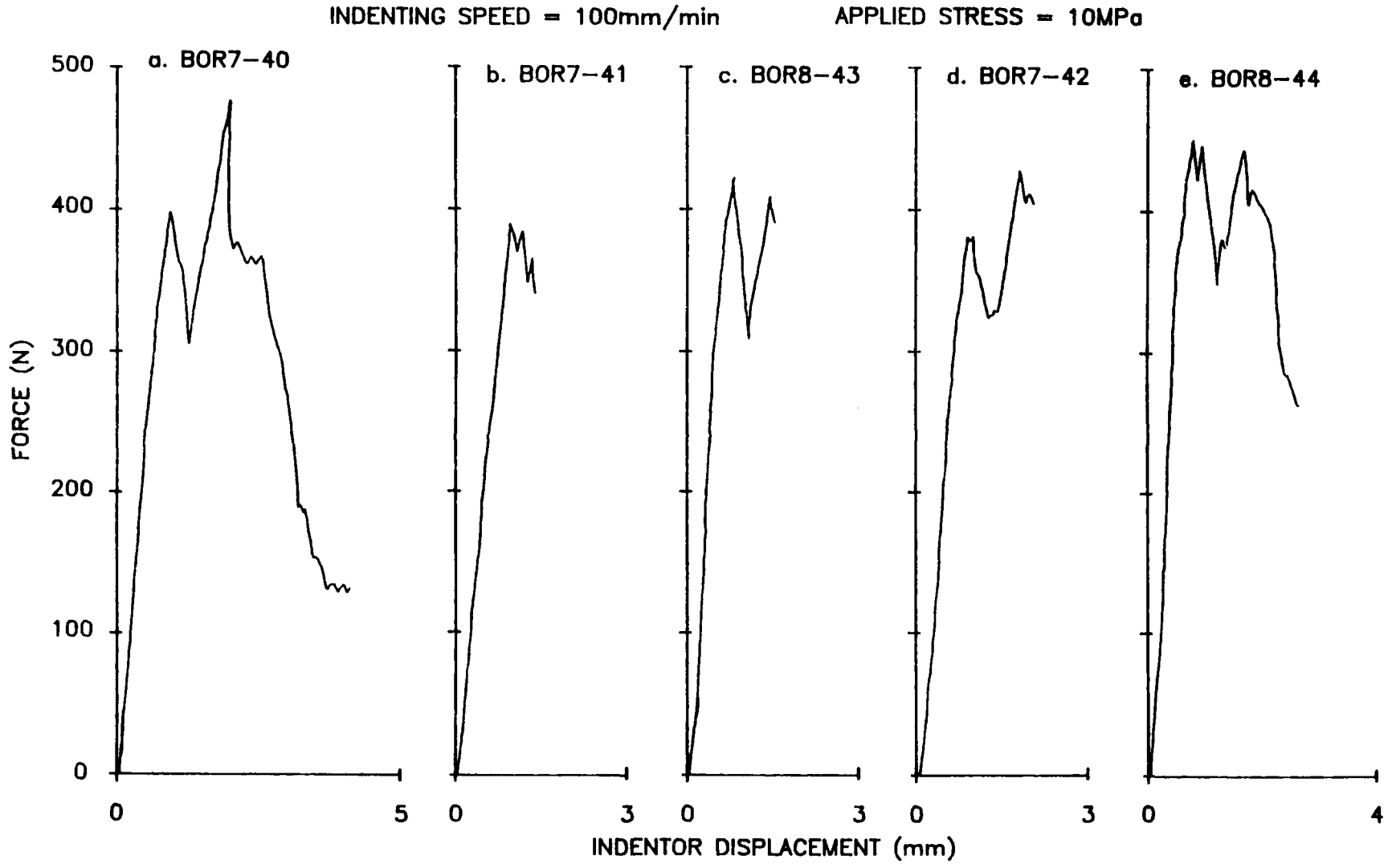

FIGURE 38. Plots of force vs indentor displacement obtained from the slow indentation experiments on the borosilicate glass composite.

IMPACTS OF GRAFIL / BOROSILICATE GLASS COMPOSITES AT ELEVATED TEMPERATURES

MATERIALS : FIBRE — GRAFIL HIGH MODULUS CARBON
MATRIX — BOROSILICATE GLASS
LAY-UP — (0,90,0,90)s

TESTING CONDITIONS : BUILT-IN ENDS
SPECIMENS UNSTRESSED
6mm CONICAL IMPACTING TUP
WEIGHT OF IMPACTOR = 0.85kg
SPECIMEN SPAN = 50mm
IMPACT ENERGY = 0.5J
IMPACT VELOCITY = 1.085m/s

FIGURE 39. Damage sustained by the borosilicate glass composite material at elevated temperatures in a 0.5J impact.

IMPACTS OF GRAFIL / BOROSILICATE GLASS COMPOSITES AT ELEVATED TEMPERATURES

MATERIALS :	FIBRE	GRAFIL HIGH MODULUS CARBON
	MATRIX	BOROSILICATE GLASS
	LAY-UP	(0,90,0,90)s
TESTING CONDITIONS		BUILT-IN ENDS
		SPECIMENS UNSTRESSED
		6mm CONICAL IMPACTING TUP
		WEIGHT OF IMPACTOR = 0.85kg
		SPECIMEN SPAN = 50mm
		IMPACT ENERGY = 1J
		IMPACT VELOCITY = 1.534m/s

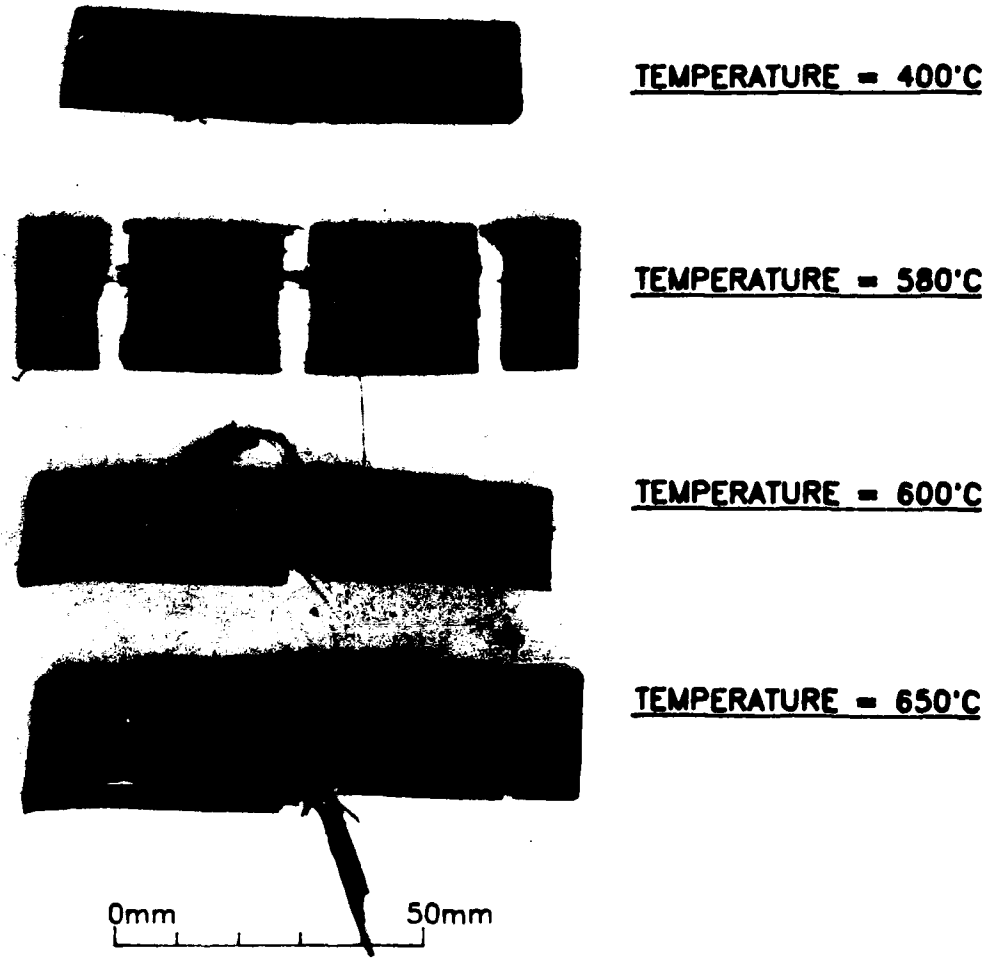

FIGURE 40. Damage sustained by the borosilicate glass composite material at elevated temperatures in a 1J impact.

BALLISTIC IMPACTS OF GRAFIL / LAS GLASS–CERAMIC COMPOSITES

MATERIALS : FIBRE — GRAFIL HIGH MODULUS CARBON
MATRIX — LAS GLASS–CERAMIC
LAY–UP — $(0,90,0,90)_s$

TESTING CONDITIONS : BUILT–IN ENDS
SPECIMENS UNSTRESSED
6mm STEEL BALL PROJECTILE
SPECIMEN SPAN = 50mm

IMPACT VELOCITY = 70m/s
SPECIMEN NUMBER : LAS2–09
EQUIVALENT IMPACT ENERGY = 2.18J
UNDERSIDE OF SPECIMEN SHOWN

IMPACT VELOCITY = 100m/s
SPECIMEN NUMBER : LAS2–08
EQUIVALENT IMPACT ENERGY = 4.45J
UNDERSIDE OF SPECIMEN SHOWN

IMPACT VELOCITY = 140m/s
SPECIMEN NUMBER : LAS2–07
EQUIVALENT IMPACT ENERGY = 8.72J
UNDERSIDE OF SPECIMEN SHOWN

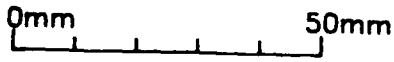

FIGURE 41. Damage sustained by the LAS glass-ceramic composite material under ballistic impact conditions.

BALLISTIC IMPACTS OF GRAFIL / BOROSILICATE GLASS COMPOSITES

MATERIALS : FIBRE — GRAFIL HIGH MODULUS CARBON
MATRIX — BOROSILICATE GLASS
LAY-UP — $(0,90,0,90)_s$

TESTING CONDITIONS : BUILT-IN ENDS
SPECIMENS UNSTRESSED
6mm STEEL BALL PROJECTILE
SPECIMEN SPAN = 50mm

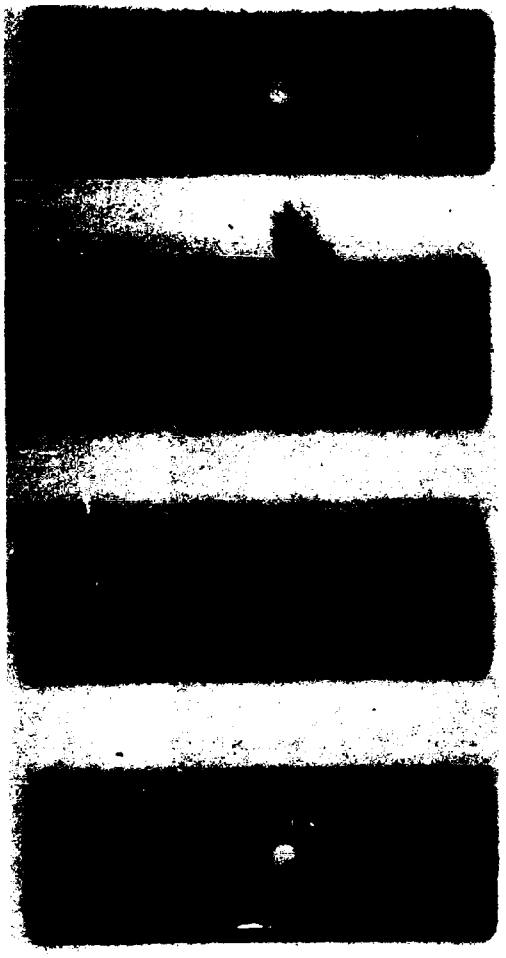

IMPACT VELOCITY = 70m/s
SPECIMEN NUMBER : BOR6-35
EQUIVALENT IMPACT ENERGY = 2.18J
UNDERSIDE OF SPECIMEN SHOWN

EXTRA PRESSING
SPECIMEN NUMBER : BOR13-68
UNDERSIDE OF SPECIMEN SHOWN

IMPACT VELOCITY = 100m/s
SPECIMEN NUMBER : BOR7-38
EQUIVALENT IMPACT ENERGY = 4.45J
UNDERSIDE OF SPECIMEN SHOWN

IMPACT VELOCITY = 140m/s
SPECIMEN NUMBER : BOR6-33
EQUIVALENT IMPACT ENERGY = 8.72J
UNDERSIDE OF SPECIMEN SHOWN

FIGURE 42. Damage sustained by the borosilicate glass composite material under ballistic impact conditions.

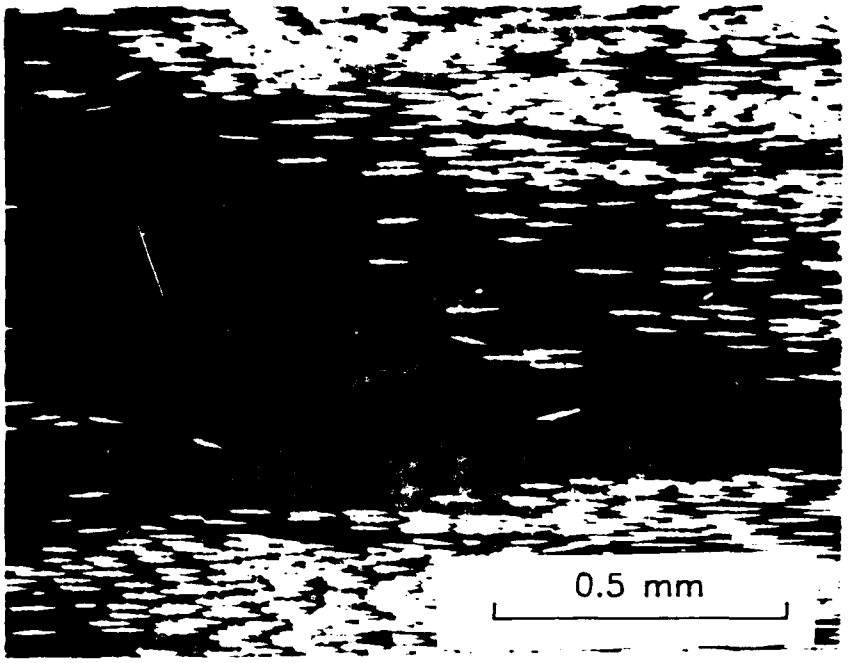

(a) Matrix microcracking in the borosilicate glass composite material.

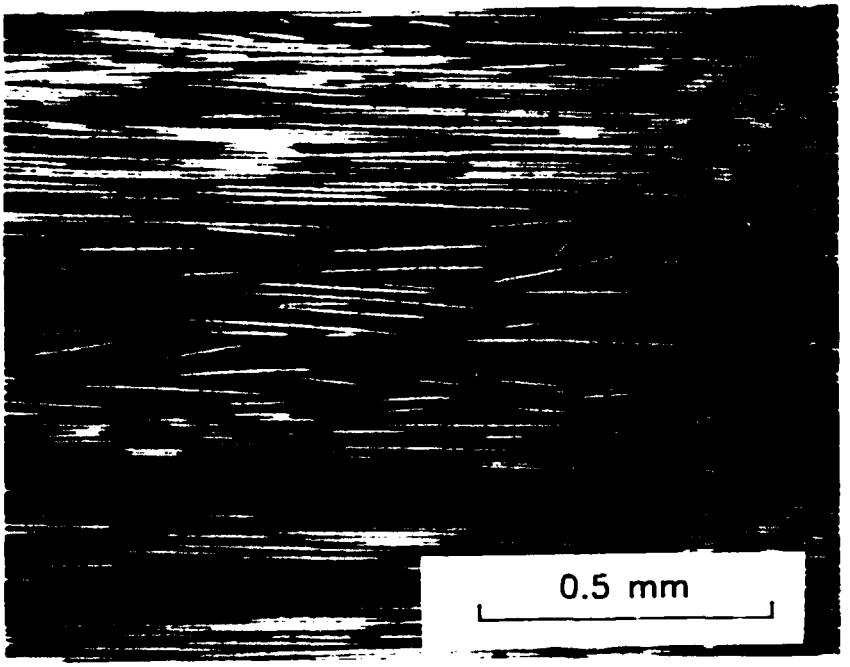

(b) Matrix microcracking in the LAS glass-ceramic composite material.

FIGURE 43. Matrix microcracking in the unidirectional ceramic matrix composite materials.

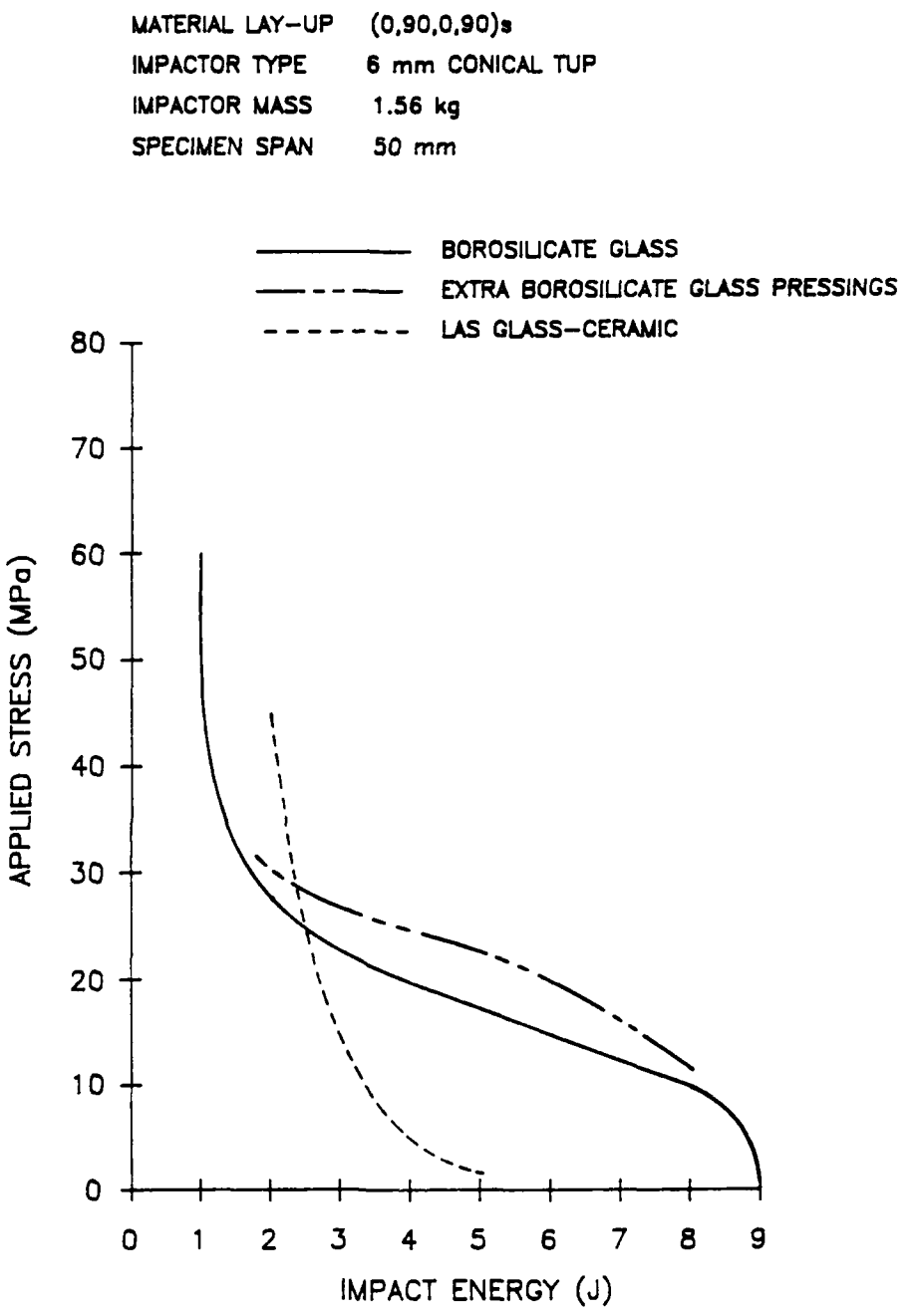

FIGURE 44. Variation of the FRACTURE / NO FRACTURE boundary over a range of impact energies and applied stresses for the Borosilicate glass and LAS Glass-ceramic composites.

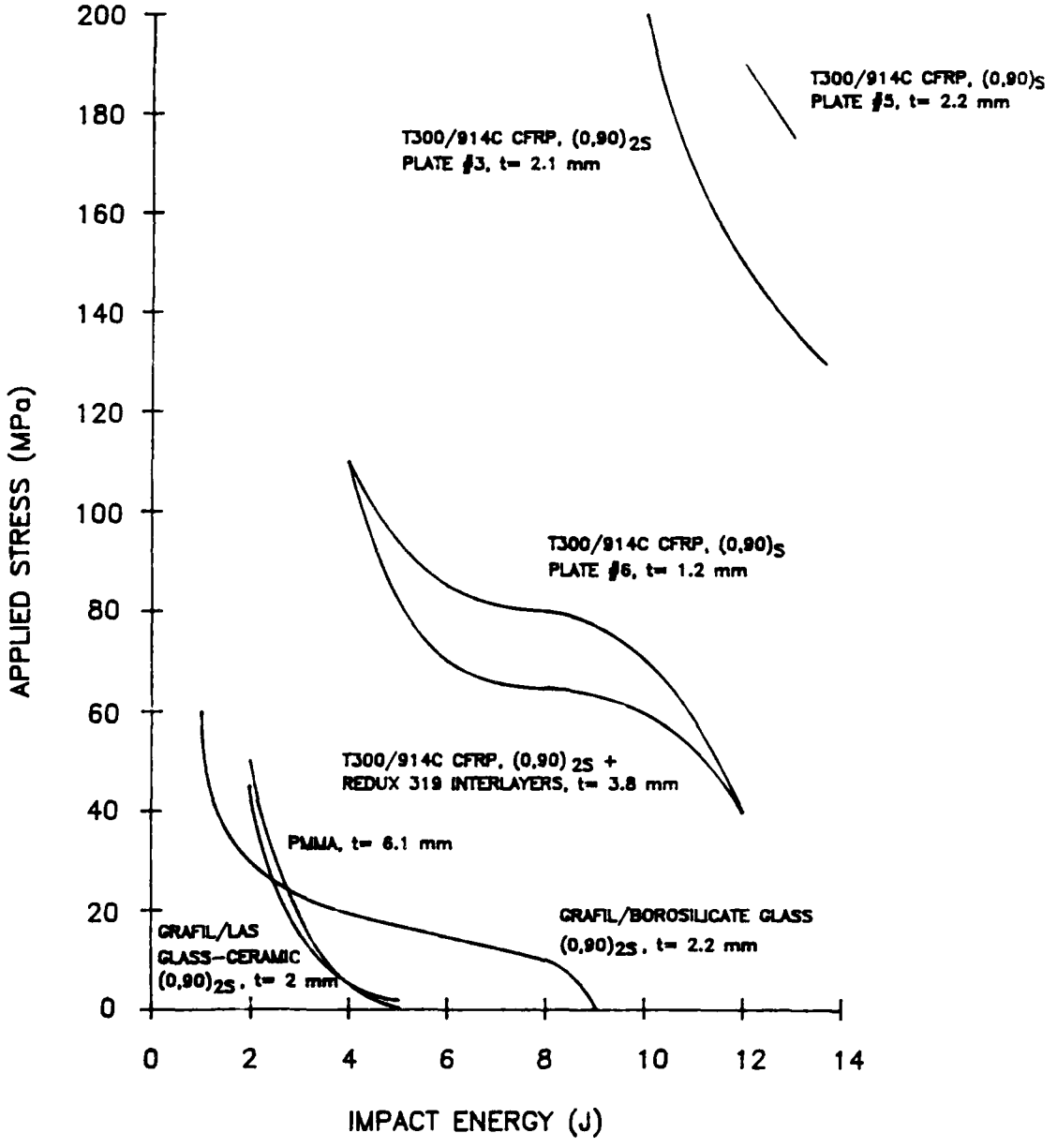

FIGURE 45. Variation of the boundary between complete and incomplete fracture for a variety of materials over a range of impact energies and applied stresses.

FIBER MATERIAL	GRAFIL H. M. CARBON
MATRIX MATERIAL	LAS GLASS–CERAMIC
MATERIAL LAY–UP	(0,90,0,90)s
IMPACTOR TYPE	6 mm CONICAL IMPACTING TUP
IMPACTOR MASS	1.56 kg
SPECIMEN SPAN	50 mm

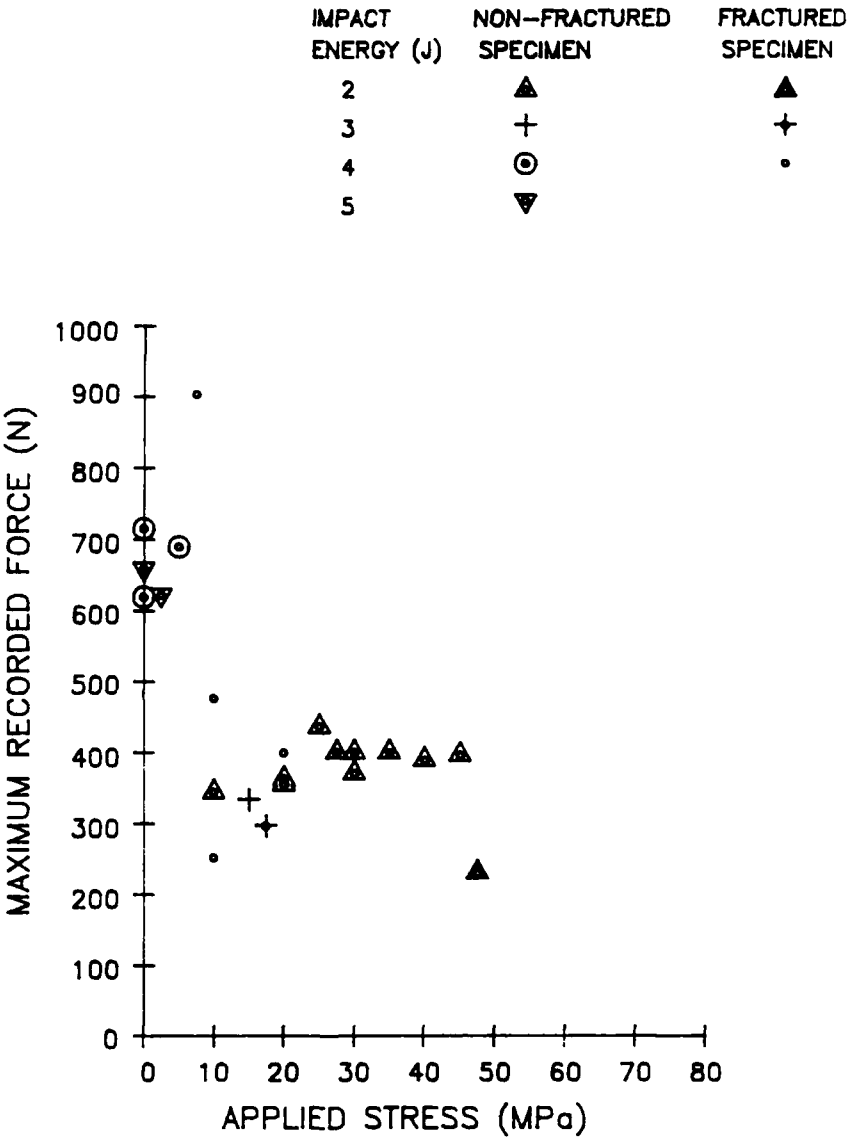

FIGURE 46. Variation of maximum recorded force with applied stress and impact energy for the Carbon / LAS glass–ceramic composite materials.

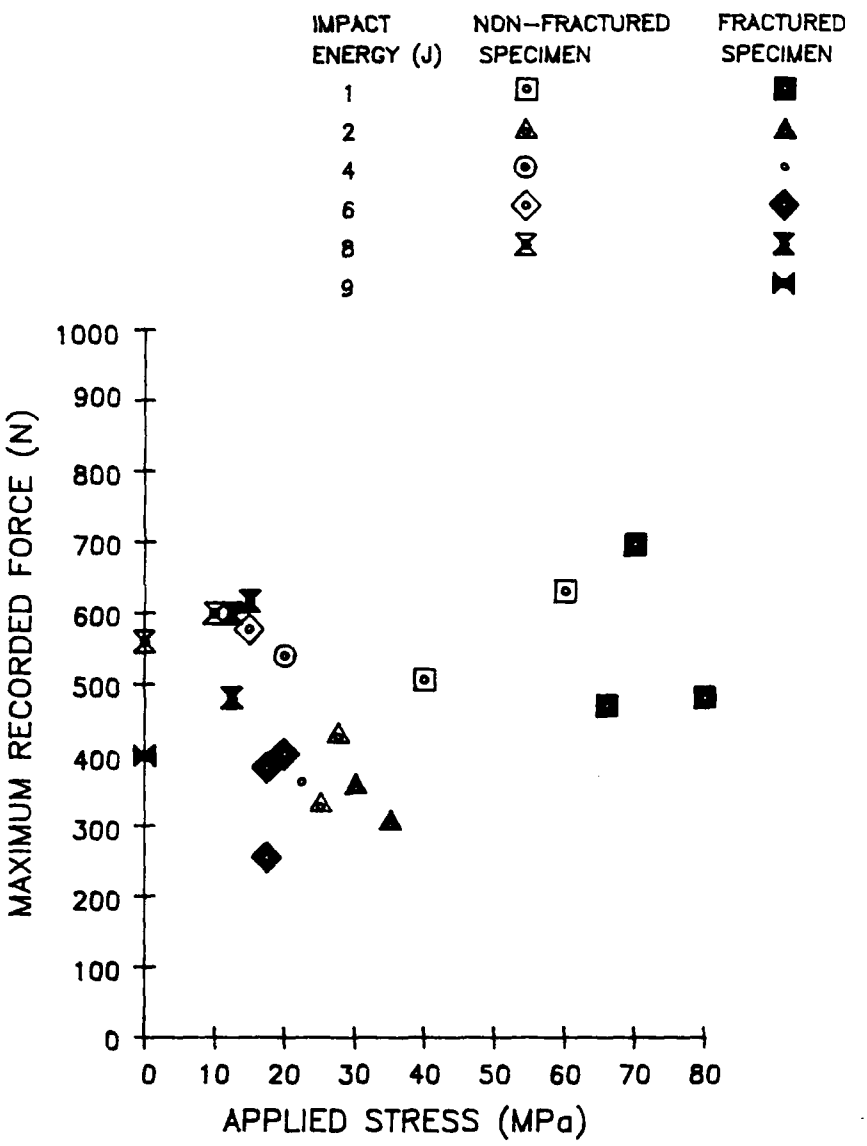

FIGURE 47. Variation of maximum recorded force with applied stress and impact energy for the Carbon / borosilicate glass composite materials.

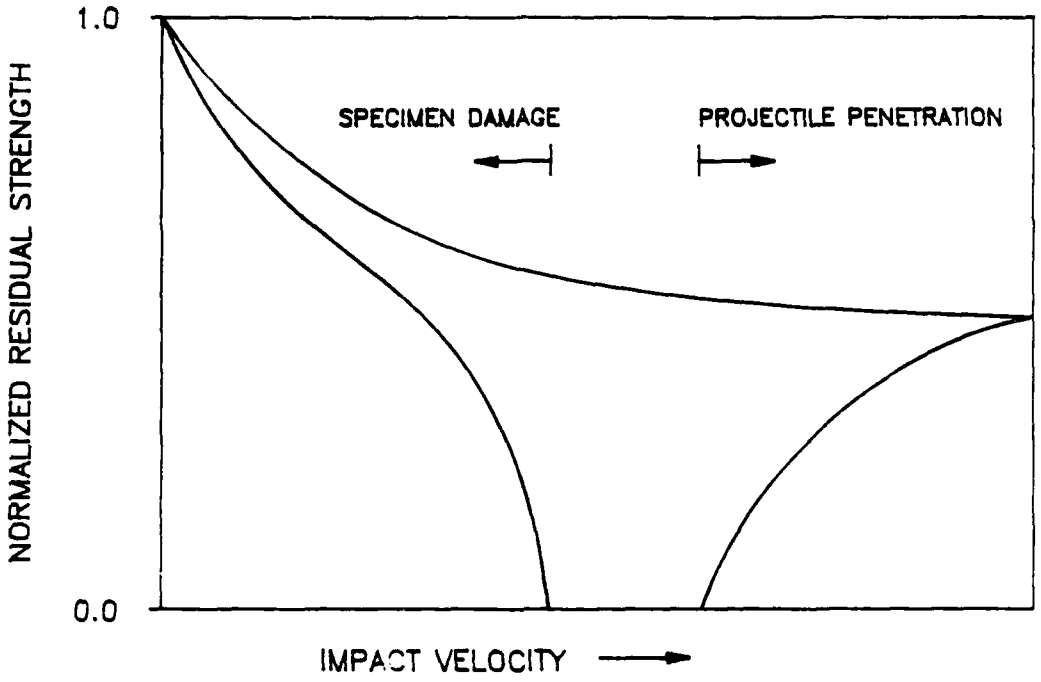

FIGURE 48. Effect of velocity on the normalized residual strength of an impacted composite [21].

U.S. GOVERNMENT PRINTING OFFICE 1988 - 548-056/04004